NTNU
Norwegian University of
Science and Technology

Causes and Impacts of Partial Shading for a Building-Applied PV System

Lovinda Ødegården

Abstract

The world as we know it today is full of technical equipment that requires energy of some sort, let it be oil, gas or electricity. With an increasing growth of the earth's population, as well as a boost in the general standard of living, it is certain that the total energy need will increase. To meet these demands one must utilize all the research available to develop the new era renewable energy and environmentally friendly technology. Solar energy is without a doubt one of the most certain sources of energy that will become a large supplier of consumer energy in the future. Thus it is important to keep on researching new ways to increase the efficiency of today's solar photovoltaic (PV) applications and keep lowering the cost of such technology.

This master's thesis has studied a building-applied PV system in Norway and investigated how well the technology performs during partial shading conditions. The PV system studied in this thesis is that of Powerhouse Kjørbo in Sandvika, near the capital Oslo. Powerhouse Kjørbo is an old rehabilitated office building and is Norway's first energy-positive office building, in its third year of operation. The building, consisting of two blocks, is meant to produce more energy than it uses for materials, production, operation, renovation and demolition during the whole of its lifetime. The energy is produced by solar panels installed at the two rooftops and on the top of a nearby parking complex.

The work began with gaining information about and understanding of the Powerhouse Kjørbo PV system and how it might be affected by partial shading. Prior to performing measurements and experimental and simulation studies of the Powerhouse Kjørbo system, a week of inspection was done at the site. Soiling of the modules by bird droppings and other pollution particles was observed as a potential factor for losses It was also found sources for cast shadows among others a vent pipe, a steel safety wire and a mussel shell lying on the surface. The findings became the background for the conducted shading experiments and simulations. The results from the experimental and simulation study were then used to estimate the impacts of selected cast shadows, and finally, on-site measurements at Powerhouse Kjørbo were conducted to compare to the previous findings.

It was found that cleaning of strings of PV modules resulted in an increased daily energy yield by up to 11 %, compared to uncleaned modules under the same environmental conditions. It was also found that all of the identified sources of partial shading had a visible impact corresponding well to what was found during the experimental and simulation studies. When analyzing the shading impacts, the I-V curve has been shown to be most useful, where the main indicator of reduced potential power production is the short-circuit current. The simulation models have been verified by real-life measurements, and proven to need some upgrades to represent a fully realistic model of a PV module or system. When measurements were performed at the PK system, it was found that the worst drop in power occurs when shading modules on their short edge. The partial shading source that had the greatest impact was shown to be an exaust vent, causing a power reduction of nearly 20 % on a string level.

Preface

This report is my master's thesis of the course TET4900, for the Master of Science study programme Energy and Environmental Engineering at the Norwegian University of Science and Technology, NTNU. This master's thesis was carried out during the spring semester of 2016, as a continuation of the work of my specialization project (TET4520), titled "Test and Demonstration of PV Systems".

The main motivation for choosing this topic for my specialization project and master's thesis, is that I believe that solar photovoltaics are and will continue to be a very important source of energy for ensuring a green electricity supply for the whole world. Around 1.1 billion people in the world do not have access to electricity, and the Sun will always be there and has an enormous energy potential. Solar photovoltaic systems are environmentally friendly and relatively easy to maintain as there are no moving parts, and the continuous development of photovoltaic technologies ensures more stable and robust ways of harvesting solar energy.

During the past year I have learnt so much about solar photovoltaic cells and modules: how they work, how they are affected by shading and environmental conditions and how they can be modelled using computer software. It has been an interesting and educational journey with new discoveries, hard work, frustration and fun – but mostly hard work and frustration.

With these words I conclude my Master of Science education, proud to soon call myself "sivilingeniør".

I hope the reader will find this master's thesis as interesting as I have.

Trondheim, July 08 2016

Lovinda Ødegården

Acknowledgment

I, the author of this project report, would like to give my heartfelt thanks to the following people for helping me on the way to fulfill what has been an exiting and enlightening master's thesis:

- My wise supervisor, professor Ole-Morten Midtgård, for his engagement and knowledge about solar photovoltaics, and his guidance and encouragement.
- My co-supervisor Peter Bernhard, Senior Consultant at Asplan Viak, for his wide knowledge and invaluable help with everything – from measurements, to cleaning PV modules, to lunch discounts in the cafeteria.
- The rest of the kind and hospitable people working at Asplan Viak, for providing me with my own temporary office and for being interested in my work.
- The Research Centre on Zero Emission Buildinngs (ZEB), for financial support for my two travels to Powerhouse Kjørbo, and an extra thanks to Professor Inger Andresen for also providing feedback on this thesis.
- The people at the mechanical workshop at the Department of Electrical Power Engineering for building the experimental PV rig, with an extra big thanks to Staff Engineer Morten Flå for quick and reliable help.
- Erik Langørgen, Staff Engineer at NTNU's Department of Energy and Process Engineering, for lending me the infrared camera.
- Carl Christian Strømberg, founder and manager of Solcellespesialisten, for providing the connector adapters on a very short notice (and outside of working hours), thus saving my PVPM measurements.
- My co-supervisor from the specialization project, Iromi Ranaweera, for her help and feedback on this thesis.
- Finally, I would like to thank my friends and fellow students for five amazing years at NTNU, with an extra thanks to Ingvild Eldegard and Odin Budal Søgnen for reading through my thesis and pointing out my many errors.

<div align="right">L.Ø.</div>

Contents

Abbreviations

The following abbreviations have been used in this thesis:

BAPV	Building-Applied Photovoltaic
BP	Bypass
E	Irradiance
IBC	Interdigitated Back Contact
IR	Infrared
I-V	Current-Voltage
MPP	Maximum Power Point
MPPT	Maximum Power Point Tracking
OC	Open circuit
PK	Powerhouse Kjørbo
PV	(Solar) Photovoltaic
PVPM	The name used for the I-V curve tracer
RBD	Reverse Breakdown Voltage
SC	Short circuit
SDM	Single-Diode Model
STC	Standard Test Conditions: AM 1.5, 1000 W/m^2, 25 °C
Wp	Watt peak

Chapter 1 | Introduction

1.1   Background and Motivation

Focusing on a sustainable future for energy consumption is one of the main drivers behind the rapid development in solar photovoltaic (PV) applications. International Energy Agency's report *Snapshot of Global Photovoltaic Markets* shows that the cumulative global installation of PV power capacity has had a great increase the past few years, with at least 227.1 GW installed by the end of 2015, which is more than 10 times the installed capacity in 2009. During 2015, there was installed up to 50 GW of new solar PV power, compared to 40 GW installed in 2014, once again setting a record of installed yearly capacity. [1]

The total installed capacity of solar power in Norway was about 15 MWp by the end of 2015, where almost 1/3rd of this capacity was installed in 2014 and 2015. The highest growth has been observed for residential PV systems, where the installed capacity in 2015 was four times that of 2014. [2] In general, the cost per installed kWp for solar power is still somewhat high, but continues to decrease along with the increasing interest for private energy demand reduction and producing electricity locally. [3] The global market for PV systems is heading towards rooftop PV being an economically attractive investment in several regions of the world – even without subsidies – which will hopefully be the case in Norway as well. [4]

Installation of solar panels on rooftops is beneficial for several parties; the PV system owner saves money from reduced electricity purchase from the power companies, and this distributed power production may help reducing the peak loads in the grid. Conventional energy consumers are heading towards becoming *prosumers*, both consumers and producers of energy, and more and more governments are adapting policies to embrace these changes. [1] An example of such a building-applied PV (BAPV) system is located in Sandvika, Norway, at the energy-positive building *Powerhouse Kjørbo.*

When finished in February 2014, Powerhouse Kjørbo's PV system had 312 kWp installed power, earning the title of Norway's largest PV system [5]. Only eight months later, this title was passed on to the 371 kWp rooftop PV system of ASKO's storage building in Vestby [6], which was expanded to 673 kWp in May 2016. In April 2016, a 720 kWp roof-mounted PV system was opened in Lillesand on another of ASKO's storage buildings. [7], [8] The company Unil is currently building a 1300 kWp PV system on a storage building in Våler, scheduled to be in operation by November 2016. [9]

BAPV systems in operation may be exposed to different environmental influences, depending highly on geographical location and climate. There may be factors such as cast shadings from nearby buildings and vegetation, exhaust particle soiling, along with weather-related influence from snow and ice, dust accumulation, leaves or bird droppings. Shading on parts of the PV system may not only reduce the power production from the affected PV modules, but also lead to a reduced performance of other modules connected in series or parallel with it. Several experimental and simulation studies have been done regarding the effect of partial shading – as will be presented through this thesis – but few studies have been conducted in a Nordic climate.

1.2 Hypothesis and Research Questions

Since the scheduled PV system was simulated in the PV system simulation software PVSyst, no studies have been conducted for the PV system at Powerhouse Kjørbo. This master's thesis is a cooperation with Senior Consultant Peter Bernhard at Asplan Viak and the owners of Powerhouse Kjørbo, where the following hypothesis has been given: *The soiling and partial shading conditions at Powerhouse Kjørbo's PV system has a significant negative impact on the PV system performance.*

Based on the hypothesis, there has been conducted a study of these partial shading sources and evaluated whether or not they should be mitigated or neglected. The main research questions for this thesis are:

1. Is the concern expressed by the hypothesis a reality or not?

2. How does the reverse bias I-V characteristic of PV cells affect the performance of

PV modules and systems under partial shading conditions?

3. How do shading-tolerant PV modules perform compared to conventional modules, and what are their advantages in a PV system exposed to partial shading?

4. Will manual cleaning of soiled PV modules lead to a significant increase in performance, or is the environmental conditions sufficient for preventing large soiling losses?

These questions have been answered by the following methods:

a) On-site inspection and measurements at the PV system at Powerhouse Kjørbo, identifying potential sources for reduced performance with focus on partial shading and soiling.

b) Conducting an in-depth literature study for understanding how a photovoltaic system and module are affected by partial shading in terms of current-voltage and power characteristics.

c) An experimental partial shading study on available test-PV modules, to obtain real-life data for PV modules under partial shading and input for computer simulation parameters.

d) Coding a MATLAB script that can calculate the current-voltage characteristics of a photovoltaic module or system based on the user's input of parameters, bypass configuration and shading conditions.

e) Creating circuit models in LTSpice for the studied PV modules, simulating shading conditions for comparison with the results from the MATLAB script.

f) Analyzing available data on weather, solar irradiance and power production for the PV system.

1.3   Limitations

Before this project started, it was planned to also study the effect of snow on the PV system. The online monitoring system was not online until March, when most of the snow had already melted. In addition, resources for quantifying the amount and density of snow were not available. It has therefore been chosen to exclude the effects of snow in this study, due to insufficient accurate data regarding snowfall and the amount of snow deposit on the PV modules at Powerhouse Kjørbo.

The outdoors shading experiments had to be conducted on sunny, cloudless days. Due to the unpredictability of the weather, each experiment was more or less spontaneous. During this semester, there has also been few days with sufficient direct irradiation to perform shading experiments and I-V measurements.

The logged data from the online monitoring system at Powerhouse Kjørbo are not measured at string level but for the whole inverter which is connected to four or six strings with two different operating voltages. Thus it becomes harder to determine which power losses come from which shading sources, in addition to the modules being exposed to uneven amounts of soiling. This has affected the certainty of several of the quantitative estimates done in this thesis.

The resources for performing on-site measurements were limited. Powerhouse Kjørbo is located in Sandvika, while the author of this thesis and measuring equipment were located in Trondheim. The PV system is also in full operation, and doing measurements on a string level involved disconnecting parts of the system, which must be done under professional supervision.

The data and results obtained in this thesis had limited to showing impacts of partial shading at specific times and environmental conditions, not so much quantification. The desirable outcome of the results would be an estimate of the potential losses as a function of time, but the available resources during this work are not sufficient for drawing such confident conclusions. It was planned to perform simulations in PVSyst to make such calculations, but the already made model of Powerhouse Kjørbo in PVSyst was not made available.

1.4 Thesis Outline

As the experiments, simulations and on-site measurements at Powerhouse Kjørbo were done in between each other, the structure of this report may seem a bit disorganized. The simulations, experiments and measurements were all performed to support and provide information for each other. As this thesis presents results from various sources, they will be discussed as they are presented, looking back and connecting the results to previous findings through the text. Information about Powerhouse Kjørbo's PV system has been presented first, as the basis and inspiration for the theoretical, experimental and simulation studies conducted in the following chapters.

Chapter 2 presents background information about PV system of Powerhouse Kjørbo.

Chapter 3 presents the relevant theoretical background for the simulations, measurements and analysis, assuming that the reader has some elementary knowledge about photovoltaics and PV systems.

Chapter 4 presents the setup and results from the experimental study of shading on PV modules and the impact of bypass diodes.

Chapter 5 presents the methodology and results from computer simulations in MATLAB (numeric) and LTSpice (electrical circuits), using the obtained results from the shading experiments to determine parameters.

Chapter 6 presents the results from on-site measurements at Powerhouse Kjørbo's PV system, focusing on selected sources for partial shading and the effect of cleaning modules. This chapter is supposed to round up the previous chapters and connecting the findings.

Chapter 7 presents the a summary of the results, conclusions for the work of the thesis, along with suggestions for further studies.

Chapter 2 | Background: The Powerhouse Kjørbo PV System

The object of study in this thesis is building-applied photovoltaic (BAPV) at Powerhouse Kjørbo, a case of building-applied photovoltaics (BAPV). Powerhouse Kjørbo is an office building located in Sandvika, near Oslo. The goal is to identify sources and impacts of reductions in performance for this PV system, focusing on partial shading. The findings from inspecting the Powerhouse Kjørbo (PK) PV system will then be further studied by experimental I-V curve measurements and computer simulations to understand and quantify the impacts of the found partial shading conditions. Obtaining data for analyzing the PV system performance was done by online monitoring of irradiance and power at inverter level, thermal imaging of the module surface, and I-V curve measurements at string level. These data were to be compared to the experimental and simulation results.

Some of the information presented in this chapter has been found in private documents borrowed from Asplan Viak and Entra, unavailable to the public. The contact person for this thesis regarding the rooftop PV system at PK has been Peter Bernhard, Senior Consultant at Asplan Viak. Mr. Bernhard gave a tour of Powerhouse Kjørbo on March 7th, providing information orally regarding the PV panels and inverters on Block 4, Block 5 and the garage building. Because of this, some of the information does not have any references.

Remark: *Due to numerous mentions of Powerhouse Kjørbo, the acronym "PK" may be used in the text. As the theoretical part of this thesis is presented in the next chapter, some terms may not be explained in the current chapter.*

2.1 About Powerhouse Kjørbo

Powerhouse Kjørbo is an old office building in Sandvika, Norway, from 1980 consisting of two blocks, which has been rehabilitated and made into a modern, energy-positive building as the first of its kind. The term "powerhouse" refers to a building that will have produced more energy than it has consumed in total through its lifetime – including construction, operation, and demolition – which in PK's case is 60 years. The PK project was finished in February 2014, and was initiated by the alliance *Powerhouse*, a collaboration involving Scandinavian companies dedicated to energy-positive buildings. One of these companies is the consulting firm Asplan Viak, who is currently renting the office building. [10], [5]

After the renovation, the building's energy demand was reduced by 90 %, which was a result of optimization of known technologies for ventilation, insulation and lighting. In addition, the energy demand was reduced further by integrating a geothermal well for heating and cooling, and installing solar panels of state-of-the-art quality on the rooftops. [5] Building-applied photovoltaics (BAPV) refers to a solar PV system that is installed after construction of the building. This distinguishes BAPV from building-*integrated* PV (BIPV), which means that the PV panels are a part of the building construction, like for instance PV panel roof tiles.

In august 2015 Entra Eiendom, the owner of the PK building, decided to renovate another block in the same building complex to be a part of PK. This addition to PK is scheduled to be finished by July 2017, and includes an expansion of the total PV system as well. [11]

2.1.1 Planning the PV system

When referring to the PV system of PK in this thesis, the PV modules installed at the nearby garage building are included. An overview of the building complex and garage building with the rooftop PV systems pointed out is presented in Figure 2.1. The compass indicates the North direction. Note that on Block 5 there are no modules installed at the southern corner of the roof. The reason for not placing PV modules here, was that it was not permitted to cut down the nearby trees. However, after PK was finished, these

trees were cut down anyway. En energy storage solution was also considered for the PV system, but was not deemed economically feasible due to the large cost of batteries.

Figure 2.1: The Powerhouse Kjørbo area, showing locations for Block 4, Block 5 and the Garage building. (Screenshot from Google Maps)

Prior to construction, a simulation analysis of the PV system was performed using the software PVSyst by the installers of the PV system at PK, Solkompaniet Sverige AB (at that time named Direct Energy AB). PVSyst is a tool for detailed simulation of the energy yield of a specified PV system. Solkompaniet performed a simplified simulation of the three rooftops separately, with some differences from the design that was actually built. The simulation was run with 936 modules, at 0° tilt and 100 % power loss due to snow from December to March. They have not included any other shading in the model, but specified "near shading losses" of 2.4 % for Block 4 and 1.1 % for Block 5. The result was a theoretical electricity production of 229 000 kWh/year, with an average production of 210 000 kWh/year during their lifetime of 30 years. To compensate for degradation of approximately 0.5 % per year, the final installed system included 18 modules more than the simulated case. (Source: PVSyst reports borrowed from Solkompaniet and Peter Bernhard)

Figure 2.2 shows the monthly solar electricity production for 2015, separating between the three rooftop PV systems. During January, February and December, the total energy

yield only 1570 kWh, which is due to snow covering the rooftops. For April–August the PV energy production is larger than the consumption. The total solar energy production for 2015 was measured to be 221 380 kWh, while the measured total electricity consumption at PK for 2015 was 228547 kWh. The PV system is dimensioned for these numbers balance each other each year, but due to a technical error, approximately 6000 kWh were lost between May and June 2015.
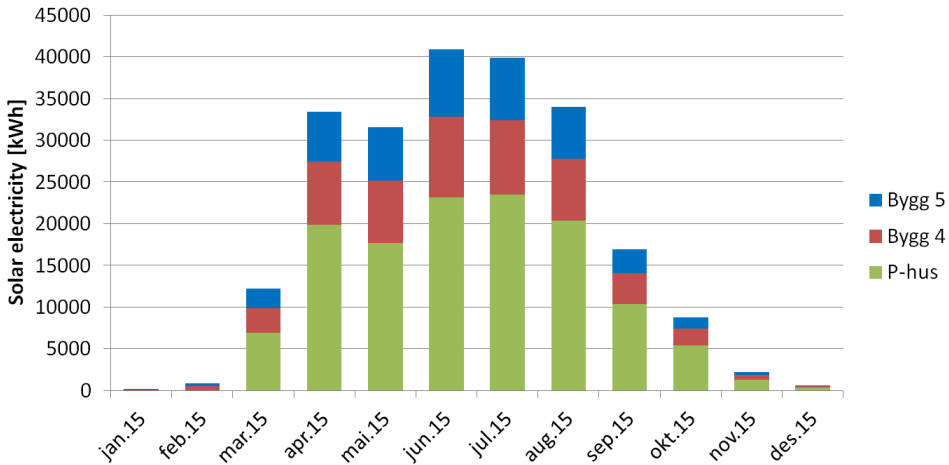
Figure 2.2: Monthly solar electricity production at Powerhouse Kjørbo from 2015.

2.2 PV System Information

Powerhouse Kjørbo's PV system has been in operation since April 2014 and has an installed peak power of 312 kWp. The PV systems at Block 4 and 5 supply the PK building itself, while the garage building PV system supplies power to itself, 30 charging stations for electrical vehicles and a nearby building with a gym for the employees at Kjørbo.

The operational PV system consists of 954 modules covering approximately 1555 m^2, divided among the three rooftops. The distribution of PV modules, installed power and orientation is presented in Table 2.1. The azimuth angles that are given in the Tables are approximations done using Google Maps, comparing the direction to the indication of North. There are mainly two ways of defining the azimuth angle; using either North or South as zero degrees. In this report, the reference will be South with positive direction

clockwise, accordingly to the Sunny Portal user manual, [12]. At Block 4 and 5, half of the modules are facing approximately Southeast (SE) and half is facing the Northwest (NW). At the garage building, the orientations are close to East-northeast and West-southwest, but these will here be referred to as Southwest (SW) and Northeast (NE).

Table 2.1: My caption

Rooftop	No. of modules	P_{PEAK}	Azimuth
Block 4	212	69.3 kWp	-35° (SE) / +145° (NW)
Block 5	180	58.9 kWp	-35° (SE) / +145° (NW)
Garage	562	183.8 kWp	-110° (NE) / +70° (SW)
TOTAL	**954**	**312 kWp**	-

All PV modules are mounted in a horizontal position with a tilt angle of 10 °, and every other row of modules is facing separate directions, as shown in the photo of Figure 2.3. As seen in the photo, the snow melts from the top and slides downwards, so the horizontal positioning of the modules ensures less lost power due to snow covering the modules. Another practical solution worth mentioning is that the edge around the roof of Block 4 and 5 is adapted in a manner that makes the wind push the PV modules down, instead of having the wind lift the modules which might break the mounting rack. This solution also provides the modules with a natural cooling which may increase the performance (read more about temperature effects in section 3.3.4).

Figure 2.3: A photo of a part of the roof of Block 4 from March 10th, while there was still snow on the modules. (Photo: L. Ødegården)

2.2.1 PV module specifications

The PV modules used at PK are of the model *SunPower E20-327*, which is a mono-crystalline PV module, made by the American energy company SunPower. It will be referred to as the "SP-E20" module. The PV module's relevant data are presented in Table 2.2. More detailed specifications are provided in the module's data sheet, [13], and in the installation manual, [14]. This module has 12x8 PV cells in series, i.e. 96 in total. The PV cells are of the type SunPower Maxeon Gen (Generation) II, having an efficiency of 20.4 %, which is well above average for mono-crystalline cells.

The module has three bypass diodes of the Schottky type with ratings 15 A and 45 V Peak Inverse Voltage (PIV). There are two diodes for two substrings of 24 cells, plus one diode for a single substring of 48 cells [14]. It is not specified how these substrings are connected, but most likely the two short substrings are the two outer columns on each side to achieve symmetry. The module is designed so that the bypass diodes are not activated for small cases of shading, but rather as an extra mechanism in case of severe shading and thus minimizing the maximum power loss. With a small reverse breakdown voltage of -5.5 V these modules are so-called "shading-tolerant" [15]. These important properties will be discussed further in the next chapter, presenting the theoretical background for understanding the effect of partial shading on PV modules.

Table 2.2: Relevant data for the SunPower E20-327 PV module. [13], [15]

Parameter	@STC
Peak power (P_{MAX})	327 Wp
Rated voltage (V_{MPP})	54.7 V
Rated current (I_{MPP})	5.98 A
Open circuit voltage (V_{OC})	64.9 V
Short circuit current (I_{SC})	6.46 A
Module efficiency (@STC)	20.4 %
Temperature coefficient for P_{MAX}	-1.2426 W/°C
Temperature coefficient for V_{OC}	-176.6 mV/°C
Temperature coefficient for I_{SC}	3.5 mA/°C
Reverse breakdown voltage	-5.5 V
Module area	1.63 m^2

2.2.2   Inverters

At PK, the PV system uses multistring inverters. The inverters used at PK are all of the type Sunny Tripower (STP) made by SMA Solar Technology AG, but with three different power ratings; one rating for each rooftop. The different inverters' ratings are presented in Table A.1 in Appendix A.1. Table A.2 to A.4 summarize the PV modules and inverters for each roof. As seen in the tables, the inverters can have four or five parallel strings at input A (see Table A.1), plus one string at input B, with one independent MPPT at each input. The modules connected to input B are typically strings experiencing the most variable shading conditions, while the strings connected to input A should be in as similar operating conditions as possible, i.e. the strings' maximum power points should be at the same voltage.

String nomenclature

Figure A.1 to A.3 give a visual presentation of the string configurations where each string is colored and given a label. V stands for "vekselretter", meaning "inverter" in Norwegian, and each inverter is labeled with a number between 1–4 for the Blocks and 1–8 for the garage. The letters A and B describe which input terminal the string is connected to. When referring to a specific string later, the three buildings are abbreviated "B4" for Block 4, "B5" for Block 5 and P for the garage (parking) building. For example, B5_V4A3 is the string connected to inverter 4 at Block 5, to input terminal A3.

2.3   Logging and monitoring data

2.3.1   The Sunny Portal

During March 2016, the inverters at PK were connected to the *Sunny Portal* made by SMA Solar Technology AG. In brief, the Sunny Portal is an Internet portal set up by SMA Solar Technology, where PV system owners can monitor and download information and data. Available data are e.g. the PV system's power and energy production, irradiance, weather, performance ratio, amount of CO_2, money saved, and more. [12] For this thesis, the power production and irradiance are the most interesting data for analyzing

performance, and impacts of partial shading. These data for Block 4 and 5 were available on a 15 minute basis from March 8th, and the garage building inverters were online from March 23rd. The production data is presented visually as curves and can be downloaded as Excel-compatible files for numerical analysis. The data from PK's Sunny Portal are not public, but have been granted access to in relation to this project.

Temperature and global irradiance sensors were installed at the garage building with the same orientation as the PV modules there – one for each direction. These were connected to the Sunny Portal and logging 15 minute mean values from April 13th. There has not been installed such a sensor with the orientation of Block 4 and 5. The irradiance and temperature data will therefore not be applicable for Block 4 and 5.

2.3.2 Sunny WebBox

The Sunny WebBox is a monitoring device communicating between the inverters and the Sunny Portal. A WebBox is installed per rooftop, sending data to the Sunny Portal via Bluetooth. It is possible to log into the WebBox via Internet browser to access instantaneous production data on string level, monitoring current, voltage and power. Though such data would be ideal for the analysis of this thesis, these data are not logged. [12]

2.3.3 Meteorological data

The closest weather station to Sandvika is located in Asker, approximately 6.5 km away from Sandvika. Table B.1 in Appendix B presents the daily average precipitation (snow and rainfall) from February 1st to June 1st, according to Norwegian Meteorological Institute. The dates marked in yellow are the dates spent on site, and the dates marked in green are the dates studied when cleaning the modules on the garage.

2.4   Malfunctions and repairs March–June 2016

Through the work of this thesis, there has been some occurrences of inverter and WebBox malfunctions. The recorded malfunctions were as follows:

- Inverter P_V5 failed some time between 19:00 on March 25th and 6:00 on March 26th. According to the weather data in Appendix B, there was a rainfall at this time, which might have been the "cause of death" for P_V5. P_V5 was producing the same power as the similar inverters at random times since then, but on a majority of the time the production was zero.
- On May 1st and 4th inverter P_V2 began to malfunction. The largest rainfall recorded in Appendix B happened on May 1st, strengthening the assumption that rain has been the cause of inverter failure.
- Once in a while, the communication between the WebBox and Sunny Portal fails, resulting in some time intervals lacking data.
- The temperature sensor oriented South-west on the garage building failed on May 10th, switching between showing absolute zero (-273 °C) and unreasonably high temperatures up to 100 °C through the day.

On May 9th, technicians from Solkompaniet came to PK to repair the malfunctioning inverters. The problem seemed to be solved for inverter P_V2, but it began failing again on May 30th. After the repair, P_V5 was put back in operation successfully with one string disconnected. This can be observed in the Sunny Portal as a production that is consequently lowered by approximately 1/6th. After searching for the malfunction cause, the technicians from Solkompaniet were fastening the connectors to the back of all the modules at the garage building. Until then, the cables had been lying on the ground, exposed to water and dust (see Figure 2.4). This was the most probable cause of the inverter failure, but was not confirmed.

2.5   On-Site Shading Inspection

As a preparation for the outdoor experiments and the I-V curve measurements at PK, a week of inspecting the site was conducted from the 7th to the 11th of March. This

Figure 2.4: One of the MC4 connection cables lying on the ground, covered in dirt. (Photo: L. Ødegården)

consisted of walking around the rooftops of Block 4, Block 5 and the garage building, identifying and documenting partial shading and soiling on the modules, in addition to planning which strings would be most similar in production for later comparison. During this week, there was still snow on the modules, which was completely melted on March 10th for Block 4 and 5. Configuring the Sunny Portal was also done during this week, involving labeling the inverters and strings, and changing the data logging frequency from 1 hour to 15 minutes. The second trip to PK took place from the 3rd to the 10th of May. During this period, measurements of current-voltage characteristics and thermal imaging using an infrared camera were performed.

2.5.1 Cast shadows

Block 4 and 5 both had multiple sources for cast shadows causing partial shading of modules, while no such shades were observed at the garage building. Figure 2.5 and 2.6 show the identified sources of cast shadows that affect the PV modules at Block 4 and Block 5, respectively. All the identified cast shading sources come from constructions and installations at the PK building itself. The black shapes represent the sources for the shadow, while the dark circular area around it is an approximation of the shadow's range through the day. Note that they are drawn approximately as they were observed in May; the shadows' lengths and angles will change through the year.
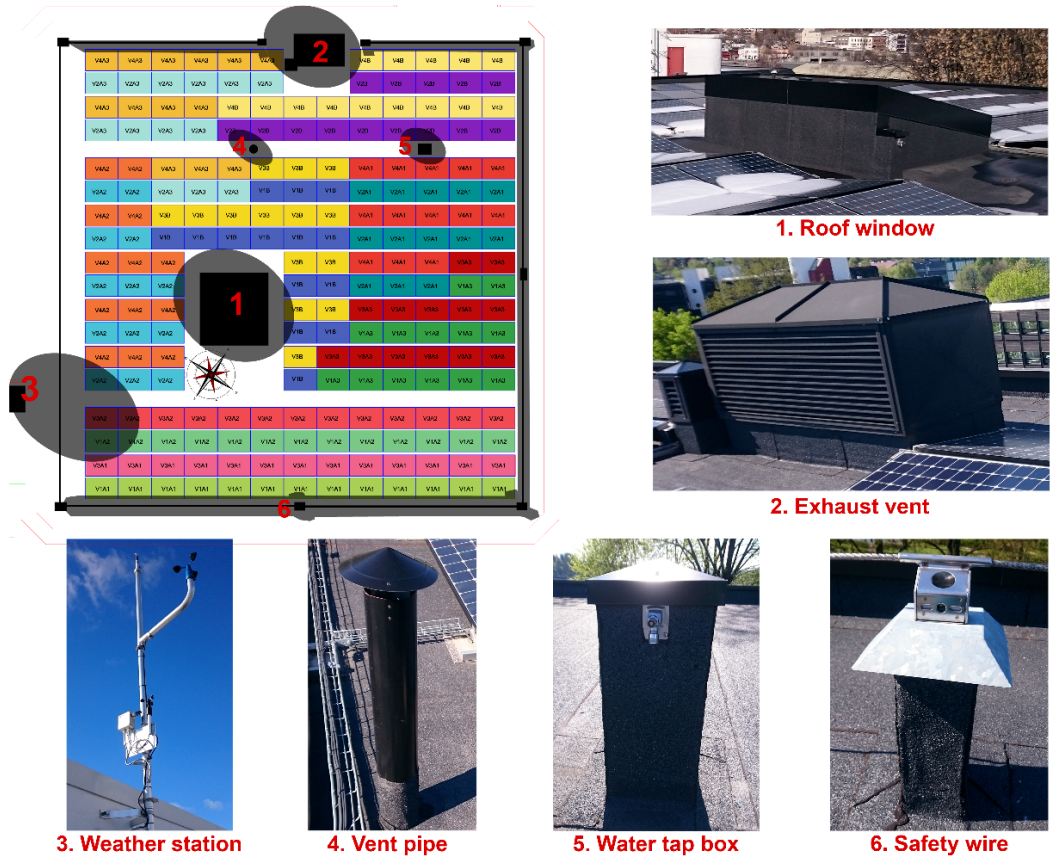
Figure 2.5: Identification of cast shadows at Block 4. (Drawing fom Entra, Asplan Viak, photos by L. Ødegården)
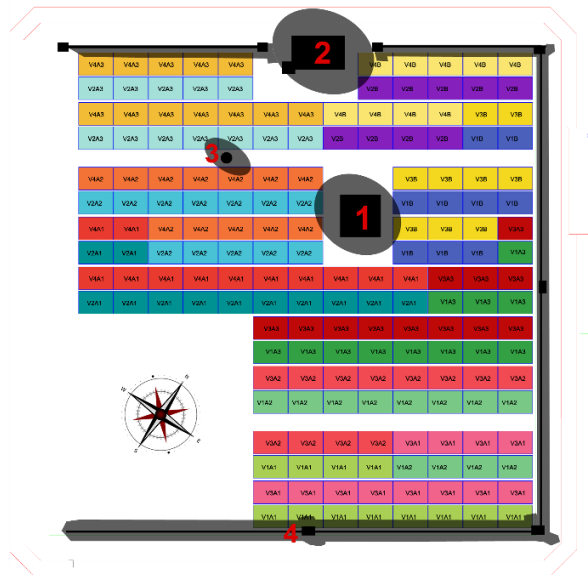
Figure 2.6: Identification of cast shadows at Block 5. (Drawing fom Entra, Asplan Viak, photos by L. Ødegården)

The safety wires were measured approximately 0.85 cm in diameter and produced cast shadows on several of the modules at both Blocks. The wires were fastened 8–10 m apart and drooping somewhat in between the mounts, producing different shadows on the modules. Figure 2.7 presents four different modules with in the same substring B5_V1A1 (South-east), 10:20 May 10th. The most severe shading is for the module in front of the safety wire mount (second photo from the left), while two modules were not shaded at all due to the drooping of the wire. The shadows did not stretch across more than two rows of cells at a time. Shading from the wire was not observed on the North-east and South-west edge of the modules on either of the Blocks, as the wires were placed further from the modules at these edges.
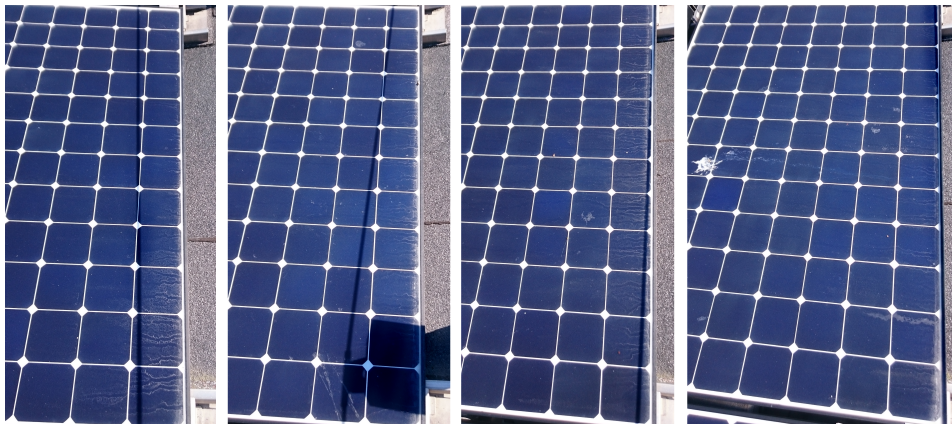
Figure 2.7: Cast shadow from the steel safety wire at Block 5, 10:20 May 10th. (Photo by L. Ødegården)

The exhaust vents, roof window at Block 4 and roof hatch on Block 5 may produce cast shadows affecting the short side of the modules and may potentially affect the whole module. This kind of shading is worse than for shading on just a part of the module horizontally, as will be explained in the next chapter. In March, the vent pipes and water tap box were observed to cast shading on the two lower substrings throughout the day, the cap of the vent pipe being large enough to cover a whole cell – see Figure 2.8.

Figure 2.8: Cast shadow from the vent pipe at Block 5, 12:40 March 8th. (Photo by L. Ødegården)

The largest shading observed during the first inspection in March, was shading from the weather station located at the interconnection between Block 4 and 5, where some parts of the construction are much taller than the rooftops. This casts a large shadow at Block 4, as seen in the photo of Figure 2.9, taken on March 8th. In May there was no cast shadow from the building interconnection, only from the weather station. An important difference between the shading from the weather station compared to the other shading sources, is that the weather station is located further away, thus allowing more diffuse and reflected light to reach the module. This can be seen in the blurry and weaker shadows in Figure 2.9 compared to for example the shading from the pipe.

Figure 2.9: Cast shadow from the weather station and parts of the building, 13:15 March 8th. (Photo by L. Ødegården)

2.5.2   Surface soiling and solid objects

After the snow melted, the dust particles trapped in the snow could be seen on the modules as a rather thick layer of pollution, mostly affecting the lower part of the modules. An example is shown in Figure 2.10, displaying the differnce between a clean and soiled module, taken shortly after the snow had melted on Block 5, and before the first rainfall. The same amount of soiling was observed for all the three rooftops, while the snow at the garage building did not melt for another week or so.
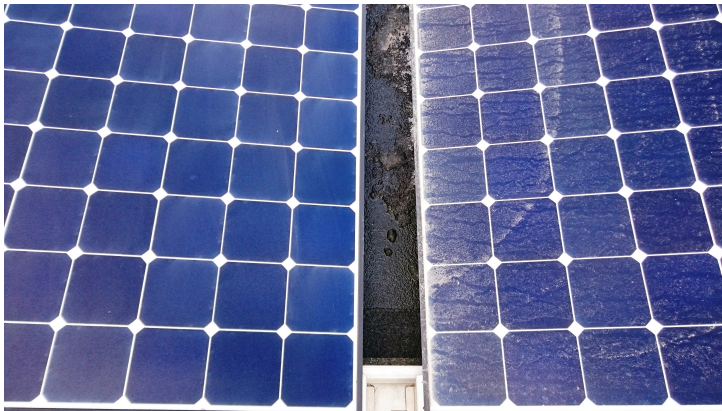
Figure 2.10: Cleaned (left) and uncleaned (right) module after the snow melted completely, taken 13:45 March 11th. (Photo by L. Ødegården)

During the inspection, the following sources of surface soiling was noted:

- PK is located next to a highway with much traffic. This will most likely be a source of carbon-based particles from vehicle exhausts and road dust from the asphalt.
- As can be observed from the map overview in Figure 2.1, there are several trees and vegetation nearby PK, which may be a source of pollen, leaves, etc.
- PK is adjacent to the ocean, which may be a source of salt particles.
- Since PK lies near the ocean, there were also observed many seabirds, mostly seagulls, which are likely the source of the droppings observed on the PV modules.
- Seagulls are also known to open seashells by dropping them from a height to crush them, which is probably the cause for the blue mussel shells found on the roof, some of them on top of PV modules. This could also potentially cause cracks and scratches on the modules, but no such damage was observed.

Examples of typical pollutants for rooftop PV systems are sand and soil from the ground, carbon-based particles (ash) from vehicle or industrial exhausts, salt from the ocean, and pollen from vegetation. These are tiny, solid particles of various sizes, shapes and compounds, which can block sunlight from the PV cells to different extents. Studies have shown that different compounds and particle sizes give impacts of different severity, where ash has proved to be among the worst compounds. [16] The effect of different types of soiling will not be studied here, but it will be investigated whether cleaning soiled modules has a significant impact on the PV module performance.

Regarding bird droppings, these are assumed to have a greater impact on reduction of effective irradiance, as they are more dense and are not as easily cleaned by rainfall as a thin layer of dust particles. [17] In March, right after the snow melted, there were little to no bird droppings observed on the modules, but there were some traces of old dropping stains. When returning to PK in May, the amount of seagull droppings was drastic for some of the modules on all of the three rooftops. The most severe case is shown in Figure 2.11, which is for a module affected by both excrement and shading from the vent pipe at B4_V2B. The issue of seagull droppings is not new to the owners of PK. Earlier, a shock track was installed along the edge of the roofs of Block 4 and 5 to mitigate the problem, but the droppings still seems to be an issue.

Figure 2.11: A module severely soiled by seagull droppings in addition to partial shading, taken 10:30 March 10th. (Photo by L. Ødegården)

Chapter 3 | Literature Review and Theory

To be able to evaluate the impact of partial shading at Powerhouse Kjørbo, it is necessary with an in-depth understanding of the phenomenon. This chapter presents a literature review, containing the relevant background theory for comprehending the computer simulations, practical experiments and analysis of the results. The theoretical background will briefly present design and modelling of solar PV cells and modules, factors that can influence the performance of a PV system, what the consequences might be and how to mitigate the undesirable effects. The main focus will be on electrical properties regarding shading, bypass diodes and reverse characteristics for illuminated solar cells, while theory concerning the mechanical construction and semiconductor physics will only be briefly discussed. The theoretical background will also be angled towards the PK PV system and the relevant type of modules.

Remark: *This thesis assumes that the reader has basic understanding of solar photovoltaic cells, in terms of how they produce electricity and how they are modelled as an electrical circuit. The reader should also have elementary knowledge about how to set up the current-voltage equations and how power electronics can be applied to connect a PV system to a power grid. Parts of this text has also been used in previous work of this thesis' preparatory work [18], with larger or minor changes.*

3.1 Solar Irradiance

Two main terms are used to quantify the incoming solar energy that can be converted into electricity by means of solar photovoltaics: *irradiance* (also called insolation or solar radiation, here symbolized by E), which describes solar *power*; and *irradiation*, the solar *energy*. Irradiance is a measure of power per surface area, measured in W/m^2. Solar

irradiation corresponds to the time integration of the irradiance over a specified interval, measured in J/m^2.

The amount of energy reaching the Earth's surface varies with several factors, where the angle that the receiving surface has towards the Sun is among the most significant factors. The irradiance (light intensity) at a given surface depends highly on the geographical location, the time of day, and on the season of the year, as the Earth tilts differently in relation to the Sun throughout the year. [19]

The solar irradiance reaching a PV cell surface can take several possible paths, and can be divided into three categories: *direct*, *diffuse* and *reflected* irradiance. The effective irradiance reaching a PV cell will be a combination of these three, commonly denoted by *global* or *effective* irradiance, E_{EFF}. On sunny days, direct irradiance typically account for 70–80 % of the global irradiance [20]. The direct irradiance is light travelling straight from the Sun to the PV cell surface, and has the highest energy density of the three categories. Diffuse irradiance occurs when the light is scattered due to molecules and other aerosols (clouds, pollution, etc.) in the atmosphere, while reflected irradiance comes from light being reflected by the ground and other surfaces. [21] The three kinds of irradiance are illustrated in Figure 3.1.
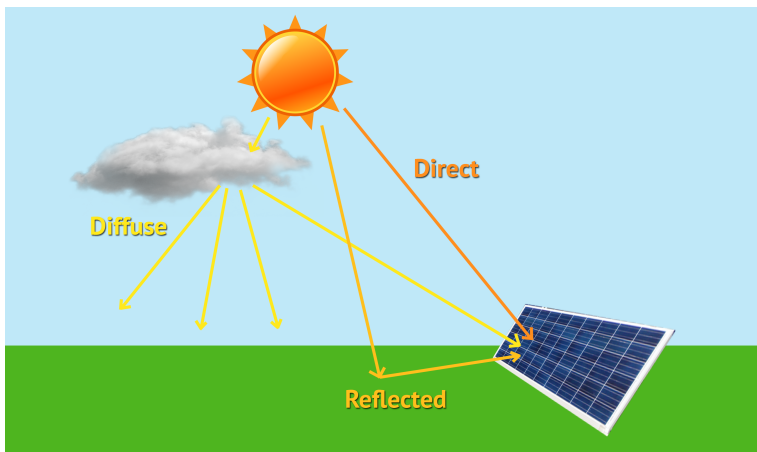

Figure 3.1: A simple illustration describing the three types of solar radiation. (Based on an illustration from [21], p. 410.)

3.2   Photovoltaic Module Design

3.2.1   Cell, substring, module, string and array

A PV *module* consists of a series connection of some number of PV cells. A number of series-connected modules is referred to as a *string*, and an *array* denotes one or more strings in parallel. Series-connected modules share the same current, and parallel-connected modules have the same voltage. The term *substring* will be used for the series-connected PV cells within a module which share a bypass diode (see section 3.4.3).

3.2.2   Crystalline silicon solar cells

The most common material used for producing commercial PV cells is crystalline silicon, including the two types of cells studied in this report. Data from the German website Solar-Server indicate that the price of silicon PV modules have dropped almost 70 % from 2010 to 2015, which is a result of the rapidly growing market for solar panels [3]. Crystalline silicon PV cells can be divided into two types: *mono-crystalline* and *poly-crystalline.* As the names indicate, mono-crystalline silicon cells consist of one single silicon crystal and typically has a uniform dark blue, almost black color, while the poly-crystalline cell consists of many smaller crystals and is speckled and blue. Typical efficiencies for commercial PV cells are 15–20 % for mono-crystalline and 14–16 % for poly-crystalline. [22]

3.2.3   Front-contact vs. Interdigitated back-contact (IBC)

Figure 3.2 shows close-ups of the two types of PV cells studied in this work. The cell on the left has its contacts (electrodes) both at the front (negative) and the back (positive). The front has a so-called metal grid consisting of "busbars", the two thick vertical lines, and "fingers", the very thin horizontal lines, for collecting the photo-generated charge carriers. Such so-called screen-printed PV cells is the simplest and most mature fabrication technology, currently dominating the market for commercial PV cells. [23] The right-hand cell has both the positive and negative electrodes on the backside of. The

main advantage of placing the contacts on the back is that more of the front-side area
can absorb photons, increasing the available power per cell area and thus the efficiency.
Figure 3.3 illustrates a cross-section of the two described designs. Another important
advantage of all-back-contacts is an increased robustness in the cell interconnections
of the module, considering thermal expansion and other physical stresses. As for the
deep blue color compared to the black front-contact cell, this is due to the anti-reflective
coating. [15]
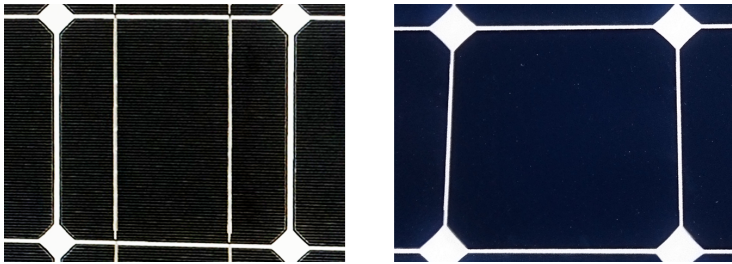
*Figure 3.2: The front-contact SoloSol module (on the left, source: Solcellespesialisten) and the
all-back-contact SunPower E20 module (Photo by L. Ødegården).*
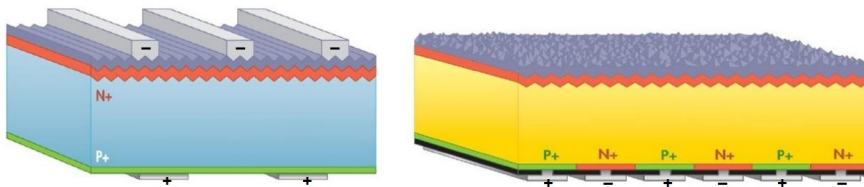
*Figure 3.3: An illustration depicting a cross-section of the front-contact design to the left vs. the
(interdigitated) back-contact design. (Adapted from [15])*

3.3 Modelling of PV Cells

3.3.1 Circuit and mathematical representation

The single-diode model (SDM) – presented in Figure 3.4 – is concluded to be sufficient
for modelling in this project, as it gave satisfying results in previous work [18]. The
photo-generated current, I_{PH}, is the current generated by the photons absorbed in the
PV cell. I_{PV} denotes the output current of the cell. The diode and its behavior represent
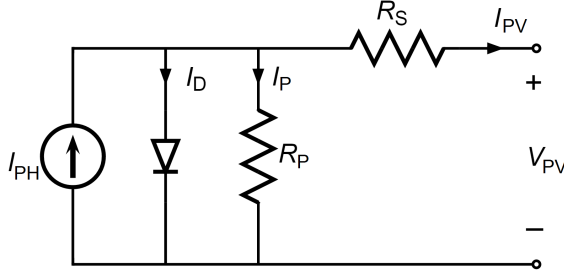
Figure 3.4: The single-diode model for a photovoltaic cell. (Adapted from Wikipedia)

a reduction in the output current I_{PV}, dependant on the cell's material properties, temperature and voltage. [24] The parallel resistance R_P represents leakage currents avoiding the p-n junction, i.e. the present alternative paths for the photon-generated free carriers. The series resistances R_S accounts for ohmic losses in the contacts and conductors of the cell or module. The equation linking current and terminal voltage for N PV cells in series is derived from the SDM as [24]:

$$I_{PV} = I_{PH} - I_D - I_P = I_{PH} - I_0 \cdot (e^{\frac{q(V_{PV}+NR_S I_{PV})}{NAkT}} - 1) - \frac{V_{PV} + NR_S I_{PV}}{NR_P}, \qquad (3.1)$$

where the parameters are as indicated in Figure 3.4, and I_0 is the reverse saturation current of the diode (typically in the scale range of a few nanoamperes), T is the temperature of the cell in Kelvin, q is the electron charge (1.602×10^{-9} C), k is the Boltzmann constant (1.381×10^{-23} J/K), and A is the ideality factor, which is equal to 1 for an ideal diode and between 1 and 2 for an average commercial PV cell. [24], [25] The voltage across the diode, V_D, is given by

$$V_D = V_{PV} + NR_S I_{PV} \qquad (3.2)$$

3.3.2   Current-Voltage Characteristics

The I-V curve of a PV cell (or module/substring) describes the possible operation points in terms of combinations of current and voltage for a given operating state, and can be very useful for analyzing performance and detecting for instance shading, surface

pollution or defects. The I-V characteristic of a PV cell in illuminated conditions has a typical shape as the green curve in Figure 3.5. The shape of the power curve is typically like the blue curve in the figure. [24] For a series-connection of several cells or modules, the resulting I-V curve is equivalent to the sum of the individual curves along the voltage axis.
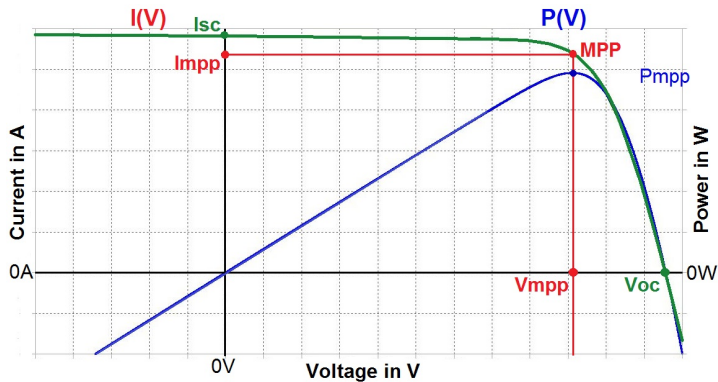
Figure 3.5: Typical I-V curve (green) with its power curve (blue) and maximum power point marked in red. (Based on figures from [26] and [18].)

The I-V curve has the characteristic parameters V_{OC}, the open-circuit voltage, and I_{SC}, the short-circuit current which is approximately equal to I_{PH} when $R_S << R_P$ [27]. The I-V curve has a maximum power point (MPP) located at the "knee" of the curve, given by V_{MPP} and I_{MPP}. These four parameters are indicated in Figure 3.5, and the rated values of these parameters for a PV module are normally specified by the manufacturer. To achieve maximum power extraction from the PV system, it is desirable to keep the terminal voltage at V_{MPP}. A PV module, string or array can be forced to operate at the MPP at all times, using maximum power point tracking (MPPT) to control the terminal voltage through power electronics. [28]

3.3.3 Change in series and parallel resistance

An ideal solar cell has an infinite R_P and $R_S = 0$. In other words: low parallel and high series resistance reduces the performance of a PV cell in terms of maximum available power. [29] Typical values for R_P and R_S are somewhat unclear in the available literature, the same as for which values are regarded as "low" or "high". According to [30], R_P may

vary from some 10 Ωcm^2 (low performance) to some 10 $k\Omega cm^2$ (near ideal). According to [31], the typical value for a commercial PV cell is in the 1000 Ωcm^2, which for a cell of $15 \times 15 cm^2$ is 4.44 – 44.44 Ω for 1000 and 10000 Ωcm^2, respectively. According to both sources, R_S is supposedly lying in the 0.5–1(1.3) Ωcm^2 range, corresponding to 0.0022–0.0044 Ω for a $15 \times 15 cm^2$ cell.

Studies such as [29], [32] and [33] have proved that both the series and parallel resistance change value with effective irradiance and temperature for silicon PV cells. Both the series and parallel resistance value will increase drastically with decreasing irradiance below 200–300 W/m^2, and a lesser decrease above this irradiance, as seen in Figure 3.6 showing experimental results for R_P versus irradiance. These results indicate that if the effective irradiance is reduced by 80 % and more due to clouds or shading, the resistances will be significantly larger than for irradiance levels near 1000 W/m^2.
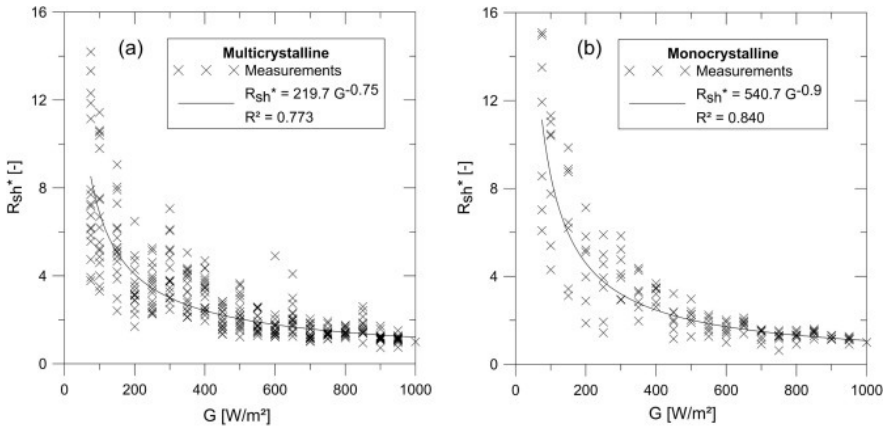
Figure 3.6: Measured relative values of parallel (shunt) resistance for different irradiance levels, for multi-crystalline and mono-crystalline PV modules. (From [29])

If the I-V curve is available, R_P can be estimated using equation 3.3. This is a valid approximation when R_S is small. [29] This will be used when estimating the effective parallel resistance for shaded and unshaded parts of I-V curves later in the experimental and simulation chapters. R_S will not be studied in this report.

$$R_P \approx R_{P,0} = -\frac{dV}{dI}\bigg|_{I=I_{SC}} \tag{3.3}$$

3.3.4   Irradiance and temperature dependence

The effective irradiance and temperature on a fixed PV module surface will change through the day and through the seasons of the year, due to the varying angle towards the Sun and weather conditions. The temperature level is determined by the ambient temperature and the level of irradiance, and affects the electrical processes in the semiconductor material. The photo-generated current, and thus also the SC current, is almost directly proportional to the effective irradiance, with a small temperature dependence. [34] Therefore, measuring I_{SC} and comparing it to the rated value at STC with E = 1000 W/m^2 will indicate the irradiance level at which this current was measured. Typical impacts on crystalline silicon from an increased temperature is a small increase in I_{SC}, a decrease in V_{OC} and a decrease in P_{MAX}. For the three parameters it is common for the manufacturer to specify temperature coefficients at STC, given in either percentage or Ampere/Volt/Watt, per degree Celsius or Kelvin. [35] These are here denoted by μ. Approximated methods for estimating I_{SC} and P_{MAX} for a given irradiance and temperature level are [34]:

$$I_{SC} = \frac{E_{EFF}}{E_{REF}}[I_{SC,REF} + \mu_{Isc}(T - T_{REF})] \qquad (3.4)$$

$$P_{MAX} = \frac{E_{EFF}}{E_{REF}}[P_{MAX,REF} + \mu_{Pmax}(T - T_{REF})], \qquad (3.5)$$

where the coefficients are given in and A/°C and W/°C. If the coefficients are small in absolute value – which is usually the case for I_{SC}) – or the temperature deviation from the reference is small, the temperature term of the equations can be neglected. This more simplified approximation assumes a direct proportionality with the effective irradiance, E_{EFF}. The formulas can also be solved for the reference value, for estimating the value at STC. Regarding V_{OC}, this approximation is not valid and changes in V_{OC} will not be studied further here.

3.3.5   Modelling shading

Cast shadows are only produced by direct radiation, as these rays are travelling in a straight line and will be blocked all at once if an object is placed between the Sun and the PV cell. [20] The further away the source of shading is, the more diffuse and reflected irradiance can find its way to the PV cell, as these rays are coming from arbitrary directions. This may be observed as a blurry shadow, while an object shading at a close distance will produce a more crisp shadow, as pointed out in section 2.5.1 on page 15. The same effect of diffuse irradiance can be seen during a cloudy sky; shadows will be more blurred out and weak because of the low amount of direct irradiance. A non-transparent object lying directly on the PV cell surface will give the most drastic irradiance reduction. [21]

When estimating the impact of shading, a good indicator is I_{SC}, representing the effective irradiance as mentioned above. The reduction in effective irradiance is determined by the shaded area and the level of shading, i.e. how much irradiance the shaded area receives compared to an unshaded case. According to [36], a shading ratio can be defined as $S = \frac{A_{SHADE}}{A_{CELL}}$, and the SC current of the shaded cell can be estimated by

$$I_{SC,SHADEDCELL} = J_{SC,SHADE} A_{SHADE} + J_{SC,ILLUM} A_{ILLUM}, \tag{3.6}$$

where J denotes the current density and A the area of the shaded or illuminated parts of the cell. In the case that the irradiance and thus current density of the shaded area is zero, (e.g. an object lying on the surface) the SC current of the shaded cell is equivalent to the case of the whole cell being shaded by an object that removes a portion of the irradiance equal to S, i.e. $= I_{SC,SHADEDCELL} = I_{SC,ILLUM.CELL}(1 - S)$. This assumes that the SC current for an illuminated cell is known, such that $J_{SC,ILLUM} = \frac{I_{SC,ILLUM.CELL}}{A_{CELL}}$

For estimating the reduced effective irradiance due to shading on parts of a cell, equation 3.4 (ignoring the temperature term) can be combined with equation 3.6, obtaining the following equations for the effective irradiance for the whole cell as an average and for the shaded area alone:

$$E_{\text{EFF,SHADEDCELL}} = E_{\text{SHADE}} S + E_{\text{ILLUM}}(1-S) = \frac{I_{\text{SC,SHADEDCELL}}}{I_{\text{SC,ILLUM.CELL}}} E_{\text{EFF,ILLUM.CELL}} \qquad (3.7)$$

$$E_{\text{SHADE}} = \frac{E_{\text{ILLUM}}}{S} \left[\frac{I_{\text{SC,SHADEDCELL}}}{I_{\text{SC,ILLUM.CELL}}} - (1-S) \right] \qquad (3.8)$$

If the whole cell is shaded, the shading ratio $S = 1$, which gives

$$E_{\text{SHADE}} = E_{\text{EFF,SHADEDCELL}} = \frac{I_{\text{SC,SHADEDCELL}}}{I_{\text{SC,ILLUM.CELL}}} E_{\text{EFF,ILLUM.CELL}} \qquad (3.9)$$

Finding E_{SHADE} provides information about the reduction in irradiance for the shaded parts of a module, which will depend on the distribution of direct versus diffuse and reflected irradiance. [21]

3.4 Operation Outside the first I-V Quadrant

Figure 3.5 on page 27 shows the current-voltage operating points in the first quadrant, together with the characteristics in the second and fourth quadrant. If a current larger than a PV cell's short-circuit current is forced through it, there will be a negative voltage across the cell, i.e. it goes into reverse bias. As seen from Figure 3.5, the power turns negative, meaning the cell is "consuming" power. This power is mostly dissipated as heat, and can cause a drastic temperature rise in the PV module material, which may cause irreversible damage. [36] Consumption of power in a cell will also be the case if a voltage larger than V_{OC} is applied across the terminals, which may happen during e.g. shading in a parallel connection of modules. The current I_{PV} will be flowing into the cell. This is undesirable, so it is common to install *blocking diodes* in series with the cells of a module or a string of modules. This changes the I-V curve by keeping the current at zero for voltages above V_{OC}. [37]

There are several ways a PV cell can go into an operation mode outside the first quadrant. Causes for this can be defects and damages, cast shadows from trees and buildings on whole or parts of the module, objects such as leaves lying on the module surface, soiling by dust bird droppings, and snow and ice. In addition to reducing the module output

power, the module material may be degraded and permanently damaged. In this thesis, the factors in focus will be cast shadows, objects on surface and to some extent soiling.

3.4.1   Reverse characteristics of a cell

The I-V characteristics in the second quadrant is called the reverse characteristics (PV cell is reverse biased). In this part of the I-V curve, the diode in the model is blocking, causing the current exceeding I_{SC} (I_{PH}) to flow through R_P, i.e. the high-resistance alternative current paths. This can cause a large power dissipation, and if the parallel resistance uneven across the cell area in, so-called hot spots may arise which can cause the cell to crack or the back plate of the module to melt if the temperature is high enough. [38], [36]

The expression for V_{PV} for the SDM with I_{PV} higher than the cell's SC current and cell voltage below zero is equation 3.10 [39]. When $R_S << R_P$, the slope of the curve, $-\frac{dV}{dI}$, will be dominated by R_P.

$$V_{PV} = R_P (I_{SC} - I_{PV}) - N R_S I_{PV} \tag{3.10}$$

3.4.2   Reverse breakdown

For an increasing I_{PV}, the voltage continues following equation 3.10 until the diode voltage reaches its *reverse breakdown voltage*, V_{BD}, also called *peak inverse voltage (PIV)*. In this thesis the breakdown voltage is defined as the minimum voltage that makes the diode start conducting in reverse [40]. For voltages below the breakdown voltage, the diode current is expressed by a backwards diode characteristics. This means that all the current exceeding the SC current will flow through the diode for voltages significantly lower than V_{BD}. The voltage stabilizes at a voltage approximately 0.5–0.6 V below V_{BD}, and the increase in dissipated power is only determined by the increase in current. Reverse breakdown of a PV cell is illustrated as a circuit in Figure 3.7 and as an I-V curve in Figure 3.8.
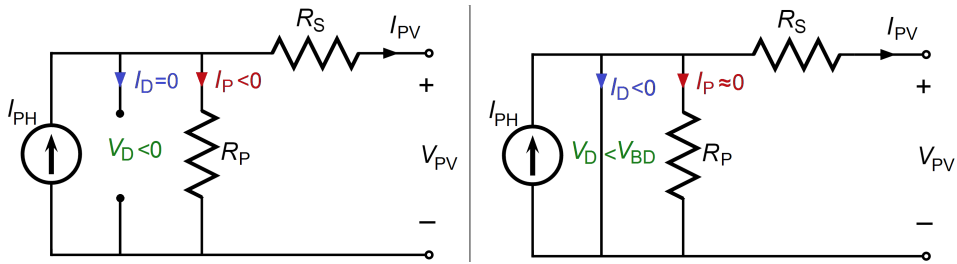
Figure 3.7: Equivalent circuits for reverse bias for voltages below zero and above V_{BD} (left) and after reverse breakdown (right). The short circuit is an approximation valid after full breakdown.
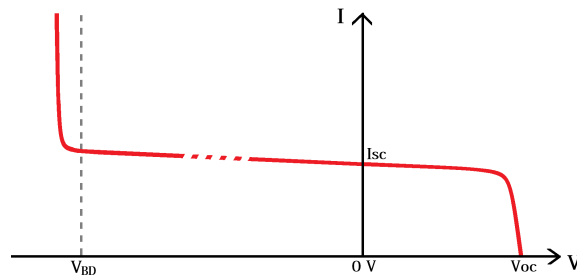
Figure 3.8: I-V curve of a PV cell in first and second quadrant, including reverse breakdown. (Based on a figure from [26])

Typical values for reverse breakdown voltages are in the range of -12 to -20 V for poly-crystalline PV cells and down to -30 V for mono-crystalline cells [41], [15]. Reverse breakdown is generally unwanted, so when designing a module a "rule of thumb" is that the reverse breakdown voltage (RBDV) of a PV cell should be greater in absolute value than the number of cells in series times V_{MPP} (or V_{OC}) of one cell (≈ 0.5 V) plus the forward voltage of any bypass diodes [42]. The more negative V_{BD} is, the more cells can safely be connected in series if reverse breakdown is to be avoided.

Without going into too much detail, there are different types of reverse breakdown for a crystalline PV cell. According to an experimental study, three types have been found for poly-crystalline silicon cells: Early breakdown, occurring at small negative voltages (-4 to -9 V) due to surface aluminum contamination; defect-induced breakdown (-9 to -13 V); and avalanche breakdown (below -13 V), a steep current increase where V_{BD} depends on the doping concentration in the material. [38] The typical RBDV values mentioned above apply to the type avalanche breakdown.

3.4.3   Bypass diodes

Most PV modules produced today are equipped with bypass diodes, installed in anti-parallel with some number of PV cells (a substring), or across the whole module. The purpose of bypass diodes is to to prevent shaded cells going into a large reverse bias, by providing an alternative path for the module current exceeding the SC current of a shaded substring. Activation of a bypass diode causes lost voltage – and thus power – from the non-shaded cells in the substring, but spares the shaded cell(s) from large negative bias and damage. Bypass diodes are also essential when connecting several modules in strings. If one module should fail or be subject to shading without a bypass path, the current through the whole series-connection will be reduced.

A bypass diode is reverse biased (blocking) in normal operation (no faults or irradiance mismatches). The diode will start conducting when the voltage across the substring becomes negative, thus forward biasing the diode. [26] The voltage across the substring will then stabilize at the forward voltage of the bypass diode. The resulting negative voltage across the shaded cell will be limited to the forward voltages of the non-shaded cells (due to the excess current flowing through the PN junction) plus the bypass diode forward voltage. This implies that the fewer cells there are in a substring, the less power will be dissipated in the shaded cells. Since the bypass diode's forward voltage contributes to the negative voltage of the shaded cells and additional power loss, it is desirable to keep this voltage as low as possible. [43] Schottky diodes are commonly used as bypass diodes because they generally have a low forward voltage of 0.15–0.45 V, compared to conventional PN junction diodes which may have a forward voltage from 0.6 up to 1.7 V, according to [44]. There are also newer solutions called "active bypass diodes (switches)" with even lower forward voltage, but these are not studied here.

To illustrate the impact of integrating bypass diodes in a PV module, consider a module with three substrings with n cells each. Substring 1 and 2 are unshaded, and one cell is shaded 50 % in substring 3, as shown in Figure 3.9. Figure 3.10 shows the I-V curves for the described module on a substring level, and Figure 3.11 shows the same curves at a module level. The lowest SC current in a substring can be read from the voltage approximately 0.5–0.6 V ($V_{\text{OC,CELL}}$) below the knee point of the current step-down, which

is marked by the grey line in Figure 3.10. Reverse breakdown is not included in the curves, as they by module design will not occur if the bypass diodes are functional.
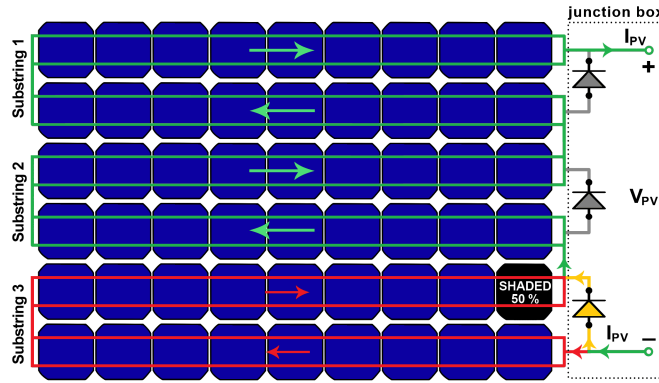
Figure 3.9: *A module with three bypass diodes in a shaded situation. Bypass diode 3 is activated. (Based on a figure from [26]*
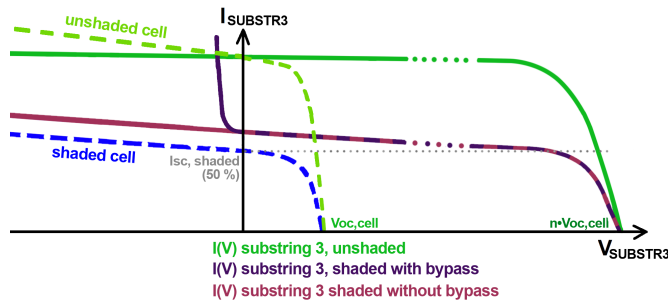

Figure 3.10: *I-V curves for a substring of n cells, one cell is shaded 50 %. The curves show the impact of having a bypass diode in anti-parallel. (Inspired by [37])*
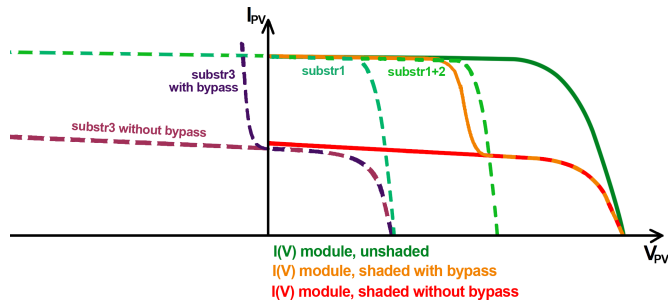

Figure 3.11: *I-V curves for one cell in substring 3 shaded 50 %. The curves show the impact of having a bypass diode on substring 3. (Inspired by [37])*

As the curves in Figure 3.10 and 3.11 show, the bypass diode of substring 3 causes the negative substring voltage to stabilize at the bypass diode forward voltage (purple curve) instead of decreasing to large negative values (pink curve). This results in a module I-V curve that follows the orange curve in stead of the red curve (which stops at 0 V because a blocking diode is assumed present) in Figure 3.11. The bypass diode salvages more of the maximum output power, reducing it to about 2/3 of the unshaded maximum power, as I_{MPP} is almost the same and V_{MPP} is 2/3. Approximately half of the maximum power is lost for the case without bypass diodes (and even less for a higher shading percentage). This has been proven in studies such as [18], [45], [46].

As mentioned, the resulting I-V curve is the sum of all individual cell voltages along the voltage axis. Shading several cells in the same series connection will result in curves like Figure 3.10 and 3.11, but with a flatter curve for the shaded substring due to increased effective parallel resistance. The slope of the shaded substring's curve will depend on the resulting R_{P}, which will change value with the shading ratio (effective irradiance) and the number of cells shaded. When there are several cells shaded at different levels, the most shaded cell will determine the current and slope at the step-down knee point in the module I-V curve, where the voltage begins dropping and the associated bypass diode activates at the current level that makes the voltage of the substring negative. The other shaded cells in the same substring will contribute to the voltage drop – and thus a steeper slope – if the substring current surpasses their SC currents. In case of shading on several substrings, the resulting I-V curve will have several current steps with knee points at the lowest SC current in each shaded substring. [45], [46]

3.4.4   Soft reverse breakdown and shading-tolerance

While reverse breakdown of PV cells are generally considered harmful to the material, it is possible to modify the semiconductor material to make the RBDV magnitude lower for avalanche breakdown. Studies have verified that it is possible to predetermine the RBDV by changing the doping profiles in the semiconductor material (for more details, [47] is recommended). With a RBDV of small magnitude, typically $|V_{\mathrm{BD}}| < 5$ V, a shaded cell will have its own "bypass" mechanism, where it allows a large current to

pass through the substring in exchange for a "small" power dissipation in the cell. The maximum dissipated power will depend on and be limited by the RBDV of the material. By exploiting this property, less power may be lost from a module or substring. In case of a module with soft breakdown cells and bypass diodes, shading of one single cell will not necessarily activate the bypass diode as it would for a conventional module. Thus, the power production from the non-shaded cells in the same substring are not lost due to the bypass. [43] Modules using PV cells with this property can be called *shading-tolerant* modules. [15]

A "controlled" reverse breakdown occurring at small RBDV is sometimes referred to as a *soft breakdown*. This name refers to the fact that the PV cell can recover from reverse breakdown without taking damage. This kind of breakdown occurs uniformly over the cell area, instead of in one or several spots for cells as may happen unintentionally due to locally reduced RBDV. This uniform breakdown is less harmful to the cell, as the reverse current is spread across a larger area reducing, the current density and evenly distributing any temperature rise. [47] The I-V curve for a shading-tolerant module with one cell shaded will look similar to the orange curve in Figure 3.11, but with the step-down covering the RBDV value plus the forward voltage of the cell. Figure 3.12 shows the difference between a shading-tolerant module (light blue curve) and a module relying on bypass diodes (orange curve) as in the previous section. It also shows the I-V characteristics of one shading-tolerant cell (dark blue curve).
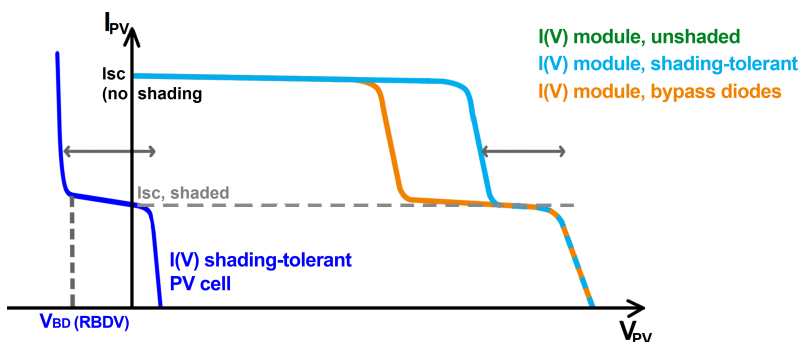

Figure 3.12: I-V curves for a module with three substrings and one cell is shaded 50 %. The curves show the difference between an unshaded module, a shading-tolerant module and a module relying on bypass diodes. (Inspired by [47])

Maxeon Gen II and Gen III solar cells

The SunPower's Maxeon IBC solar cells are good examples of state-of-the-art solar cells with shading tolerance. As mentioned, the modules at PK are made of Gen II cells with a RBDV of -5.5 V, limiting the negative voltage to about -6 V at maximum reverse current. Also available on the market are Maxeon Gen III solar cells, with an even smaller RBDV of -2.5 V and -3 V at full reverse current and higher efficiencies. Both cells have been tested and exposed to repeated reverse breakdown for hundreds of hours without lowering the performance of the cell. [15], [48] A low RBDV combined with a low maximum current is beneficial when focusing on minimizing power loss. When the maximum current of the SP E20 module is 6.46 A, the theoretical maximum dissipated power in one cell will be 38.76 W. Given the same current and Gen III cells, this maximum dissipated power would be half of this. In a study where modules with Gen II and Gen III cells were compared with a conventional front-contact module, the recorded energy losses through a day with equal shading conditions for all three modules were 8 % for the Gen III module, 14 % for the Gen II module, compared to 29 % for the front-contact module [48].

3.5   Shading in PV Systems

There can be numerous sources for shading of a PV system, from cast shadows of buildings and trees, to leaves landing on the modules, to accumulation of dust and particles. All of these will to some extent prevent sunlight (i.e. photons) from being absorbed in the PV cells, reducing the photo-generated current and thus the maximum power.

The effects of partial shading one or several cells in a single PV module have been described in the previous section, which causes series mismatches between the PV cells. A PV module with a number of m bypass diodes can be modelled as m cells in series with bypass diodes in anti-parallel. The behaviour previously described thus applies for whole strings and arrays as well as cells and modules. The total I-V curve for a series-connection of modules equals the sum along the voltage axis, while for a parallel-connection, the curves are summed along the current axis, as mentioned earlier.

3.5.1 Mismatches in a string or array

Assume again a module with three bypass diodes with the same number of cells in each substring. Figure 3.13 shows four different conditions on the same module. Figure 3.14 and 3.15 present simple illustrations resulting I-V curve when connecting these in series and parallel. The colors indicate which module contributes where, to the voltage for the series-connection, and to the current for the parallel-connection. The curves are not scaled compared to each other.
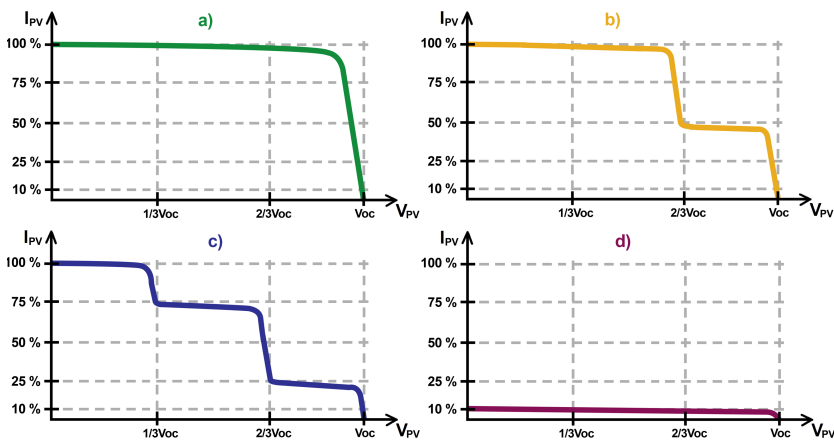
Figure 3.13: Four identical modules under different shading conditions. a) is unshaded, b) is partially shaded by 50 % on one substring, c) has partial shading on two substrings with SC current reduced to 25 and 75 %, d) has shading on all substrings, SC current reduced to 10 %.
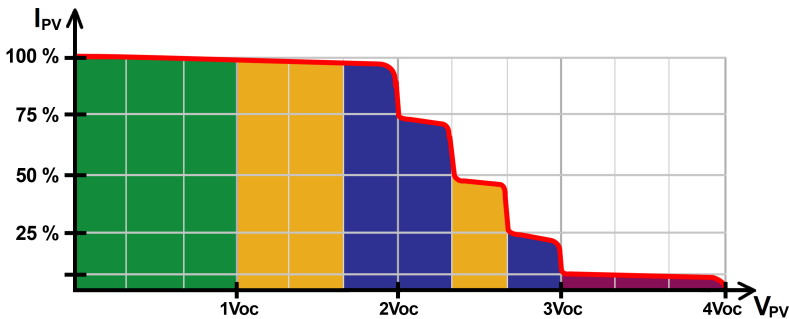
Figure 3.14: A simple illustration of the effect of mismatch in SC currents between four differently shaded PV modules in series (= string). Total I-V curve is shown in red. (Inspired by [49])
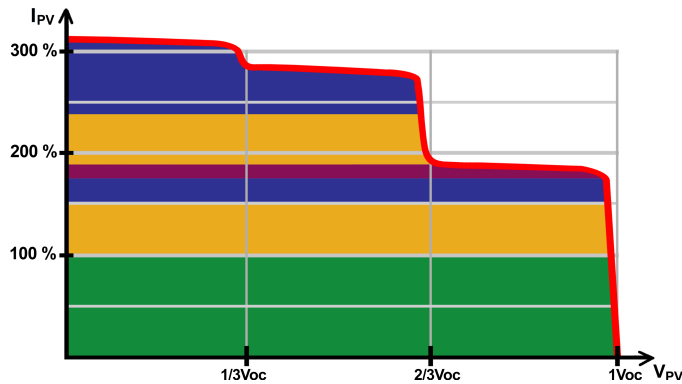
Figure 3.15: A simple illustration of the effect of mismatch in SC currents between four differently shaded PV modules in parallel. Total I-V curve is shown in red. (inspired by [49])

The same method as depicted in Figure 3.15 will apply to a parallel connection of strings (array) with mismatched SC currents. It is important to note that mismatches in arrays or strings causes the MPPT to find the MPP voltage of the *total* I-V curve, which may not give the maximum power extraction for all individual modules or strings. For the PK PV system, the inverters have multiple strings connected to a single MPPT at input A. If there is shading on one of the strings, this may reduce the interfacing voltage and operate the unshaded strings at a power level below the MPP. [49]

3.5.2   Maximum power point tracking (MPPT) issues

Another issue that may arise from mismatches – both series and parallel – is that the power electronics (converter) performing MPPT will "see" several maxima. If the MPPT strategy is so that it will look for any maximum point by e.g. the "perturb and observe" algorithm, there is a risk of operating at a local MPP, thus extracting less power from the string or array than its potential maximum power. Therefore, PV systems undergoing much partial shading through the day should have an MPPT algorithm that can distinguish the global from the local maxima. An example of such an algorithm is that the converter does frequent "current sweeps" to obtain the whole I-V characteristics and localize the global MPP. [46], [50]

Looking at the power curve for the array in Figure 3.15, this curve has three maxima where two of them are suboptimal MPPs – see Figure 3.16. In an unshaded condition, the

MPP voltage will lie between $2/3V_{OC}$ and V_{OC}. When partial shading and mismatches arise, this might cause the MPPT to look for MPPs close to the previous MPP voltage and end up finding one of the local maxima, pointed out in Figure 3.16.
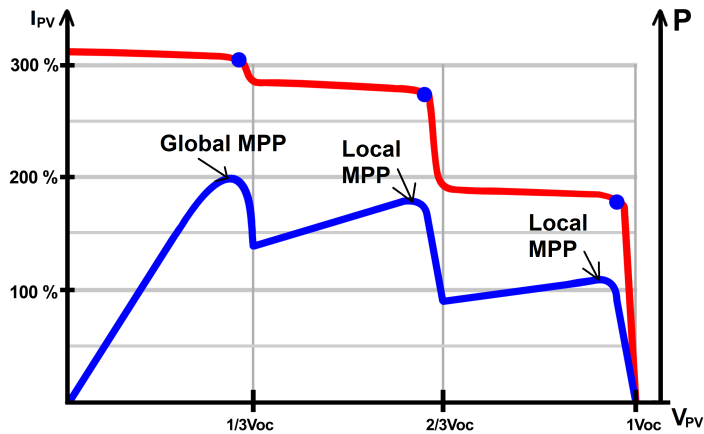
Figure 3.16: The I-V curve along with the power curve (blue) from the case of parallel-connected mismatched modules in Figure 3.15, where the maxima are marked by a blue dot. The power curve may not be correctly scaled. (inspired by [49])

The SMA inverters at PK have a MPPT function by default called *OptiTrac*, which can be extended by the function *OptiTrac Global Peak*. This function is targeting PV strings with partial shading and possible several maxima seen by the inverter. The user may specify global MPP search intervals, which is set to 6 minutes by default. While performing this search, there will some inevitable power loss. The OptiTrack Global Peak search causes a maximum power loss of 0.2 % during this search for the global MPP. Energy losses due to this MPPT function can be reduced by decreasing the frequency of sweeps, and for strings with little or no shading it may not be necessary at all. [51] It is not specified which MPPT strategy the OptiTrac Global Peak uses. A review of the different conventional and state-of-the-art MPPT strategies is neatly summarized in this paper from 2013 [52]. Upon checking the inverter settings for PK's PV system, OptiTrac Global Peak was not activated.

Chapter 4 | Experimental Study of Partial Shading

The purpose of the conducted experiments is to gain information about the effects of the different shading conditions observed at Powerhouse Kjørbo's PV system. A selection of the shading conditions were recreated at NTNU using available PV modules and various objects to produce similar shadings as the ones documented at PK. To investigate the importance and function of bypass diodes, shading experiments were also performed on a module where the bypass diodes were removed from the junction box. The purpose of the latter experiments was to validate the theoretical background and support the validity of the constructed simulation models. When analyzing the shading impacts, I-V curve is most useful. The main indicators are: 1. the drop in short-circuit current, indicating the reduction in effective irradiance; and 2. the slope of the curve near I_{SC}, where R_{P} can be estimated.

The PV modules used in the shading experiments were two modules of the type IBC SoloSol 100 CS with 100 W peak power, mounted on a mechanical PV experiment rig. For the experiments without bypass, only one module was used. The conducted experiments were performed on two clear and sunny days in Trondheim: April 11th 2016 between 10:30 and 11:30, and May 26th 2016 between 10:50 and 12:10. The theoretical background for the experiment results has been presented in the previous chapter.

Remark: *The experimental setup for this work has been similar to what was done in previous work [18]. Some text has therefore been reused in the following sections. Another remark to avoid confusion is that "IBC" is both the name of the manufacturer of the SoloSol module, and an acronym for "interdigitated back contact". The IBC SoloSol module does* not *have interdigitated back contact cells, but the SunPower modules does.*

4.1   Modules and Measuring Equipment

4.1.1   Test Module Specifications

The *IBC SoloSol 100 CS* module is made of mono-crystalline front-contact PV cells, by the Germany-based manufacturer IBC Solar. The PV module's relevant data are presented in Table 4.1, and more detailed specifications are provided in the module's data sheet, [53]. This module has 9x4 PV cells in series, i.e. 36 in total, with two bypass diodes connected to substrings of 18 cells. The data sheet does not provide this information about the bypass diodes, but the substring configuration has been confirmed in previous research [18]. This module will be referred to as the "SoloSol" module.

Table 4.1: Relevant data for the IBC 100 Wp PV module. [53]

Parameter	@STC
Peak power (P_{MAX})	100 Wp
Rated voltage (V_{MPP})	18.39 V
Rated current (I_{MPP})	5.44 A
Open circuit voltage (V_{OC})	23.11 V
Short circuit current (I_{SC})	5.82 A
Module efficiency (@STC)	14.9 %
Temperature coefficient for P_{MAX}	-0.47 W/°C
Temperature coefficient for V_{OC}	-77.88 mV/°C
Temperature coefficient for I_{SC}	1.571 mA/°C

Important differences from the PK modules

It is important to note the reverse characteristics between the two modules. The SP-E20 module uses their cells' low-voltage reverse breakdown actively, while the SoloSol module is constructed to avoid reverse breakdown of the cells. The bypass diode configuration is also different; the SoloSol have two equal substrings of 18 cells. The SP-E20 module has three bypass diodes with two substrings of 24 cells and one of 48 cells. For the SP-E20 module, the bypass diodes are not activated by shading one single cell, which is the case for the SoloSol modules. [15].

4.1.2   Measuring equipment

The device used for measuring I-V characteristics was of the type *PVPM 1000CX* from the German company PVE Photovoltaik Engineering. The PVPM 1000CX (from here on referred to as "the PVPM") is a peak power measuring device and I-V curve tracer for photovoltaic modules. This device measures and traces the I-V characteristic of the connected module given the current operating conditions, presenting the results on its display. Using an irradiance reference sensor (Phox), the device can calculate module parameters such as the series and parallel resistance, together with the I-V characteristic parameters at both STC and NOCT. For the PVPM to make successful calculations, the effective irradiance must be above 500 W/m^2 and non-varying. All these values are saved permanently in the PVPM's storage and are available for data transfer to a computer. Such equipment is typically made to test the condition of a PV module or an array/string of modules, and this device can handle up to 1000 V and 20 A. [54]. The digital viewing program *PVPMdisp* was used to export the results to a computer, where the I-V curves and calculated parameters could be viewed and exported to an Excel-compatible format for further analysis.

Accuracy of the measuring equipment

In previous studies, [18], the PV module ratings at STC calculated by the PVPM were compared to the rated values from the data sheet. The comparison showed overall small deviations, with the maximum deviation in V_{OC} at -3.2 % (referred to the data sheet). The deviation in P_{MAX} was at -1.7 %, and the deviations in I_{MPP}, V_{MPP} and I_{SC} were less than 0.7 % in absolute value. Regarding temperature coefficients, the PVPM uses $\mu_{Pmax} = -0.44\%/°C$. μ_{Isc} is not specified and is probably neglected. Calculation errors may happen due to the wrong temperature coefficients in addition to inaccurate measurement of PV module surface temperature. The PVPM user manual recommends using an external temperature sensor for more accurate calculation of parameters, but this has not been available in this work [54]. The calculated parameters and STC characteristics given by the PVPM must therefore be regarded with a pinch of salt.

4.2 Outdoor Experiment Set-up and Method

The set-up for conducting the outdoor experiments is presented in Figure 4.1. The mechanical rig that the PV modules are mounted on was constructed during previous work, consisting of a large aluminum plate and framing for holding the modules in place, wheels for mobility and an adjustable tilt angle [18].

Figure 4.1: Experimental setup for outdoor experiments. 1. Mechanical rig, 2. PVPM measuring device, 3. Irradiance/temperature sensor, 4. Connection between PV modules and PVPM through a safety switch. (Photo: Lovinda Ødegården)

The two SoloSol modules were connected in series – equivalent to one module of four substrings and 72 cells – mounted on the rig and placed where there was no shading from surrounding trees and buildings. The surface was facing the South-east with the same azimuth and tilt angle as the Southeast-directed strings at Powerhouse Kjørbo's Block 4 and 5 (-35° azimuth and 10° tilt angle). The tilt and azimuth angles were estimated using a compass and a digital protractor application for Android. The PVPM was connected to the back of the modules through a security switch, and an external irradiance and temperature sensor was fastened at the side of the rig. The experiments consisted of creating different shading conditions for the PV modules, measuring the I-V characteristics for each condition. A photo of the shading set-up was taken for each

PVPM measurement, to document which parts of the modules were shaded.

4.2.1   Weather conditions

Experiments with shading on PV modules will give the best results if conducted on days with no clouds in the sky, as diffuse sunlight does not give as defined cast shadows as direct light. Shading experiments in cloudy conditions were not conducted as the irradiance sensor does not distinguish direct and diffuse/reflected irradiance, making the results of cast shadows more difficult to quantify.

4.2.2   Test measurements

Prior to running the experiments, some test measurements were done to ensure that the PV two modules were functioning properly and similarly to each other. This was done by fixing the modules at a tilt angle of approximately 40° to receive an effective irradiance as high as possible, and connecting only one module at a time to the PVPM. One cell was shaded in a substring with a paper square and then a cardboard square, repeated for both substrings and both modules, shown in Figure 4.2. The maximum power was measured to 83.0 W for Module 1 at 902 W/m^2 (93.5 Wp @STC), and 81.7 W for Module 2 at 908 W/m^2 (91.2 Wp @STC). Both were measured at approximately 28.3 °C.

Figure 4.2: Setup for the test measurements on the SoloSol modules. (Photo: Lovinda Ødegården)

Using the estimation formula in equation 3.5 on page 29, the STC peak power was calculated as 93.6 W for Module 1 and 91.5 for Module 2, which is close to the PVPM estimation. Recall the power temperature coefficient used by the PVPM: -0.44 W//°C,

which differs from the rated coefficient of -0.47 W//°C by only 0.03 W//°C. The total estimated power for the combination of modules at STC is 185.1 Wp (184.7 W according to the PVPM), which is a significant 7.5 % lower than the rated value of 200 Wp. The reason for this may be degradation due to previous shading experiments on the modules, aging, or scratches or stains on the surface.

4.2.3 Recreated shading conditions

The first experiment session (April 11th) was dedicated to recreating shadings found at Powerhouse Kjørbo. The selected shadings for the experiments are listed below, with the material used for shading presented in Figure 4.3

- The vent outlet with a triangular cap, recreated by a plastic pipe section and a cap made of a magazine.
- The steel wire, recreated by a stiff steel wire of similar thickness.
- Blue mussel shells lying on the module, recreated by a thick cardboard cutout shaped like a shell.

Figure 4.3: The three recreations of shading at PK: The vent pipe (left), safety wire (middle) and blue mussel shell (right). (Photos: Lovinda Ødegården)

The second experiment session (May 26th) consisted of making different shadings on Module 1 alone, investigating the impact of removing the bypass diodes from the junction box. Shadings were done with and without the bypass diodes, using regular printing

paper folded into PV-cell-sized squares, and cardboard cutouts of the same size. Tape was attached to one side to make them stick to the module. As mentioned earlier, these experiments are not directly related to the PK PV system, but their purpose is to underline the importance of bypass diodes in a series-connection and to show that real-life measurements agree with the theoretical literature.

4.3 Shading Experiment Results

As presented in the theoretical background, partial shading on a substring in a module with bypass diodes results in an I-V curve with a step down in current covering a portion of the OC voltage that is approximately equal to the portion that the substring represents in the module. In a module with four equal substrings, shading one or more cells in one substring is expected to results in a current step-down covering 25 % of the OC voltage. This has been verified in studies of previous work, [18] along with other experimental studies (see e.g. [55], [56],[57])

4.3.1 Reference case, PK shading

The reference case for two series-connected modules at -35° azimuth and 10° tilt angle, effective irradiance of 627 W/m^2 and a measured temperature of 27 °C, gave the measured results in Table 4.2. Each shading measurement will be compared to this case, quantifying the reduced performance by the peak power, and shading level by short-circuit current, which as described is close to I_{PH} and and directly proportional to the effective irradiance.

Table 4.2: Measurement data for the reference case for the shading experiments.

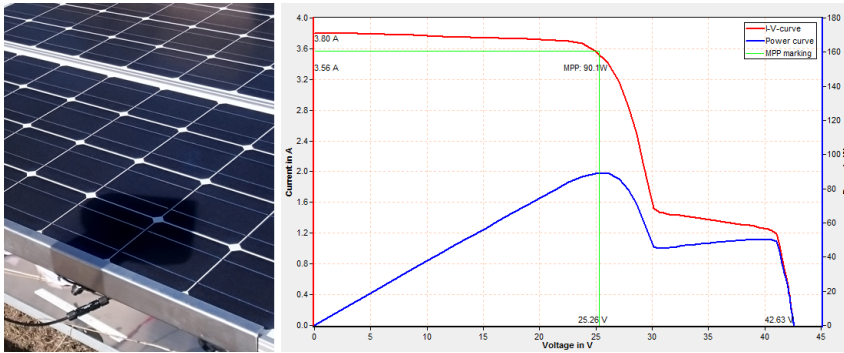| Parameter	Measured value, ref. case
P_{MAX}	117.5 W
V_{MPP}	33.1 V
I_{MPP}	3.55 A
V_{OC}	41.6 V
I_{SC}	3.73 A
R_S per module/cell	0.3870Ω/0.01075Ω
R_P per module/cell	239.13Ω/6.642Ω

4.3.2   Shading by vent pipe

Figure 4.4: Photo and I-V curve of module shaded by a "vent pipe" over one substring.
$E_{\text{EFF}} = 636 \text{ W/m}^2, T = 22.8\,°\text{C}.$
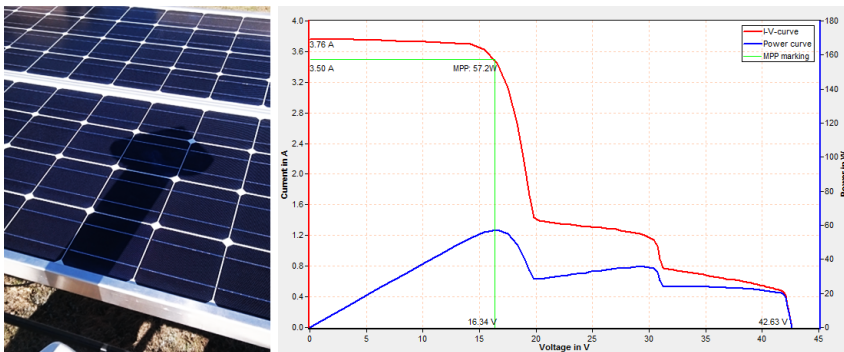
Figure 4.5: Photo and I-V curve of module shaded by a "vent pipe" over two substrings.
$E_{\text{EFF}} = 632 \text{ W/m}^2, T = 22.0\,°\text{C}.$

Figure 4.4 and 4.5 show the results of a cast shadow from the "vent pipe", affecting one and two substrings, respectively. In terms of power, P_{MAX} for the two cases were 90.1 W at 25.26 V and 57.2. W at 16.34 V, respectively. Using the reference case and equation 3.5 (page 29), the maximum power in a non-shaded is estimated as 121.19 W for the case with one shaded substring, and 118.39 W for two shaded substrings. The estimated loss of P_{MAX} is then 31.09 W and 61.19 W, corresponding to 25.7 % and 51.7 %, respectively. These results are reasonable, as the maximum power is extracted at a voltage where bypass diodes are active, losing the about 1/4th of the power for one shaded substring and half of the power for two shaded substrings.

It is important to recall that the resulting I_{SC} for a shaded substring will be characterized by the lowest maximum current in the series-connection. The voltage of a shaded cell starts to drop as soon as the substring current surpasses the lowest SC current, i.e. where the step down along the voltage axis begins at the knee point. This means that the resulting I-V characteristic is affected on how the shadow falls on the module. For the case in Figure 4.4 the cap's shadow is mostly shared between two PV cells, and the cell with the most shading is the one on the bottom left, having a shaded area of 70–75 %, corresponding to the shading ratio S. The SC current for this substring is approximately 1.47 A (where the bypass diode activates), and the lowest SC current is approximately 1.27 A (just above knee point). The reduction in SC current for the substring equals 66.7 % compared to the module SC current of 3.80 A. Using equation 3.8 (page 31) and a guess of $S = 0.73$, the estimated effective irradiance for the shaded part is 55.9 W/m^2. Since the irradiance at the shaded area is not reduced to zero due to diffuse irradiance, it is reasonable that the effective irradiance is reduced by less than the shading ratio.

In the case depicted in Figure 4.5 the shadow is covering almost the whole area of the cell in the middle of the cap part of the shadow, which is in the second substring. This reduced the SC current of that substring to 0.76 A, and the lowest SC current is approximately 0.48 A. The reduction in SC current is approximately 87.6 % for the most shaded substring and 69.5 % for the less shaded, compared to I_{SC} for the module of 3.76 A. The calculated irradiance for the shaded area, assuming a shading ratio of 95 %, gave $E_{SHADE} = 51.7$ W/m^2, which is close to the calculation in the previous case. For the lower substring in the same case the SC current is approximately 1.18 A for the most shaded cell. With a shading ratio of approximately 75 %, $E_{SHADE} = 53.8$ W/m^2, which is also close to the two previous calculations. These percentages correspond well to the percentage of SC currents, where the reductions are somewhat smaller, again probably due to diffuse irradiance.
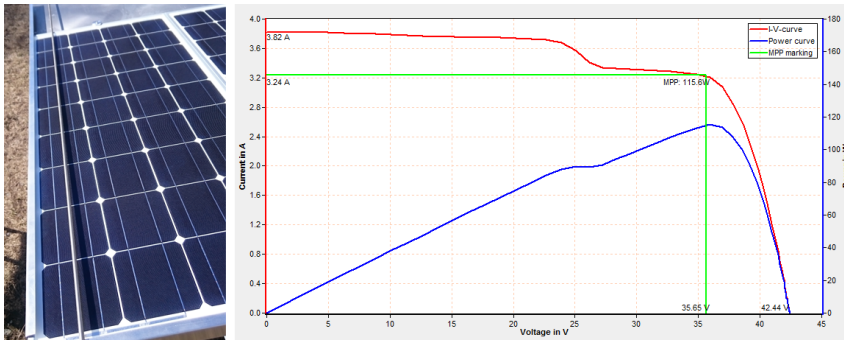
4.3.3   Shading by a steel wire

Figure 4.6: Photo and I-V curve of module shaded by a steel wire. $E_{EFF} = 639$ W/m^2. $T = 24.9\,°$C.

Figure 4.6 presents the resulting I-V curve for the setup shaded by a steel wire. P_{MAX} in this case was 115.6 W at 35.65 V. Using the reference case to estimate the maximum power in a non-shaded case gives $P_{MAX,NOSHADE} = 120.75$ W. The estimated loss in P_{MAX} is then 5.15 W, corresponding to 4.3 %. The lowest SC current of the shaded substring is approximately 3.25 A, a reduction of 14.9 % compared to the non-shaded substrings' I_{SC} of 3.82 A. During this measurement, the reduced SC current may be reduced more than the wire at PK, because the wire is located closer to the module surface, allowing less diffuse and reflected irradiance to hit the shaded area. At the given tilt angle, there is also a thin shadow present due to the edge of the mechanical rig. This will have lowered the SC current for this substring further. An additional measurement with the edge shading alone, showed a reduction of 6 %. A fair estimate of the reduced SC current due to this shading is 9 %, giving a SC current of 3.48 A.

The shading ratio is estimated to about 0.1 for the wire alone, but including the shading from the edge this is set to 0.15 when calculating E_{SHADE}. This gives an estimated irradiance at the shaded region of 3.3 W/m^2. This may be realistic as the wire is so close to the module surface, blocking most of the incoming irradiance at several angles. It is however not correct to use this value for the case at PK, as the wire is acutally placed much further away.

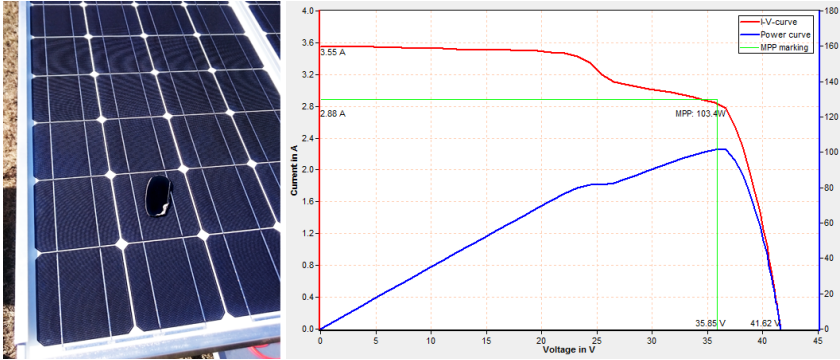### 4.3.4   Shading by a mussel shell lying on module surface

Figure 4.7: Photo and I-V curve of module shaded by a "blue mussel shell". $E_{\text{EFF}} = 596$ W/m^2. $T = 27.7°$C.

Figure 4.7 shows the result from shading the module with a cardboard "blue mussel shell". The estimated power for a non-shaded case is $P_{\text{MAX,NOSHADE}} = 111.38$ W, and with a measured P_{MAX} of 103.4 W at 35.85 V, the loss is 7.98 W, corresponding to 7.16 %. The SC current of the shaded cell was measured as 2.86 A, which is a reduction of 19.43 % compared to 3.55 A.

In this case, the shaded cell is not exposed to the shading from the edge, meaning that it does not affect the lowest SC current of that substring. The area of the cardboard shell was measured to 28.03 cm^2, giving the cell a shading ratio of 0.18. When the shading object is lying on the module surface, there will be as well as no diffuse irradiance. The reduction in SC current should therefore be more or less equal to the shading ratio, which is in this case is true if the estimations of current and shell area are correct. Using these values in equation 3.8 (page 31), the result was an irradiance in the shaded area of -47.5 W/m^2, which is likely because of some estimation errors. The expected answer was zero, as the cardboard should not let any irradiance through to the shaded area. In this experiment the size of the shell was arbitrary. In real life, these pieces of shell will come in different sizes. Their impact on the module performance will be directly connected on the size of the shell.

4.3.5 Summary of shading experiments

Table 4.3 shows the summary of the most important findings from the PK shading experiments. These reduced SC currents will be used when modelling the PK shading conditions in the simulation chapter. The reduced irradiance will be used to estimate the SC currents of the less shaded cells which could not be read directly from the I-V curves but can be estimated by calculating the effective irradiance for other cells based on their shaded area using equation 3.7 on page 31. For the shading of the blue mussel shell, the irradiance has been set to zero and for the steel wire the reduced SC current and shading ratio has been corrected for the shading of the rig's edge. Note that the steel wire was placed much closer than what is actually the case at PK. The actual impact may therefore be less than what is estimated here.

Table 4.3: Summary of the most important findings from the PK shading experiments.

Case	Total power loss	Largest cell shading ratio	Lowest I_{SC} (reduction)	Reduced E_{EFF} shaded cell
Pipe, 1 shaded sub.	25.7 %	0.73	1.27 A (66.6%)	212.6 W/m^2
Pipe, 2 shaded sub. upper substring	51.7 %	0.95	0.48 A (87.6 %)	80.68 W/m^2
Pipe, 2 shaded sub. lower substring	51.7 %	0.75	1.18 A (69.5 %)	198.3 W/m^2
Steel wire	4.3 %	0.1	3.48 A (9 %)	582.13 W/m^2
Blue mussel shell	7.16 %	0.18	2.86 A (19.4 %)	480.16 W/m^2

4.3.6 Estimating parallel resistance

Estimations of R_P are done for each of the measurements for the shaded substrings, using equation 3.3 (page 28). Note that the SC current for the whole substring is not the same as for the most shaded cell. When using equation 3.3, the step segment near the SC current of the substring is the used to estimate the slope which is almost equal to R_P. Recall from section 3.4.3 that the slope will be determined by the shaded cells and their voltage drop. The obtained R_P for the substring is divided among the shaded cells causing the voltage drop.

Table 4.4 presents the estimated values for the effective R_P in the four selected shading measurements above, calculated for the shaded section of the I-V curves, i.e. current

step-down. The R_P estimate for the unshaded case is divided among the total number of cells (72) and the average R_P per cell is divided by the number of cells in a substring (18). The parallel resistance for the shaded cell(s) is divided by the number of cells most likely to have affected the slope, written in parentheses. For the case of shading by vent pipe, the shadow is unevenly distributed among cells, but assumed to be dominated by the most shaded cells.

Table 4.4: Estimating the parallel resistance in different shading conditions.

Case	Calc. R_P	Avg. per cell	Shaded cell(s)
Reference case	119.57 Ω	6.643 Ω	-
Pipe, 1 shaded substr.	46.15 Ω	2.560 Ω	23.01 Ω (2 cells)
Pipe, 2 shaded substr. upper substring	52.50 Ω	2.917 Ω	52.50 Ω (1 cell)
Pipe, 2 shaded substr. lower substring	53.33 Ω	2.963 Ω	26.67 Ω (2 cells)
Steel wire	111.11 Ω	6.173 Ω	12.34 Ω (9 cells)
Blue mussel shell	35.55 Ω	2.058 Ω	35.55 Ω (1 cell)

The estimated parallel resistances in Table 4.4 show that the more cells that are affected by the shading (given approximately the same shading for each cell), the higher the effective R_P is. For the case of shading by a wire, 9 cells are affected. The effective resistance per cell is only reduced to 92.93 % of the reference cell R_P. For the case of shading by the mussel shell, only one cell is affected, and the resulting average cell parallel resistance is reduced to 30.98 %.

As presented in section 3.3.3 on page 27, the parallel resistance of a cell has been observed to change with temperature and irradiance. For these experiments, the temperature did not vary much; the measurements were done at temperatures between 22 and 27.7 °C. Table 4.3 presented the effective reduced irradiance for the shaded cells for which these resistance values have been calculated. According to the theoretical background the effective R_P should be highest for the cases where the irradiance is around 200 W/m^2 and close to the value near STC for irradiance levels above. The steel wire case showed the least reduction in effective irradiance and SC current, and has the effective R_P closest to the reference case, as expected.

The largest reduction in effective irradiance was measured for the shading of two substrings by the vent pipe, where one cell was almost completely shaded. The calculated R_P for this cell is by far the highest, and is almost 8 times larger than for one cell in the unshaded reference case. In the case of shading one substring with the vent pipe, it was uncertain whether to divide the parallel resistance between one or two cells, as the most shaded cell is shaded 75 % and the second-most shaded cell by approximately 50 %. The SC current of the second-most shaded cell would need to be lower than the substring SC current of 1.47 A to contribute to the slope of the curve, corresponding to a reduction of more than 61.3 %. This estimated R_P is therefore uncertain. Dividing the effective parallel resistance by two, as done in the table, gives a result corresponding to the co-relation with effective irradiance.

The most unexpected value of parallel resistance is that of the blue mussel shell case, which has been given a value of R_P that according to the other results should correspond to an irradiance somewhere between 80 and 200 W/m^2. It is unlikely that the small shading from the rig's edge contributes to the slope of the curve, so the reason for this high value may be connected to the cardboard lying on the surface or simply a measurement error.

4.4 Bypass Diode Experiment Results

To obtain some measurements without bypass diodes and to see if reverse breakdown could be reached, the junction box of one SoloSol module was opened and the bypass diodes were removed. Though these experiments are not relevant for the PV system at PK, they were useful for gaining further knowledge about PV module design and operation without bypass diodes.

4.4.1 Inside the junction box

The inside of the box is shown in Figure 4.8, indicating the location of diodes, and substring and module terminals. The bypass diodes can be pulled out and put back in without harming the junction box or the diodes.
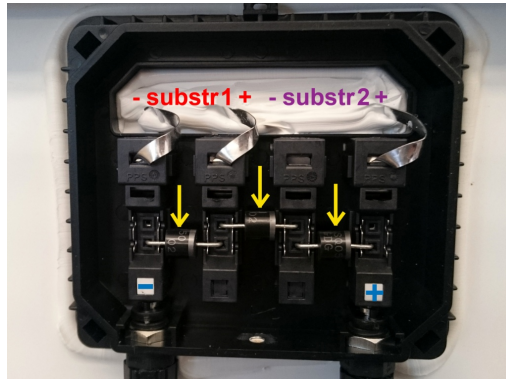
Figure 4.8: The inside of a IBC SoloSol 100 CS module's junction box. (Photo by L. Ødegården)

The junction box does not contain two diodes as expected, but three. Taking a closer look at the conductors, it appears that there are two series-connected diodes in parallel with substring 1. The reason for this is most likely that the junction box is of a standard type which can be used on modules with up to three substrings. It was probably easier and/or cheaper for the module manufacturer to install an extra diode than to use a different junction box.

When referring to substrings, "substring 1" refers to the substring connected to one bypass diode, and "substring 2" is the one connected to two diodes. From the front of the module, substring 1 is the right-hand side substring, with the module standing on its short edge, junction box on the upper end.

4.4.2   Impact of having an extra diode in series

Before removing the bypass diodes, measurements were taken on the two modules, creating the same shadings with cardboard and paper squares on each substring in turn to compare the I-V curves. The results of shading one substring compared to the other is shown in Figure 4.9 and 4.10. These figures show clearly that there is an extra voltage drop due to the extra diode of substring 2.
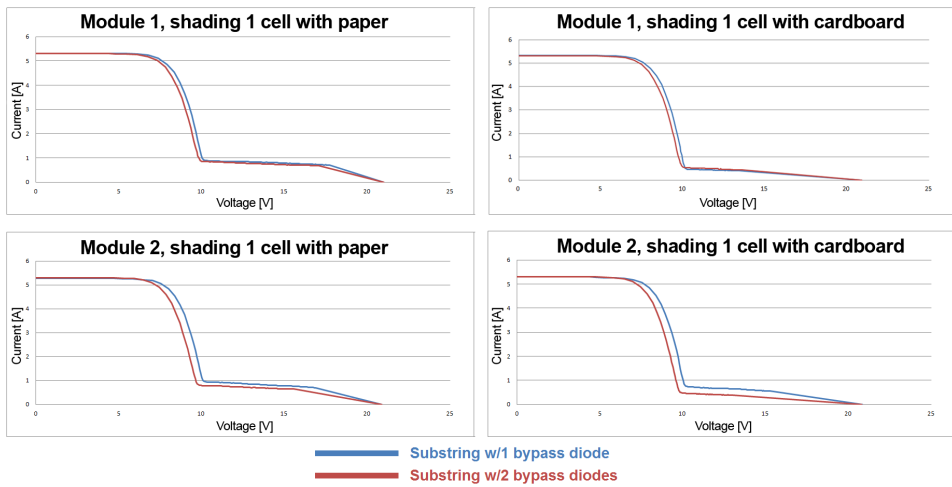
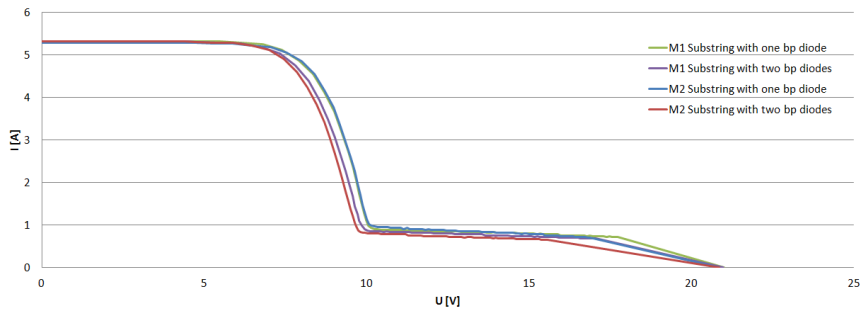*Figure 4.9: I-V curves showing the impact of having two diodes as one bypass diode for one substring.*

Figure 4.10: I-V curves for both modules when shading each substring with a paper square.

The average voltage difference between the blue and red curves were 0.35 V for Module 2 and 0.2 V for Module 1. In Figure 4.10 it can be observed that for both substrings with one diode, the I-V curves are almost identical. The difference appears when shading the substrings with two diodes in series (red and purple curves). The cause for this difference of approximately 0.15 V is uncertain. It could for example be caused by manufacturing inequalities in the diodes or in the connections inside the junction box.

4.4.3   Shading without bypass diodes

Removing the bypass diode of substring 1 and shading with a cardboard square on one cell of each substring produces the I-V curves in Figure 4.11. As expected, when shading the substring without a bypass diode, the current for the whole module is limited. The SC current when shading substring 2 is 5.63 A, while when shading substring 1 I_{SC} becomes 0.67 A. The bypass connection on substring 2 can save half the power if the substring is shaded, having P_{MAX} = 41.5 W. Without a bypass path for substring 1, 5.4 W is the maximum power available in case of shading.
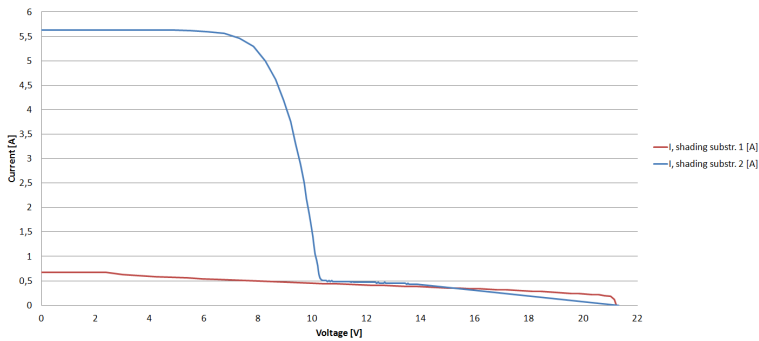

Figure 4.11: Shading substring 1 and 2 with substring 1's bypass diode removed. E_{EFF} = 962 W/m^2.

When removing one of the two diodes remaining, it was confirmed that the diodes were connected in series, functioning as one bypass path. When shading substring 2, the I-V curve of the module was more or less identical to the red curve in Figure 4.11. Figure 4.12 presents more clearly the curves with no bypass diodes, in the cases of shading 1 to 5 cells on substring 2. The curve is less steep for each extra shaded cell, as presented in Table 4.5. Shading of more cells increases the effective parallel resistance and lowers the module's SC current slightly. Some measurement error may be expected as the current values are so low.

Table 4.5: Calculated parallel resistances when shading 1–5 cells on a substring without a bypass diode.

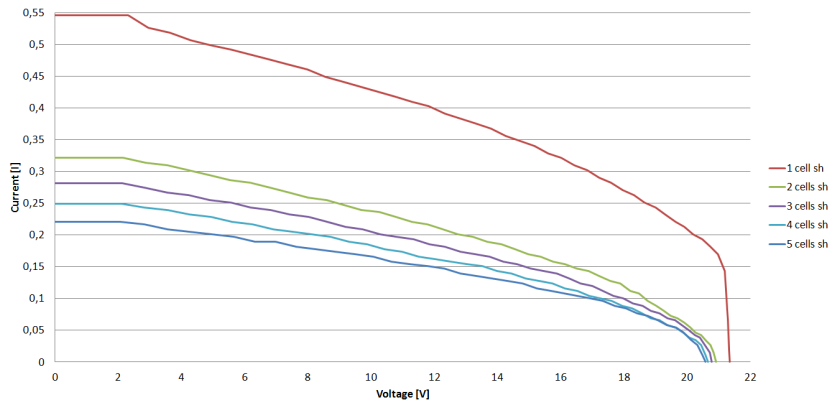| No. Cells shaded	1	2	3	4	5
Rp [Ω]	74.51	90.49	111.14	114.10	150.52
Rp, avg. per cell [Ω]	2.07	2.51	3.09	3.17	4.18

Figure 4.12: Shading substring 2 with 1–5 cells, no operating bypass diodes. $E_{\mathrm{EFF}} = 951$ W/m^2.

4.4.4 Reverse breakdown

Judging by the obtained curves in this section, reverse breakdown of a PV cell was not achieved. This would have been easiest to observe when shading one single cell, where the current should have stepped up to the values it would have had in an unshaded condition at that voltage. These results imply that the breakdown voltage of these cells must be higher than the voltage at the knee point of the curve (where the shaded cell starts to go into reverse bias), which is approximately 21 V. This is reasonable according to the typical values described in section 3.4.2 on page 32. These measurement results imply that the module is designed not to have a reverse breakdown in any of the cells in case of a failed bypass diode to avoid harmful power dissipation and heat development in the shaded cell.

Chapter 5 | Modelling and Simulation of Partial Shading

The theoretical background for understanding the shading-tolerance of the Maxeon Gen II PV cells and the SP-E20 module's use of bypass diodes in cases of partial shading has been presented in chapter 3. The results from the shading experiments were to be compared with simulations for checking if the obtained measurement data were reasonable. The circuit simulation program *LTSpice IV* together with the numerical computing program *MATLAB* (version 2016a) were used to recreate the situations from the SoloSol module experiments, and Microsoft Excel (2007) was used to further analyze the I-V and power characteristics obtained from the simulations. These tools have been chosen to demonstrate that a PV cell, module or system may be modelled using either the equivalent electrical circuit model or mathematical equations, with reasonable results.

The simulation part of this thesis has been focused on modelling partial shading and understanding the impact of using PV cells with low reverse breakdown voltage versus relying on bypass diodes. For modelling the PV cells, the single-diode model (SDM) with 5 parameters described in section 3.3 on page 25 and its mathematical equations were used. The most important aspects of the simulations were the changes in the I-V and power characteristics due to different shading conditions. The simulations would also give an understanding of the impact on the module when removing bypass and blocking diodes, and reverse bias operation. Soiling on modules has not been simulated.

LTSpice circuit models have been made for the experiment modules (IBC SoloSol 100 CS) and the modules used at Powerhouse Kjørbo (SunPower E20-327). In the constructed MATLAB script, the user may specify parameters for any type of module. Parameter values obtained from the PVPM measurements of chapter 4 have been used when simulating shading, along with values from data sheets.

5.1 Simplifications and Assumptions

The following simplifications and assumptions have been made when constructing the LTSpice and MATLAB models:

- The single-diode model is assumed representative for modelling both types of PV cell studied in this work, as the results from previous work have demonstrated the validity of this model under similar simulations [18].
- The ideality factor A is assumed constant. This may cause some deviation compared to measured voltages, but should not have a significant impact. [25]
- The short-circuit current is assumed equal to the photo-generated current and directly proportional to the irradiance, such that a reduction in irradiance can be modelled as the same reduction in I_{SC}. This is a common simplification when modelling PV cells. [27]
- The temperature is not an object of study in this chapter, and is therefore assumed constant equal to 25 ° C in all the presented MATLAB and LTSpice simulations. The models are however made such that the user may specify other temperatures.
- The diode saturation current is assumed constant and independent of temperature.
- The parallel and series resistances are considered constant parameters (to begin with).
- The temperature coefficients specified at STC are assumed valid for other irradiance levels.

5.2 LTSpice: Circuit modelling

The first simulation software used in this work is a SPICE (Simulation Program with Integrated Circuit Emphasis) type software, named LTSpice. The software is used for modelling electrical circuits on a component level and is available for free from the website of Linear Technology Corporation, a manufacturer of analog integrated circuits. [58] The resulting plots can be exported to a .txt file and opened in Excel, allowing further numerical analysis.

5.2.1 Model parameters

The models were constructed using the SDM circuit for each PV cell, and the available parameters from the PV modules' data sheets. The model was first set up for one single cell, then duplicated and series-connected, becoming a module. For the SoloSol module, values for the series and parallel resistances were taken from the PVPM measurements (see chapter 4, and for the SunPower module the parallel resistance was inspired by [15]. The diodes' ideality factors and I_0 (reverse saturation current, named "I_S" in LTSpice), along with the SunPower cell's series resistance, were found by "trial and error" until the I-V curve was sufficiently correct in terms of the rated values for V_{OC}, I_{SC}, V_{MPP} and I_{MPP}. The final parameter values for the models are presented in Table 5.1 and 5.2.

Table 5.1: Parameters used in the LTSpice model for constructing the SoloSol and SP-E20 module models. Note that the parameters are given on a cell level and STC conditions. Data from [53], [13], [15] [59].

Parameter	IBC SoloSol 100 CS	SunPower E20-327
I_{PH}	5.82 A	6.46 A
$R_{S,cell}$	0.007Ω	0.002Ω
$R_{P,cell}$	6.84Ω	6Ω
I_0 (PV diode)	1.5 nA	6.8 nA
A (PV diode, per cell)	1.142	1.278
PV diode rev. breakdown voltage	−25 V	−5.5 V
PV diode activation energy ('EG') for Si	1.11 eV	1.11 eV
PV diode junction potential	0.6 V	0.6 V

Using equation 3.1 with the parameters from Table 5.1, inserting $V_{PV} = 0$ V, $I_{PV} = I_{SC}$ and solving for I_{PH}, the photo-generated current at STC is found to be 5.8285 A for the SoloSol, and 6.4602 A for the SP-E20 module. This confirms that the approximation of $I_{PH} \approx I_{SC}$ is valid for these PV modules.

5.2.2 Diode modelling

The breakdown voltage of the bypass diodes are assumed equal to the peak inverse voltages found in the manuals [59] and [14]. The diode model parameters in Table 5.2 were adapted to silicon (PV cell) and Schottky (bypass) diode properties, and the blocking diode parameters were set to the same values as for the bypass diode [60].

Table 5.2: *Parameters used in LTSpice's diode models. Data from [14], [59], [60].*

Bypass diode parameter	IBC SoloSol 100 CS	SunPower E20-327
$I_{0,\mathrm{BP}}$	0.1 nA	0.1 nA
A_{BP}	1.05	1.05
Breakdown voltage	-50 V	-45 V
$I_{0,\mathrm{BP}}$ temperature exponent	2.0	2.0
Activation energy ('EG')	0.69 eV	0.69 eV
Junction potential	0.3 V	0.3 V

5.2.3 The final models

The finished LTSpice circuit models are shown in Appendix C.1. The voltage source connected to the module symbolizes the interfacing voltage that will depend on the load or on the MPPT control of a connected converter. LTSpice's function "DC sweep" over the connected voltage source is executed to plot the I-V and power characteristics. Table 5.3 shows the obtained characteristic parameters for the two models at STC conditions and the deviation of each parameter compared to its rated value. These small deviations imply that the models are fair representations of the real modules. However, several of the parameters have been proven to vary with temperature and irradiance – as mentioned in Chapter 3 – which may give simulation results with larger deviations compared to a real-life measurement.

Table 5.3: *The STC parameters for the two modules and the deviation of each parameter compared to their rated values. (N.B. Without blocking diode)*

Parameter, sim @STC	SoloSol	Deviation	SP-E20	Deviation
Peak power (P_{MAX})	100 W	0 %	331 W	-1.2 %
MPP voltage (V_{MPP})	18.36 V	0.16 %	54.2 V	0.91 %
MPP current (I_{MPP})	5.44 A	0 %	6.1 A	-1.34 %
Open circuit voltage (V_{OC})	23.17 V	-0.23 %	64.93 V	0.046 %
Short circuit current (I_{SC})	5.82 A	0 %	6.64 A	0 %

5.3 MATLAB: An analytical approach

Modelling a PV module in MATLAB was coded using the equations for the single-diode model presented in section 3.3 on page 25, and the parameters found by tuning the LTSpice model in Table 5.3 were used as input. A current row vector with a specified

step size is first initiated, and the voltage over the diode and the terminal of each cell with different shading conditions are calculated for each current step, creating voltage matrices. Equation 3.1 is solved for the diode voltage V_D, and the terminal voltage is calculated from equation 3.2 for one cell. For the total voltage of the module or substring, the voltages are added together column-wise for each value of the current. To solve the non-linear I-V equation, MATLAB's numeric solver function *vpasolve)* was used, which require the Symbolic Math Toolbox.

5.3.1   Pseudocode

The MATLAB script is scripted with a visual interface where the user is first asked to input the rated parameters of the module, and is then asked whether to model the module in a shaded or unshaded condition. The user then receives another interface depending on the choice of shading or not, and on whether the module has bypass diodes or not. The pop-up interfaces are shown in Figure C.3 of Appendix C.2 with the available parameters the user can choose. For simulations outside the first quadrant, the script needs to be modified, not available through the interface.

For modelling partial shading, the user specifies how many cells are shaded at each substring and at what percentage of shading. For the specified shading percentage, the script calculates the new effective irradiance and SC current for that cell by reducing them by the given percentage. The script calculates the I-V curve for a non-shaded cell and multiplies the voltage vector by the number of non-shaded cells. A row in the shaded-cell voltage matrix is added for each shaded cell, containing the I-V characteristics of that particular cell. The script checks whether the PV diode is positive (forward bias), negative (reverse bias) or has reached the reverse breakdown voltage, calculating the voltage matrix entry accordingly. The substring voltage is calculated for each step, and if it turns negative the bypass diode activates, drawing a current following the Shockley diode equation [24]. For modelling reverse breakdown, the script is very simplified. The script checks if the shaded cell's diode voltage is equal to or less than the RBDV, and if so the diode voltage is equal to the RBDV minus an additional 0.5 V.

5.3.2 Shading in a string

The script does not yet model a whole array, but a string of *M* modules could easily be simulated by multiplying the number of bypass diodes and substrings of one module by *M*. In case of modelling one or more shaded modules in a string of unshaded modules, the script can be run for an unshaded module and for each of the shaded module(s), exporting the results and adding the voltages for each current value in e.g. Excel. This method can also be used with the LTSpice model. The same cannot be done for currents in case of shading in an array, because the equations in the MATLAB script are solved for the voltages, using the known current as input.

5.4 Simulation Results: SoloSol Module

The results from this section were used to verify the simulation models, as there was actual experimental data to compare the simulations with. This gives a more solid foundation for the validity of the simulations for the SP-E20 module.

5.4.1 MATLAB vs. LTSpice modelling

The main difference between the modelling in LTSpice and MATLAB, is that the LTSpice model is more detailed, allowing the user to specify more parameters for the PV and bypass diodes. In MATLAB, each cell is modelled separately and independently of each other, while in LTSpice the whole circuit is modelled as a whole. Also, the step size for simulation in MATLAB is set to 0.05 by default due to the large use of computer memory when running. The LTSpice model is simulated with a step size of 0.01, providing five times as many data points.

The I-V and power curves of from two simulations in MATLAB and LTSpice are shown together in Figure C.4 to C.9 in Appendix C.3, for one unshaded and shaded situation for the SoloSol module, and one shaded case for the SP-E20 module. The voltages in the MATLAB script are calculated slightly higher than in LTSpice, probably due to the "more ideal" simulation of the PV and bypass diode in MATLAB, plus the fact that the blocking diode included in the LTSpice model contributed to the overall voltage drop by

0.5 V. The curves in Figure C.4 and C.5 are simulated without the blocking diode, and the voltage gap between the curves is much smaller than for the case of Figure C.8 and C.9. Lowering the ideality factor in MATLAB also seemed to close the voltage gap, as can be seen in Figure C.6 and C.7 where the ideality factor has been reduced by 0.02 (blocking diode included).

5.4.2   Importance of blocking diodes

As presented in section 3.4 on page 3.4, applying a module voltage above the OC voltage while having no blocking diodes in series with the module or string of modules, results in a negative current flow and dissipation of power in the PV cells. This is illustrated by the LTSpice simulations in Figure 5.1, showing the I-V curve for one SP-E20 module with and without a blocking diode included at the positive module terminal. The thick vertical line in Figure 5.1a indicates where the power is zero; after this the power is steeply decreasing. Increasing the voltage 5 V above V_{OC} causes almost 800 W to dissipate in the module, which is 8.3 W per cell and almost 2.5 times the peak power rating of 327 W. Increasing the voltage 10 V above V_{OC} causes a negative power of 1.9 kW according to this simulation. When including the blocking diode, there is a reduction in the OC voltage of approximately 0.5 V, which is the forward voltage of the diode.
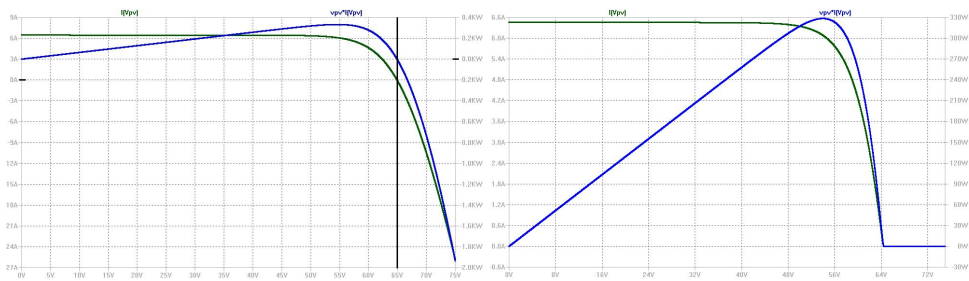
(a) I-V curve for a SP-E20 module without a blocking diode. $E_{EFF} = 800W/m^2$, no shading.

(b) I-V curve for a SP-E20 module with a blocking diode. $E_{EFF} = 800W/m^2$, no shading.

Figure 5.1

5.4.3   Impact of bypass diodes

Two diodes in series

As found in the experiments, the SoloSol module has two diodes as a bypass path on one of the substrings. Another diode is therefore added to the SoloSol LTSpice model (this was unnecessarily complicated to do in MATLAB). The result of this is presented in Figure 5.2, where the curves show clearly that the extra diode adds a voltage drop to the I-V curve (which is somewhat larger than the drop measured in the experiments). Looking back to Figure 4.9 on page 57, the simulation results can surely confirm that the PV module has one substring with two diodes in anti-parallel.
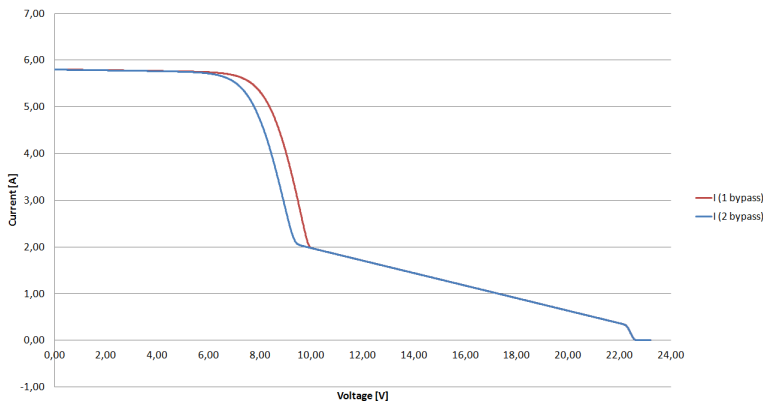

Figure 5.2: I-V curves showing the impact of adding an extra bypass diode on one substring.

No bypass diodes

Figure 5.3 shows the I-V measurement for shading one cell with a cardboard square (red), reduced SC current to 0.67 A (reduced by approximately 87 %), along with simulations from MATLAB (purple) and LTSpice (blue) for the preset value of $R_P = 6.84\ \Omega$. The curves with this value of R_P do not fit well with the measurement curve at all. The slope is much steeper than for the actual measurement, which supports the findings from the studies mentioned in section 3.3.3 on page 27 and the calculations of R_P from the PK shading experiments, i.e. that the parallel resistance should increase with decreasing irradiance. When the SC current of the shaded cell is reduced by 87 %, this should mean a drastic increase in R_P. Since the MATLAB and LTSpice are agreeing here, the value of R_P is only

changed in LTSpice. The result of changing R_P to 20, 50 and 100 Ω are shown in Figure 5.3, and it appears that the curve with R_P = 50 Ω fits the measured curve quite well, except for the slightly higher OC voltage. This voltage difference which may be because the parameters in the model are tuned to fit the rated I-V characteristic and not that of the actual module.
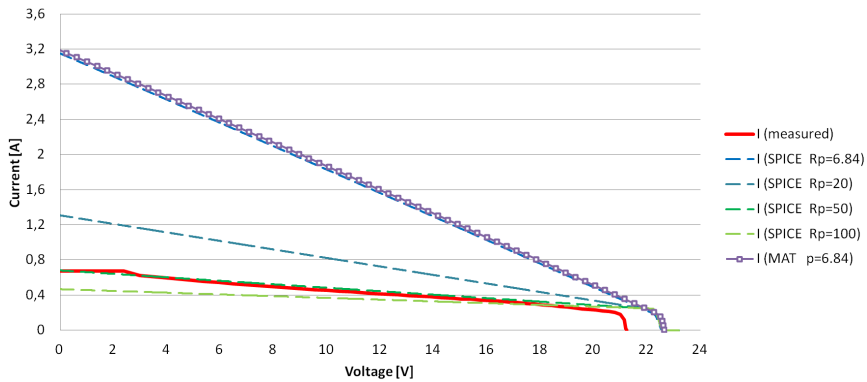

Figure 5.3: SoloSol module with no bypass diodes: Measured (red) and simulated I-V curves with R_P = 6.84, 20, 50 and 100 Ω. Measured at E_{EFF} = 963 W/m².
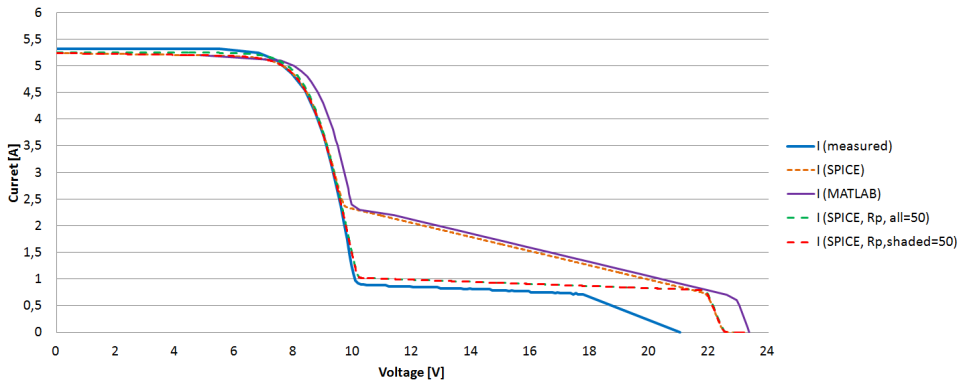
Regular bypass diode function

Figure 5.4: SoloSol module: Measured (blue) and simulated I-V curves with a) R_P = 6.84 Ω for all cells (orange), b) R_P = 50 Ω for all cells, and c) R_P = 50 Ω for just the shaded cell. Measured at E_{EFF} = 903 W/m².

One of the measurements from the shading experiments on the SoloSol module was used to compare with the simulation results to determine how realistic the computer

models are. The module had one whole cell shaded by a piece of paper (NB! in the substring with one bypass diode), reducing the current to 0.8 A, which corresponds to a reduction of 85 %. The effective irradiance was set to the same as for the measurement, 903 W/m^2. Figure 5.4 presents a comparison between the measured I-V curve (blue), the simulation in MATLAB (purple) and the simulation in LTSpice (orange). The curve from LTSpice appears to follow the measured curve well at high currents, the same for the MATLAB simulation. When the current step-down begins, the MATLAB curve starts stepping down at a higher voltage, which was noted in section 5.4.1.

The LTSpice simulation seems to be fitting very well until the voltage is above the point where the bypass diode activates. The parallel resistances are then changed in the LTSpice model to 50 Ω (green curve), which appears to be a better fit, as it did for the case in Figure 5.3. These results suggest that a more accurate model of partial shading would have to include an estimation of R_P for each shaded cell as a function of the effective irradiance of the shaded cell.

5.5 Simulation Results: SP-E20 Module

The previous section regarding the SoloSol modules have proven that both the numerical simulations in MATLAB and circuit simulations in LTSpice give reasonable results that correspond well to both the theoretical background and the measured I-V and power curves, though with a somewhat higher OC voltage. For this section, it has been chosen to only present simulations from LTSpice, as the LTSpice and MATLAB simulation results seemed to agree, and the LTSpice simulations gave a somewhat closer result to the measurements obtained during the shading experiments. The blocking diode has been excluded from these simulations.

5.5.1 Reverse breakdown vs. bypass diodes

For the SP-E20 modules, it was desired to investigate which conditions were required for the bypass diodes to activate in stead of relying on reverse breakdown of the shaded PV cell(s). A reduced SC current of 1.2 A (corresponding to a shading of 81 %) was applied

to one PV cell at a time, for the 24 cell substring and the 48 cell substring in turns. The results are shown in Figure 5.5 and 5.6, respectively.
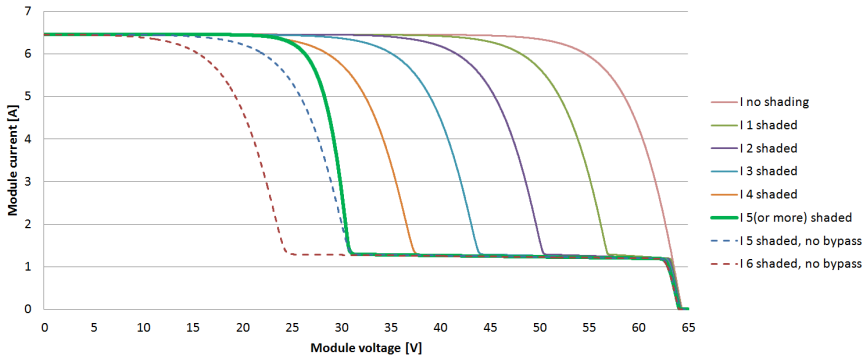

Figure 5.5: I-V curves for shading 0–6 cells 81 % on the 48-cell substring. The green curve shows where the bypass diode activates.
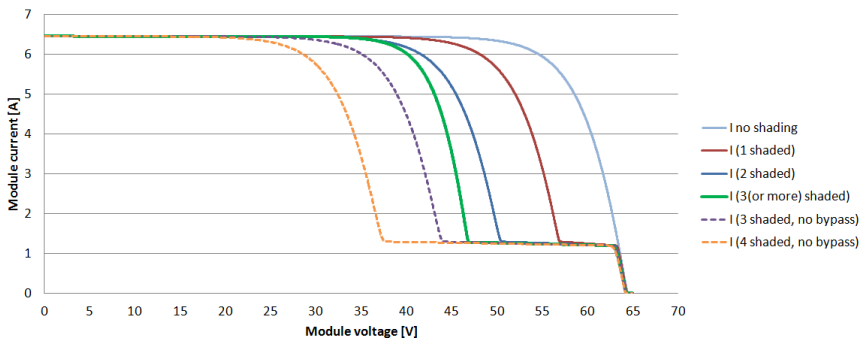

Figure 5.6: I-V curves for shading 0–4 cells by 81 % on the 24-cell substring. The green curve shows where the bypass diode activates.

When shading on the 48-cell substring, it is expected that more cells need to be shaded before the bypass diode activates, compared to shading on the 24 cell substrings. Given that one cell will have a voltage of approximately -6 V after reverse breakdown (as claimed by [48] and [15]), the voltage difference between each I-V curve should be about 6 V, as one can see is the case in both Figure 5.5 and 5.6. The bold green curve shows the activation of the bypass diode, which occurs when shading 5 or more cells in the 48-cell substring and when shading 3 or more cells in the 24-cell substring. This activation happens at 3 or 5 cells, independent on the level of shading, according to this model. The bypass diodes activate after a voltage drop of approximately 16.7 V for the 24-cell

substring and at a drop of 33 V for the 48-cell substring.

The number of shaded cells required to activate the bypass diode can also be guessed by a simple calculation. Given that all cells are operating at their MPP voltage, which is $\frac{54.7}{96} = 0.57V$, the voltages the shaded cells need to overcome before activating the bypass diode are approximately 24 × 0.57 V = 13.68 V and 48 × 0.57 V = 27.36 V. These voltages divided by 5.5 V becomes 2.48 (rounded up to 3) and 4.97 (rounded up to 5), respectively. In the case that the cells in the module had been of the Maxeon Gen III type with a RBDV of 2.5 V with a maximum reverse voltage of -3 V, the amount of shaded cells could most likely have been doubled before the bypass diode activated.
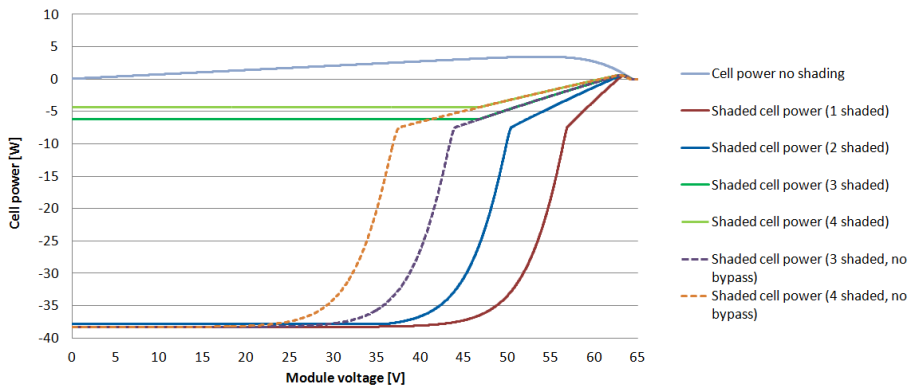

Figure 5.7: Dissipated power in one shaded cell, when shading 0–4 cells by 81 % on the 24-cell substring. The bypass diode is active for the green curves.

Figure 5.7 shows the dissipated power for each shaded cell when shading 0–4 cells on a 24-cell substring. The maximum dissipated power is about 37 W for the simulated case, close to I_{SC} × 6 V = 38.76 W. A MPPT would force the module to operate at its MPP, which would be at the knee point of the curve. This would give a loss in maximum power of approximately 35 per shaded cell until the bypass diode activates. After the bypass diode activates, the dissipated power stabilizes at a much lower level (see the green curves in the figure), which decreases for a larger number of shaded cells as they divide the power dissipation amongst them. 35 W is not a small power dissipation for a single cell, but as mentioned earlier, the cells have been tested for sustained reverse bias and does most likely degrade from this [48].

5.5.2   PK shading situations

To simulate the effect of the shadings found at PK, an estimation of the reduction in short-circuit current is made for each shading. These values can be used in the simulations, giving an indication of how the IBC type SP-E20 modules respond to the shadings in terms of I-V and power characteristics. From the experiment results in section 4.3 the estimations in Table 5.4 have been used. For shading of by the vent pipe, equation 3.7 was used to estimate the effective irradiance (and thus the reduced SC current) for each shaded cells with different shading ratios, S. Assuming the reduced irradiance in the shaded area, E_{SHADE}, is the same for cast shadows from the roof vent and roof hatch, some simulations of shading on all substrings along the module's short edge were also conducted. The parallel resistance is already quite high (63 Ω per cell, compared to 6.84 Ω for the SoloSol module), so the value of R_P has not been changed for each shaded cell.

Table 5.4: Experimental values for estimating reduced SC current in simulations of PK shading.

Case	No. of shaded cells	E_{SHADE} (% of E_{ILLUM})	Reduced SC current (% of I_{SC})
Vent pipe	4–8	9 %	$9\% \times S + 100\% \times (1 - S)$
Steel wire	12	10 %	91 %
Mussel shell	1	0 %	81 %

The Figures D.1 to D.7 in Appendix D show which cells were shaded and which SC current values that were used for them, for the most interesting simulations. All simulations were done at the same illuminated irradiance $E_{\text{EFF}} = 800$ W/m^2 and T = 25 °C, giving I_{SC} = 5.168 A. The resulting I-V and power curves are plotted together with the unshaded I-V and power curves for comparison, and are shown in the Figures 5.8 to 5.14. The simulated unshaded (reference) case has a MPP at 263 W.
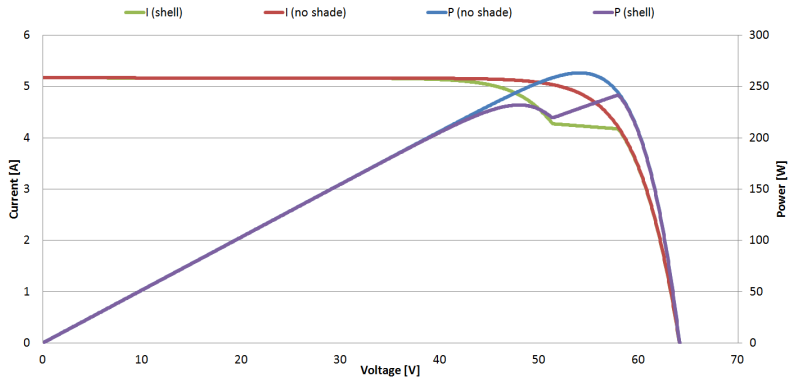
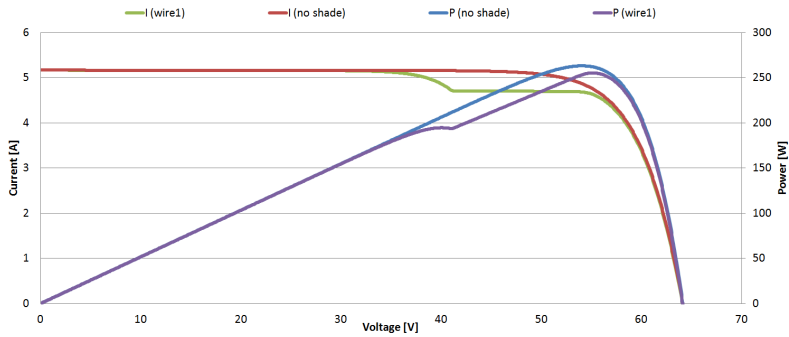*Figure 5.8: I-V and power curve for shading by blue mussel shell.*

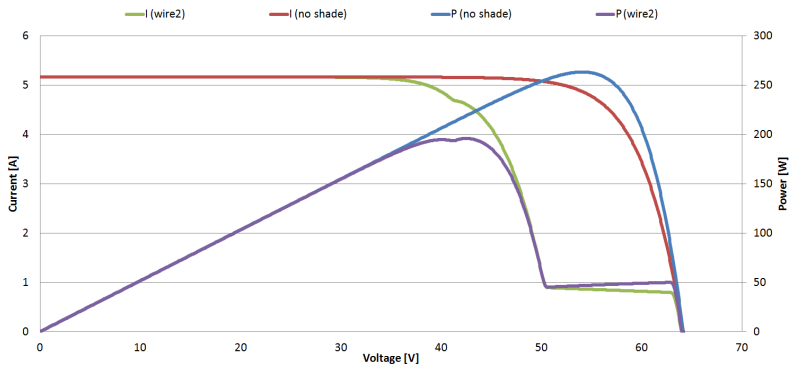*Figure 5.9: I-V and power curve for shading by steel wire, without the wire mount (1/2).*

Figure 5.10: I-V and power curve for shading by steel wire, including the mount for the wire. (2/2).
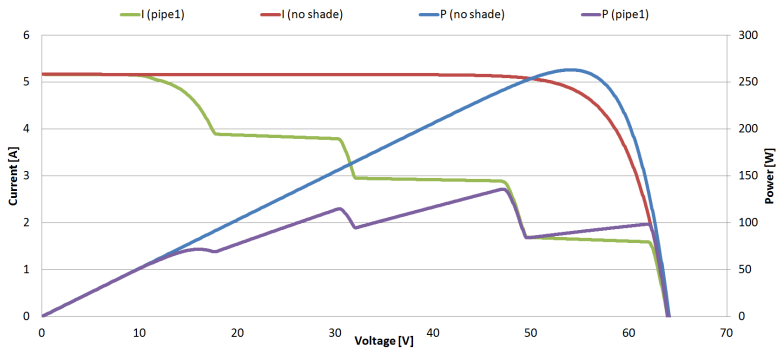
Figure 5.11: I-V and power curve for shading by vent pipe, shaded area distributed among two cells in each row (1/2).
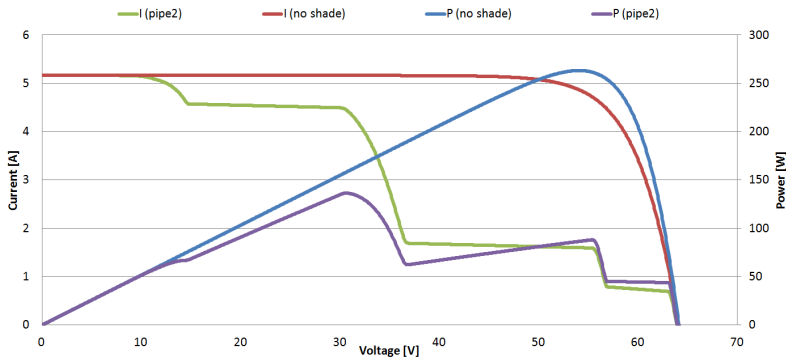

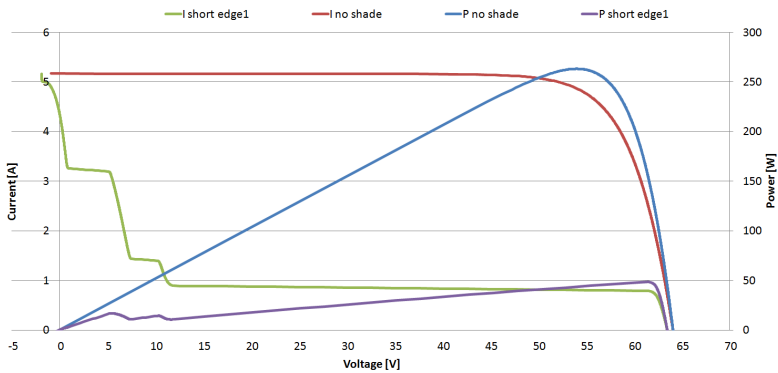Figure 5.12: I-V and power curve for shading by vent pipe, the shade being more unevenly distributed in area (2/2).

Figure 5.13: I-V and power curve for shading on the module's short edge, covering two columns.
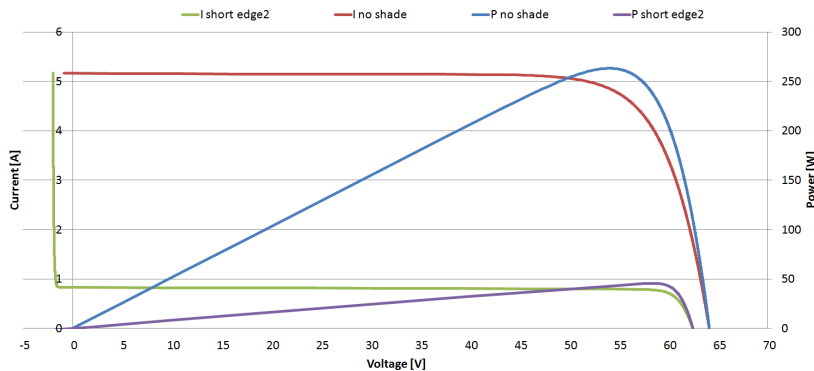
Figure 5.14: I-V and power curve for shading on the module's short edge, covering four columns.

Blue mussel shell

The result of shading part of a cell on the SP E-20 module by a mussel shell was as expected: The shaded cell goes into reverse bias when the current reaches its SC current, and breaks down after a drop of approximately 6 V, as seen in Figure 5.8. The power curve shows two MPPs, where the right-hand side maximum is the global one with P_{MAX} = 241 W. This means that the maximum power is drawn from this module at a voltage level where the current equals the SC current of the shaded cell, i.e. having the cell going into reverse breakdown would result in a greater power loss in this case.

Steel wire

The steel wire shading was first modelled by equally shading all cells on one row (i.e. half of a 24-cell substring), as seen in Figure 5.9. Afterwards the mount holding the wire was included as a more drastic shading of 85 % reduction in SC current, shown in Figure 5.10. The impact of equally shading 12 cells shows a very small drop in the maximum power due to the small reduction in SC current, where P_{MAX} is reduced from 263 W (reference case) to 255 W. For this case as well as for the previous case, the maximum power extraction requires that the shaded cells do not go into reverse bias.

For the second case of shading by wire and wire mount, the MPP reduction is quite drastic. The two cells with 85 % reduced SC current breaks down, and the rest of the shaded cells activate the bypass diode, as can be seen in the small step at 4.7 A. The

global MPP occurs at a voltage level above the activation of the bypass diode, but after the reverse breakdown of the heavily shaded cells. The P_{MAX} in this case is 195 W, corresponding to a loss of about 1/4 of the reference case's maximum power.

Vent pipe

Two cases are presented for shading by the vent pipe: one where the area of the shadow is evenly distributed between two cells in each row (Figure 5.11) and one where the shadow is covering most of one cell in the middle substring, like in the experiments (Figure 5.12). The current step-downs clearly show the reduced SC currents for the shaded cells and how many cells are shaded at this level. In the case of Figure 5.11, the bypass diode for the shaded 24-cell substring activates at approximately 32 V since four cells are shaded. This can be seen from the voltage drop around 2.9 A, which is limited to approximately 18 V, corresponding to three cells at full reverse voltage.

It is in such cases that the presence of a global MPPT system is essential. In these cases of several and unevenly shaded cells, the power curve has multiple MPPs. For these two cases where there are three different levels of shading, there are four MPPs in each curve. In a more realistic case where the shading is further unevenly distributed among the cells, there will be more MPPs. Having a MPPT system that just finds *a* maximum power point without knowing whether or not it is the global one, the system will have several "fake" MPPs at which it risks operating at. Global MPPT strategies such as the "current sweep" described in section 3.5.1, will be most useful in this kind of partial shading condition. According to [61], studies have found that MPPT systems operating at the wrong maxima can cause power losses up to 70 %. In the simulated case of Figure 5.11, operating at the lowest MPP would result in a power output of only 72 W, which is 47 % lower than the global MPP of 136 W.

Shading on the short edge of the module

Figure 5.13 and 5.14 show the results of shading a SP-E20 module on its short edge. In the latter case, all bypass diodes must activate to allow currents higher than 0.8–0.9 A to pass through the module, where the voltage across the shaded module is negative

due to the forward voltage of the bypass diodes. If the module is placed in series with unshaded modules, it is expected that the peak power drops by an amount close to the power of one module at the given irradiance of 800 W/m^2. As the curves show, the most shaded cells with SC current at 0.8 A dominates the voltage drop in both cases. The MPP is located at a high voltage and is therefore almost the same in both cases. The loss in peak power for this module is quite drastic at more than 80 % for both cases.

5.5.3 Summary of SP-E20 shading simulations

Table 5.5 summarizes the findings from the simulations of shading on a SP-E20 module. The least impact is from the case of shading by the steel wire alone, reducing the peak power by only 3 %. The mussel shell also has a relatively small impact and is not expected to give a large reduction in peak power when connected in series with unshaded modules. The largest reduction of maximum power is seen from shading by the roof vent or roof hatch, which affects all three substrings. The peak power losses are estimated at more than 80 % of the maximum power in an unshaded case. When shading by the vent pipe across two substrings, the peak power drops to almost half of the peak in the unshaded case. As seen in the table, the MPP voltage for each case differs from the reference case, which can cause parallel mismatches. This will be studied in the next section, when simulating some of these cases in a string.

Table 5.5: Summary of the results from simulating shading on PK modules.

Case	P_{MAX}	P_{MAX} loss	V_{MPP}	I_{MPP}
No shading	263.2 W	0 %	54.0 V	4.87 A
Vent pipe, even shadow	135.9 W	127.3 W (48.4 %)	47.1 V	2.89 A
Vent pipe, uneven shadow	136.4 W	126.9 W (48.2 %)	30.6 V	4.46 A
Steel wire	255.3 W	7.9 W (3.0 %)	55.1 V	4.63 A
Steel wire with mount	195.8 W	67.4 W (25.6 %)	42.5 V	4.61 A
Mussel shell	241.4 W	21.8 W (8.3 %)	57.9 V	4.17 A
Short edge, small shade	48.4 W	214.8 W (81.6 %)	61.6 V	0.785 A
Short edge, large shade	45.5 W	217.7 W (82.7 %)	58.8 V	0.775 A

5.5.4   Shading simulations on string level

To perform a simulation of partially shaded modules in a string using LTSpice, the voltage source must be exchanged for a current source. This is the same strategy as used in the MATLAB model, where the current undergoes a "DC sweep" from 0 A to I_{SC} and the voltages are added together for each current value. To recreate a "real" situation from PK, four strings from Block 5 are selected for modelling: B5_V2A3, where one module is shaded unevenly by a vent pipe; B5_V1A1, which is subject to shading on several modules from the safety wire; B5_V1B, shaded slightly on the short edge of the module by the roof hatch; and B5_V4B, shaded on a large part of the module by the roof vent. The results are presented in Figure 5.15 to 5.18, and summarized in Table 5.6. Note that the colors of the curves have been changed compared to the previous figures.
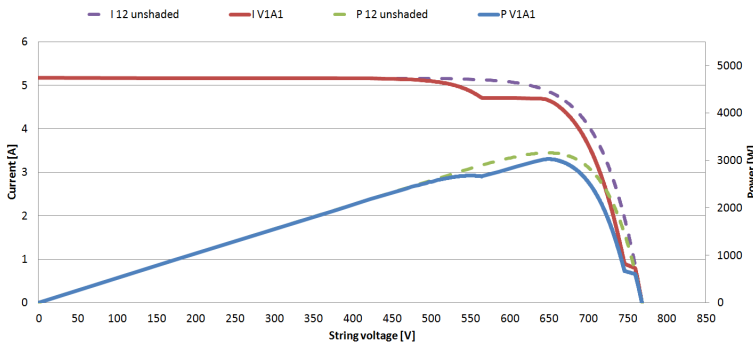

Figure 5.15: I-V and power curve for string B5_V2A3, one module shaded by pipe vent as in Figure 5.12, 11 unshaded.
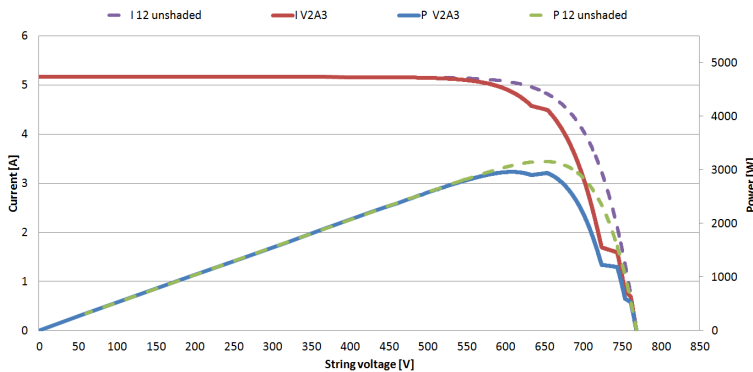

Figure 5.16: I-V and power curve for string B5_V1A1, one module shaded by wire and wire mount as in Figure 5.10, five shaded by wire as in Figure 5.9, six unshaded.
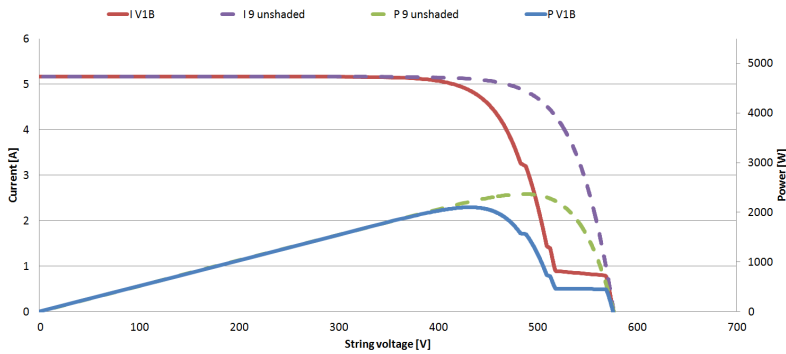
Figure 5.17: I-V and power curve for string B5_V1B, one module shaded on the short edge (by the roof hatch) as in Figure 5.13, 8 unshaded.
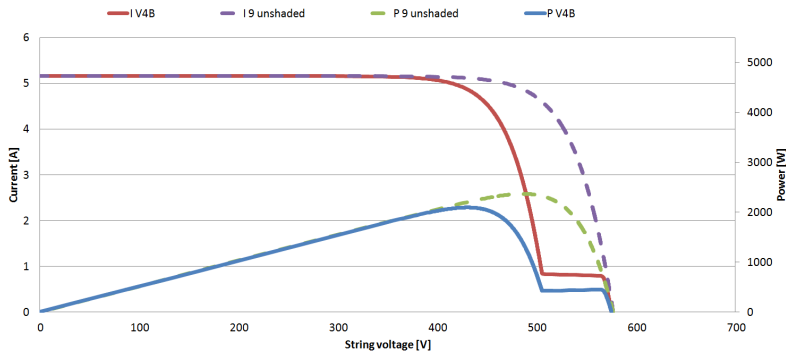

Figure 5.18: I-V and power curve for string B5_V4B, one module shaded on the short edge (by the exhaust vent) as in Figure 5.14, 8 unshaded.

Table 5.6: Summary of the results for shading on the strings V1A1, V2A3, V1B and V4B at Block 5.

String	P_{MAX}	P_{MAX} loss	V_{MPP}	I_{MPP}
12 unshaded (input A)	3158 W	0 W	648.5 V	4.87 A
B5_V1A1 (pipe)	2961 W	197 W (6.25 %)	651.4 V	4.64 A
B5_V2A3 (wire)	3026 W	132 W (4.19 %)	608.9 V	4.86 A
9 unshaded (input B)	2368 W	0 W	486.8 V	4.87 A
B5_V1B (short edge, small)	2102 W	266 W (11.23 %)	432.9 V	4.85 A
B5_V4B (short edge, large)	2096 W	272 W (11.49 %)	431.2 V	4.86 A

Mismatch losses

As Table 5.6 shows, the voltages at the MPP were different from each case. When the inverters at Block 4 and 5 have three strings at input A, there is risk of parallel mismatch losses (as described in section 3.5.1, page 39). When the strings have a different MPP

voltage, the combined parallel MPP voltage may not be equal to either of these. This means that neither of the strings will be operated at their MPP, causing lost potential power. This phenomena is described in the experimental and simulation study of the paper [62]. It was found that parallel mismatch losses can be 3 % and 9 % for a MPPT with multiple strings, depending on the level of shading in the system and on each string. The losses are smallest when the strings are equally shaded, as they will have the same MPP voltage. For instance, if the two simulated cases of B5_V2A3 and B5_V1A1 were connected in parallel, the difference of MPP voltages would be 42.5 V apart. Parallel mismatch losses will not be an issue for the strings at input B, as they have their separate MPPT.

Series mismatch losses are also present in these simulated cases. Studying the case of shading by vent pipe, the drop in P_{MAX} for the whole string was 197 W, while the loss of maximum power for the shaded module alone was 127.3 W. The series mismatches cause the extra P_{MAX} drop of 70 W. The same can be observed for the cases for shading at the module's short edge: 266 W is lost at string B5_V1B versus 214.8 W lost in the module alone; 272 W is lost at string B5_V4B versus 217.7 W in the module alone.

The largest string losses have been found to occur in the strings where the shadow affects the most substrings, i.e. in string B5_V1B and B5_V4B. The modules affected by these shadings are placed in strings with their separate MPPT, which indicates a well-planned string configuration. Even though B5_V2A3 (vent pipe) has larger losses than B5_V1A1 (wire), the wire shading is affecting more modules, which may reduce the MPP voltage and cause parallel mismatches. B5_V1A1 is connected in parallel with the strings B5_V1A2 and B5_V1A3, which according to the illustration in Figure 2.6 on page 17 in Chapter 2 have no sources of cast shadows. According to the simulation, these strings may have a MPP voltage at 648.5 V, which is about 40 V higher than the MPP voltage for string B5_V1A1.

Potential MPPT losses

In terms of MPPT, partial shading that is unevenly distributed creates more MPPs, which increases the risk of the inverter operates at a maximum that is not the global one. The

cases with the most risk of the occurrence of this, are the case of shading by wire and by vent pipe, as can be seen in the I-V an power curves. The cases where the SC current of the shaded cells is the most reduced gives the most severe consequences of operating at a MPP that is not global. Using the case of string B5_V4B as an example, operating at the local MPP to the right of the global one gives a power output of approximately 430 W, which is a lost power of 79 % referred to the global MPP of 2096 W.

5.5.5 Other notes on the simulation results

Regarding other shading sources found at PK, shading from the water tap box can be compared to shading by the vent pipe. The roof window can be compared to the shading of the roof hatch. The shading impacts from the weather station cannot be estimated from these simulations, as the distance from the modules and reduced irradiance due to the cast shadow is unknown.

It is important to keep in mind that these results are valid for a limited period of time of the year and time of the day, as the shading conditions will vary. The presented simulations may present the worst cases, i.e. when the shadow has the largest effect. These simulations have been focused on instantaneous I-V curves and maximum power. To estimate the lost energy over time, other simulation software must be used. PVSyst, in which the PV system of PK has been modelled before, is recommended to use for this estimation. The identified sources of cast shadows found in this thesis have not been directly included, which could be beneficial to understand which shading objects caused the largest energy losses, and potentially considered mitigating.

Chapter 6 | Powerhouse Kjørbo On-Site Measurements

To be able to make confident conclusions regarding the impact of partial shading at Powerhouse Kjørbo's PV system, on-site measurements were a valuable part of this thesis. These measurements would also complement the previous theoretical, experimental and simulation study. Thanks to Peter Bernhard at Asplan Viak and the technicians at Solkompaniet, the PV system – which is otherwise in full operation – was made available for performing I-V curve tracing on a string and module level.

6.1 PK Measurement Methodology

For obtaining data for evaluation, various sources were used: thermal imaging by an infrared camera, the PK PV system's online monitoring service Sunny Portal and WebBox, and the PVPM I-V curve tracer. This chapter will present the measurement setup and results regarding 1. infrared (IR) images of shading and soiling, 2. the effect of cleaning a PV module or string, and 3. the effect of partial shading.

6.1.1 Thermal imaging

An infrared (IR) camera was borrowed from NTNU's Department of Energy and Process Engineering to investigate the thermal impacts of shading and soiling, and looking for potential defects in the PV cells at PK. The IR camera used in this work was of the model FLIR E60. Thermal imaging in the IR camera is done by detecting infrared radiation (heat), converting it to an electronic signal, and then calculating and mapping the temperature on a visual image. [63] IR images is useful for checking a PV system's condition, as it can detect manufacturing defects, cracks, faulty interconnections, bypass diode failure, etc. To minimize the disturbance of reflections from the sun and clouds, it is wise to point the camera towards the PV module surface at an angle between

5–60°, where 0° is perpendicular to the module surface. Reflections can result in images showing "false hot spots", giving temperature calculation errors. The optimal IR image for PV modules would be at the back of the module, where the measurements would be done closer to the cell itself instead of through glass, but this was not feasible here. [64]

The measured temperatures indicated in the obtained images may not be 100 % accurate, due to lacking information for specifying the parameters. The relative humidity, reflected temperature and the emissivity of the PV module surface were not known, so they had to be guessed. Relative humidity was set to 50 %, reflected temperature was set to 20 $^\circ$C and the distance was mostly set to 1 m. The emissivity was set to 0.90, inspired by emissivity values for tough glass given by FLIR [64]. It is possible to measure and calculate the exact values for the mentioned parameters, but limited time and resources did not allow this. However, the measured temperature *difference* should give a fair representation of reality, and the temperature difference is more useful for this analysis.

6.1.2   I-V curve measurements

Professional supervision

First, it is necessary to emphasize that handling PV modules and strings under load can be dangerous. The strings that were measured at PK had an open-circuit voltages up to 700–800 volts and should be handled with care under supervision by professional technicians. The planned measurements at PK were coordinated with the arrival of the technicians from Solkompaniet, as they were repairing the malfunctioning inverters at the garage building and fastening the loose connectors. After discussing with the technicians how the I-V curve measurements were to be done and receiving some instructions, the technicians could confirm that the I-V tracing measurements were safe to perform.

Single module I-V curves

While the technicians were lifting up all the modules at the garage building to expose the connectors, there was an opportunity to disconnect a single module for some quick I-V curve measurements. A module soiled by dust and seagull droppings was chosen,

and the I-V curve was measured before and after wiping off most of the filth with water and paper towels. These two measurements on the single module was done on May 9th around 14:30. Further measurements on module level were not possible.

String I-V curves

The PVPM measurements on selected strings were conducted on May 10th, from 12:30 to 13:30 and 15:20 to 16:15. The procedure for measuring at a string was as follows, and the steps are visualized in Figure 6.1:

1. Make sure the PVPM safety switch is off and that the irradiance sensor is placed in the correct orientation.
2. Turn off the AC switch for the chosen inverter, thus disconnecting the whole inverter from the grid.
3. Remove the DC switch on the inverter.
4. Unscrew the cover of the inverter.
5. Disconnect the chosen string and connect to the PVPM connectors.
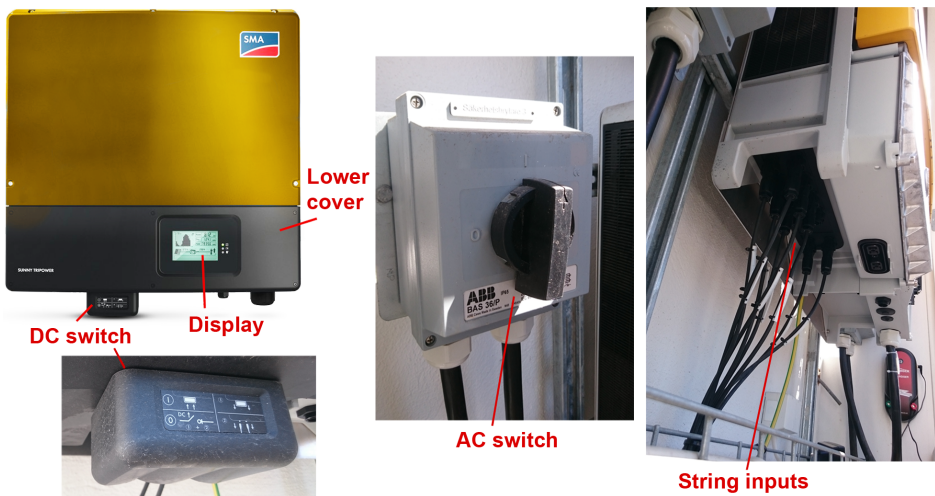6. Turn on the PVPM safety switch.

Figure 6.1: Photos showing the inverter, the AC and DC switches, and the string inputs exposed with the cover off. (Inverter image source: SMA, photos by L. Ødegården)

MC4 connector adapter

The standard plug for PV module are of the type MC4 connectors, which is also used by the PVPM. There is one male and one female plug, making them easy to "plug and play" and hard to connect wrongly. During the inspection, it was found that the SMA STP inverters use a different kind of connector than the MC4. These DC plug connectors look similar to the MC4, but have somewhat thicker pins and they may not be interconnected. Both connectors are shown in Figure 6.2, the MC4 to the left and the SMA DC plug to the right. To perform the I-V curve measurements with the PVPM, a connection adapter was necessary, having MC4 in one end and SMA's plugs in the other. This adapter was ordered from Solcellespesialisten in Fredrikstad.

Figure 6.2: MC4 connectors (to the left) vs. SMA's DC plug connectors. (MC4 image source: www.courtiestown.co.uk, photo by L. Ødegården)

PVPM measurement inaccuracy

The obtained I-V curves do not have a reference other than the theoretical I-V curve from the simulations in chapter 5. Preferably, measurements should have been done on a single, clean and flawless SP-E20 module at nominal operating conditions, to gain a better insight of the reduced performance and to verify the constructed LTSpice and MATLAB models. Also, when tracing the I-V characteristics of a whole string, the resolution of the measurements is quite low compared to measuring on a single module. This makes it more difficult to interpret the I-V curve shape as the level of detail is quite low. Therefore, only selected measurements that showed shading impacts clearly have been included.

6.1.3   SunCalc: a tool for estimating the Sun's position

SunCalc.org free online service coded by Torsten Hoffmann, and combines Google Maps with an estimation of the Sun's trajectory through the day based on the user-specified geographical location, date and time of the day. [65] This tool was used as an aid for estimating shading conditions at a specific time, for comparison with the power production data from the Sunny Portal. Estimated shading conditions at 10:00 and 11:00 are presented in Appendix **??**, and were constructed by visual inspection of SunCalc's calculations for the selected times. The SunCalc images from the time of I-V curve measurements are shown in Appendix F.1, calculated at the beginning and end of the two measuring sessions.

6.2   Results: Thermal Imaging

The IR camera measurements were taken on May 4th and May 10th in the middle of the day. The ambient temperature noted as 11–13 °C for May 4th and 15–18 °C for May 10th. The most interesting IR images captured at PK are presented in Figure 6.3 to 6.6. The highest measured temperature was 80 °C, measured where a cell was partially shaded by the roof hatch in Figure 6.3. The partially shaded cells heat up in the unshaded area as a high current is pushed through it, causing power dissipation. In the case of Figure 6.5, the shaded middle substring appears to be bypassed, and the three partially shaded cells in the outer substring are dissipating power. For the vent pipe in Figure 6.4, the partially shaded cells are not heated up, indicating that the substring is bypassed. The thermal images of the seagull droppings showed that the dropping spot itself was hotter than the cell affected by it. In general, the seagull droppings had a temperature 5–8 °C above the cell it shaded.
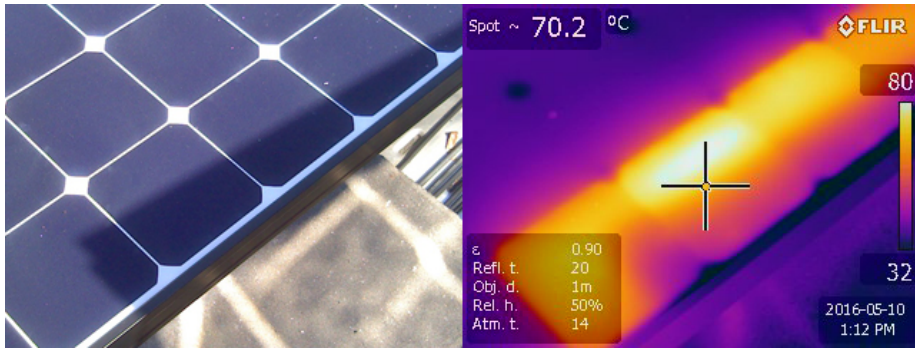
Figure 6.3: Thermal image of the cast shadow of the roof hatch. Taken May 10th, 13:12.
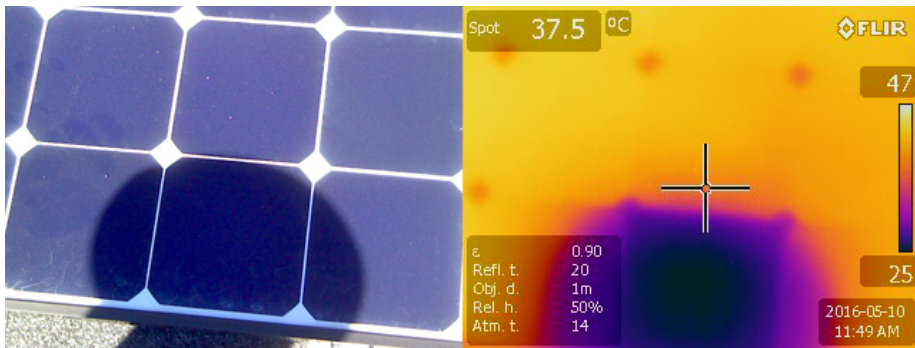

Figure 6.4: Thermal image of the cast shadow of the vent pipe. Taken May 10th, 11:49.
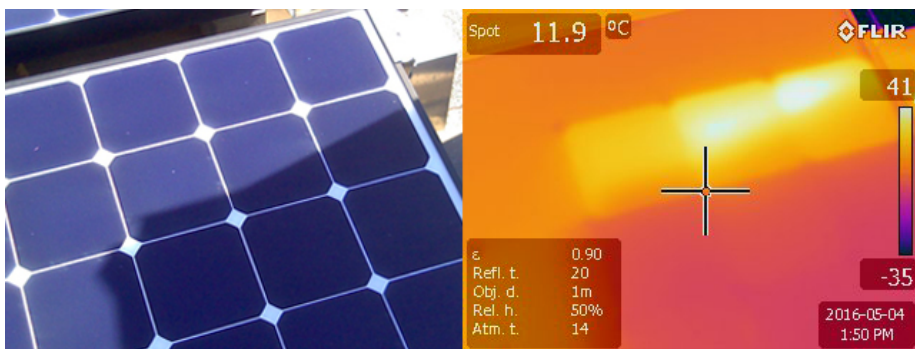

Figure 6.5: Thermal image of the cast shadow of the exhaust vent. Taken May 4th, 13:50.
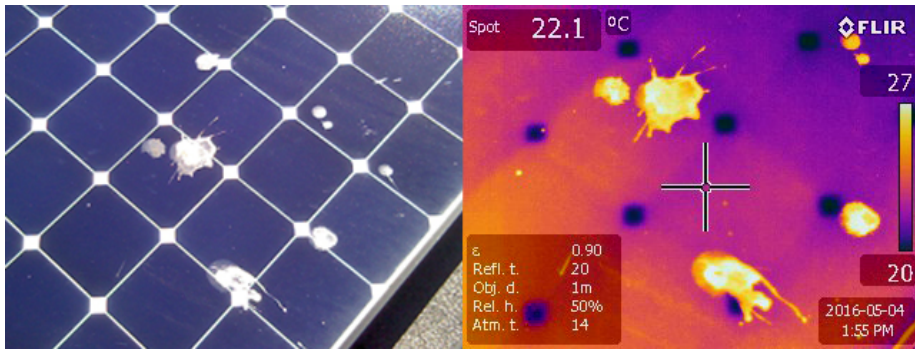
Figure 6.6: Thermal image of some seagull droppings. Taken May 4th, 13:55.

Thermal degradation studies such as [66] have found that hot spots in crystalline silicon can withstand up to a critical temperature of 150 °C before taking significant damage. If the temperature should exceed 150 °C, there is risk of melting the encapsulation material, discolouring the back sheet and for temperatures above 200 °C the PN junction may suffer irreversible damage. This particular test was done on a 60 cell poly-crystalline module. The test also shows that the temperature rise has a positive correlation with decreasing hot spot size. In the Maxeon PV cells, where the reverse breakdown occurs uniformly, any "hot spots" will not be confined to a small area unless there was some impurities or cracks. [66] According to the SP-E20 data sheet, the module can operate in the temperature range -40 to +185 °C, [13]. Comparing these critical temperatures to the IR images found at PK, neither the soiling nor the partial shading seem to be able to cause any dangerous temperature rise. This indicates that the power dissipated in shaded cells (maximum 35–37 W, as found in the simulations) is most likely not sufficient to cause thermal degradation of the cells.

6.3   Results: Cleaning of Modules

6.3.1   Cleaning one single module

The before and after photos of the PV module on which I-V measurements were performed are shown in Figure 6.7. It may not be very visible in the photos, but the uncleaned module had an even layer of dust, some dust accumulation on the bottom due to rain,

and two protruding seagull dropping stains. The module was cleaned by wet paper towels and did not become completely clean, as it was left with dirty water streaks and some leftovers from the seagull droppings. The measurements were done at 892.5 and 893.5 W/m^2 respectively, and the temperature was approximately 35 °C for both cases. The obtained I-V curves were exported to Excel to plot them on the same axes, and the result is shown in Figure 6.8 (a) and (b).

Figure 6.7: Photos showing the PV module before (left) and after (right) cleaning.
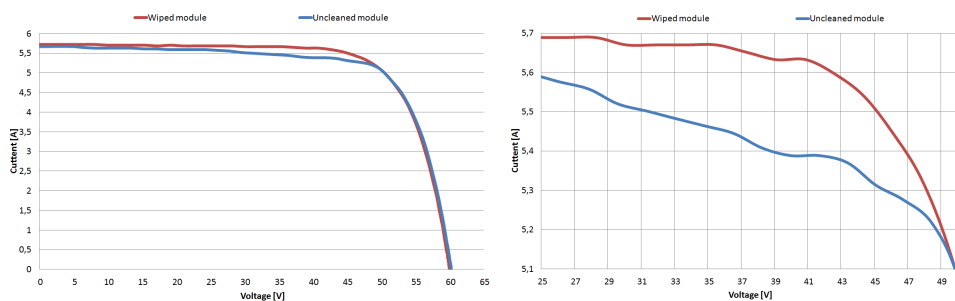
(a) Full 1st quadrant I-V curves. The black square indicates the I-V range of Figure 6.8b.

(b) Closer view of the steps of the I-V curves.

Figure 6.8: I-V curves for the module before and after wiping.

Table 6.1 shows the calculated values from the PVPM. The I-V curves and the results in the table show that cleaning the module increases the SC current by almost 0.1 A, indicating that the whole module receives more irradiance when cleaned. The largest increase is seen in the measured parallel resistance, which increases by almost 81 Ω when cleaned, indicating less leakage current. Though it is not very clear in the depicted curves, there are two steps in the current that cover approximately 6 V each, indicating

reverse breakdown of PV cells. The ones going into reverse breakdown are most likely the two cells most covered by seagull droppings. Table 6.1 also shows an increase in peak power of 1.3 W, which corresponds to only 0.5 %. The gain in maximum power by cleaning this module was not much, but given that the performance of all modules can be increased by cleaning them, the total gain may add up to be significant.

Table 6.1: Measurement results from before and after cleaning the module.

Case	P_{MAX}	$P_{MAX,STC(PVPM)}$	I_{SC}	R_S	R_P
Uncleaned	254.5 W	299.4 W	5.673 A	0.9120 Ω	645.71 Ω
Wiped	255.8 W	307.7 W	5.726 A	0.938 Ω	726.26 Ω

Using equation 3.5 from page 29, assuming $P_{MAX,STC}$ is 327 W, and using the temperature coefficients from the SP E20 module's data sheet, the theoretical power for a clean module at 35 °C and 893.5 W/m^2 is calculated to be 281 W. The measured value is 25.3 W lower, indicating that the module is still not operating at its theoretical performance. The PVPM calculated the peak power of the cleaned module at STC to be 307.7 W, which is 19.3 W lower than the theoretical value of 327 W. It can be seen in the red curve for the cleaned module that there is still some voltage drop, which may be the cause of this deviation. This is most likely due the fact that the module was not completely clean, and potentially also degradation or measurement errors.

6.3.2   Cleaning of strings

The results from cleaning whole strings have not been documented in terms of I-V curves, but they are quite visible in the logged data from the Sunny Portal. For this experiment, the modules at the garage building were most suited, considering that they do not experience shading that may obscure the results. For the garage building, the three inverters with the same azimuth angle and number of modules (P_V1, P_V2, P_V3 and P_5, P_V6, P_V7) appeared to give an approximately equal production. For this reason, it was chosen to clean all the modules connected to P_V1 and P_V5, and compare these to P_V2 and P_V6, respectively.

The cleaning was executed March 22nd, the same day that the WebBox for the garage building was installed. Production data from the garage building are only available from

March 23rd, so there is no data before the cleaning to compare with. Figure 6.9 shows the power for P_V1–V4 for March 23rd, where it can clearly be seen that P_V1's power is the highest – even larger than that of P_V4 which has one more module. Figure E.1 to E.6 in Appendix E show a comparison of P_V1 and P_V2 for March 24th to March 28th, showing that P_V1's production stays on top the following days. Note that the graphs for March 27th and 28th are shifted one hour to the right; this is because of the daylight saving time where the clock is set one hour ahead.
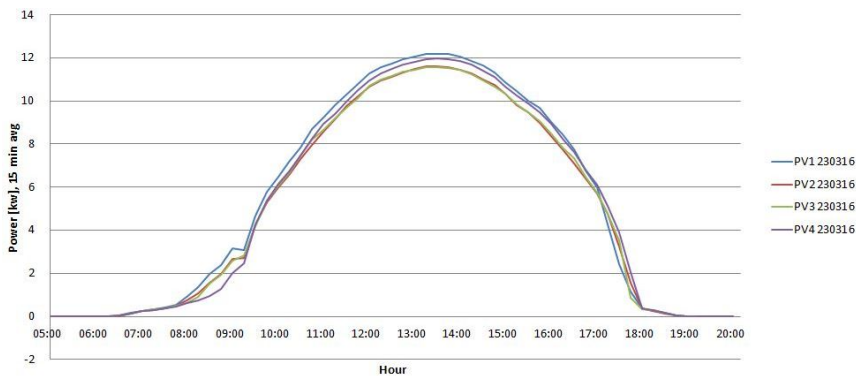

Figure 6.9: Power of inverters P_V1, P_V2, P_V3 and P_V4 for March 23rd.

The daily energy yield for P_V1 and P_V2 in kWh, together the difference between them, are presented in Table 6.2. The numbers show that the average difference in energy yield between V1 and V2 decreases after the cleaning March 23rd to March 26th, and suddenly becomes significantly smaller on March 27th. According to the weather data in Appendix B, a rainfall occurs as of March 26th, resulting in a reduced difference in production between P_V1 and P_V2. The following days, the difference in energy yield is smaller than before March 26th, but there is still a consistent positive difference. This indicates that the rain washed away most of the soiling on P_V2 and P_V3, which previously kept them from producing as much power as the clean strings of P_V1. The fact that the difference in energy yield decreases after the cleaning and before the rainfall on March 26th, could indicate that P_V1 is exposed to a new accumulation of dust and soiling.

Table 6.2: Daily energy yield between inverter P_V1 (cleaned) and P_V2 (not cleaned).

Date	Energy yield P_V1 [kWh]	Energy yield P_V2 [kWh]	Difference [kWh]	Gain by cleaning, ref P_V2
3/23/16	81.528	76.678	4.850	6.33 %
3/24/16	44.626	42.34	2.286	5.40 %
3/25/16	39.656	38.601	1.055	2.73 %
3/26/16	55.436	53.292	2.144	4.02 %
3/27/16	9.379	9.221	0.158	1.71 %
3/28/16	10.977	10.815	0.162	1.50%
3/29/16	18.729	18.481	0.248	1.34 %
3/30/16	45.764	45.406	0.358	0.79%

For the Northeast-oriented modules, the same phenomenon was observed; there was a significant difference in power production from March 23rd, which decreased little by little the following days. Unfortunately, P_V5 failed on March 26th, most likely due to the rainfall. Therefore, there are only three days of available data from P_V5 as of March 23rd. Nonetheless, the results are as clear as for the case of cleaning P_V1. Figure 6.10 shows the difference in power production on a 15 minute average between P_V5 and P_V6, and Table 6.3 shows the gained energy yield from cleaning P_V5. The gained energy yield is even larger for the NE-oriented module, where almost 11 % more energy was produced at P_V5 compared to P_V7 and 8 % compared to P_V6. Assuming these strings are otherwise equal, this implies that both P_V6 and P_V7 are affected by soiling; P_V7 even more so than P_V6.
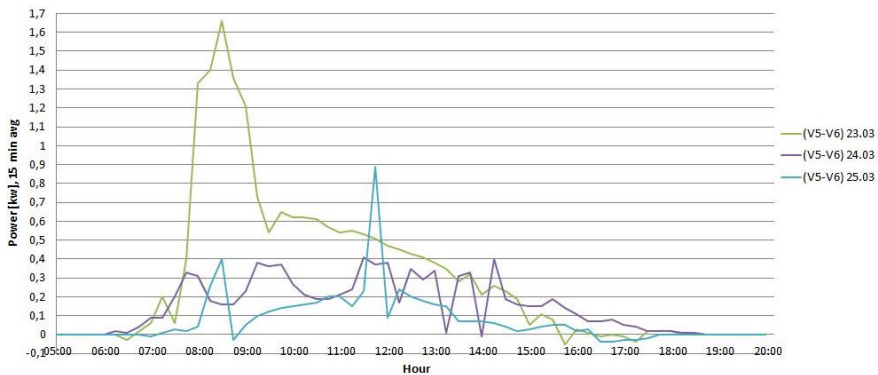

Figure 6.10: Difference in power production between P_V5 and P_V6.

Table 6.3: Daily energy yield between inverter P_V5, (cleaned), P_V6 and P_V7.

Date	Energy yield P_V5 [kWh]	Difference P_V6 [kWh]	Difference P_V7 [kWh]
3/23/16	65.144	4.837 (+8.02 %)	6.325 (+10.75 %)
3/24/16	45.239	2.439 (+5.70 %)	2.903 (+6.86 %)
3/25/16	31.716	1.011 (+3.29 %)	1.362 (+4.49 %)

6.3.3 Theoretical vs. measured power per module

To support the findings from the effect of cleaning modules, the weather data from Appendix B was used to select four dates close to and far from the last precipitation. May 2nd and May 5th were chosen as dates close to rainfall. For April 28th, the last rainfall was recorded as 0.1 mm on April 25th, while for May 12th, the last rainfall was recorded on May 4th, meaning the modules would have been exposed to soiling for eight days. For March 24th, this was two days after cleaning the modules of P_V5, and the last precipitation of 0.5 mm was recorded 10 days earlier. The maximum production for one module was calculated for each 15 minute mean irradiance and temperature (1 hour average for March 24th), using equation 3.5 on page 29 and assuming $P_{\text{MAX,STC}}$ = 327 W. The logged 15 minute mean power from the Sunny Portal was divided by the number of modules and compared to the theoretical maximum power values, and the results are presented in Table 6.4. Only the NE-oriented modules are chosen because of the malfunctioning temperature sensor for the SW orientation.

Table 6.4: Average deviation from theoretical production, calculated for average power per module for the Northeast-oriented modules.

Date	Diff P_V5 [%]	Diff P_V6 [%]	Diff P_V7 [%]	Diff P_V8 [%]
3/24/16	11.06	15.28	16.11	17.53
4/28/16	12.17	11.80	12.35	12.06
5/2/16	17.49	17.47	18.26	18.47
5/5/16	11.94	12.90	12.14	11.15
5/12/16	28.16	14.24	14.08	15.14

The absolute lowest deviation from theoretical average power per module is 11.06 % for P_V5 on March 24th, which shows clearly the effect of cleaning the modules of this inverter. The deviation is up to 6.5 percentage points lower compared to the worst case of P_V8. The numbers from May 5th and May 12th indicate a reduced performance

by 1–4 percentage points due to soiling from dust accumulation and bird droppings, though the modules have not been inspected during this period to confirm the amount of soiling. The rest of the deviation from theoretical maximum power does most likely come from remaining soiling (as the seagull droppings are not removed easily by rain), mismatch losses, conductor losses and measurement errors. The results from April 28th and May 2nd are showing the opposite; a much larger deviation is shown for May 2nd, the day after a heavy rainfall of 23.7 mm. This could mean that the rain left dirty water stains on the modules, which was then washed away between May 2nd and May 5th, but cannot be confirmed. Recall that the weather station closest to Sandvika is 6.5 km away, and therefore the weather recorded in Asker may differ from the actual weather in Sandvika.

Also, it is worth mentioning that the deviation from the theoretical power per module is quite large in all cases. According to a test of different types of PV modules was done by *Energimyndigheten* in Sweden, the SunPower E20-327 module gave a maximum power under STC of 310 Wp, which is 5 % lower than the rated value. [67]. Assuming that this is the case for these modules, the deviation percentages in Table 6.4 are reduced by 4–6 percentage points, which may be more reasonable numbers. In section 6.3.1 on page 88 it was found that the PVPM estimated a rated power at STC to be 307.7 W. This supports the findings from the test by *Energimyndiheten* regarding the SP-E20 module. Even if the cleaned module in section 6.3.1 was not completely clean, it should not have reduced the power by as much as 19 W. The maximum power output from the SP-E10 modules should therefore be investigated closer, as the theoretical yield from the PV system may be up to 5 % lower than estimated if the test in Sweden and this thesis' measurements are correct.

6.3.4   Evaluation of cleaning effects

A white paper from 2012, [68], reviews published literature on the effects of soiling on PV system performance. The studies show that soiling may have a large negative impact on the performance and that the level of soiling is strongly co-related with weather conditions and nearby surroundings (vegetation, roads, birds, etc.). A study

from California, USA, the highest monthly soiling losses was measured at up to 20 % during a dry year, with a yearly loss of up to 7 %. In a study from Málaga, Spain, the daily energy loss due to soiling has been shown to increase as a function of time without rainfall. When there was approximately four months without rainfall, the daily losses were at almost 25 %; for periods with frequent rainfall, the daily losses did not exceed 5 %. [68]

The Norwegian climate may not be comparable to that of either Spain or California. A master's thesis regarding soiling on PV modules in a Nordic climate, conducted at Kjeller – not far from Sandvika – found that the efficiency loss of PV modules dropped by 0.2–0.3 % after one week of bring exposed to soiling. The measured losses were found to be dependant on the density of the soiling, and they were consistent with an average power loss of less than 1 %, suggested by the software PVSyst for a typical Middle-European climate. [69] Considering the location and weather data of PK, the PV system will be exposed to sufficient precipitation through the year to keep the losses due to dust accumulation to a minimum compared to cases such as the one presented in the literature study mentioned above, [68].

The "advantage" with shading due to soiling by dust is that the reduction of effective irradiance is uniform across the modules, which will avoid mismatch losses. However, when soiling from bird droppings are also present, mismatches may occur if the soiling level is severe. As the measurements for the single module before and after a quick cleaning showed, the increase in maximum power was very small even though there were two quite large dropping stains on the module. Therefore it may be assumed that unless a module is heavily soiled by bird droppings, the reduction in performance will not be significant. Considering the cost of cleaning the modules manually, it may be beneficial to let the natural rainfall clean the modules.

6.4   Results: Partial Shading Impacts

Three sources of data have been used in the attempt to quantify the impacts of the different shading sources: Production from the Sunny Portal, I-V curve measurements on individual strings, and two instances of instantaneous data from the WebBox. I-V curve measurements were conducted in two sessions on May 10th: from 12:30 to 13:30, and from 15:20 to 16:15. On the same day, instantaneous string data were obtained from a two hour access to the WebBox. Since there was not found any sources of cast shadows at the garage building, this section will only present results from Block 4 and 5. Most of the results will be from Block 5, as the impacts on power production seem to be more apparent, as can be seen in the production curves in Appendix F.2.2.

As described in section 3.3.5 on page 30, the impact of cast shadows is largest when direct radiation represents most of the global irradiance. To identify the selected shadings in the power production data from the Sunny Portal, a selection of the three sunniest days have been selected due to their complete and even irradiance data. The selected dates were March 16th, April 12th, May 8th and June 5th, and the measured irradiance though the day is shown in Appendix F.2 together with the production from each inverter shown in the Figures F.8 to **??**. The overview of strings shown in Figure A.1 and A.2 in Appendix A.2 have been used together with the tool SunCalc. The position of the Sun was found at the occurrence of a dip in production, which indicated which cast shadows were most likely to have caused the power reduction for a given inverter at a given point in time. SunCalc is however used with caution, as the accuracy of its calculations are unknown.

6.4.1   Limitations of the partial shading investigations

Some important notes regarding the limitations of the findings in this chapter are:

- It is difficult to quantify the impacts of each source of shading over time when power production data are not available on a string level. In addition, the uneven level of soiling impacts on each string may affect the measurements due to series and parallel mismatch losses, obscuring the direct impact of shading alone.

- As mentioned in section 6.1.2, the detail level of the PVPM measurements on a string level is rather low due to the large voltage steps, so the shaded I-V curves

have been interpreted with caution.

- The shading impacts quantified in this section are only estimated at specific dates and times, and will not be able to reveal something about the partial shading losses over time as the impact depends highly on weather conditions. The findings here will mainly serve the purpose of determining the significance of the partial shading impacts.

- As there are no irradiance or temperature data in the same orientation as the modules of Block 4 and 5, the loss of power compared to a theoretical value cannot be calculated using the Sunny Portal data. The estimated losses have therefore been calculated by comparison to modules least affected by shading if measurements are available at the same irradiance and temperature level.

- Due to the uncertainties above, only the most evident and reliable findings will be presented. The presentation of cast shading impacts have been sorted by strings for the sake of tidiness.

6.4.2 Shading on B5_V2A3: vent pipe

According to SunCalc and on-site observation on May 10th, there should be no other cast shadows on any other modules connected to B5_V2 when shading by the vent pipe occurs on (see Appendix F.1). This can also be observed in Table F.1 in Appendix F.3, showing the instantaneous currents on a string level. The current of B5_V2A3 is 3.64 A, which is 0.28–0.34 A lower than for B5_V2A1 and B5_V2A2 at the voltage level of 587.4 V. The power drawn from the shaded string is thus 199.6 W lower than for the other strings. In the simulation results, it was found that an estimate of lost power for a string with one module shaded by the vent pipe was 6.25 % (see Table 5.6 on page 79). Assuming that string B5_V2A1 is completely unshaded, the loss of 199.6 W corresponds to 8.5 %. This percentage is fairly close, but without knowing how the shadow hit the affected module(s), they cannot be compared with certainty.

At the time of the measurement, the pipe cap shadow was divided between four cells on the two lower rows, as shown in Figure 6.11. Figure 6.12 shows the I-V curve with the vent pipe shading (red) and with the cap is removed (blue), leaving no shading on the

module. The voltages are shown from 500 V and up, as the curves were identical below this value. As the curves imply, there is a visible voltage drop due to the pipe shading. A cell breakdown can also be observed, highlighted in the figure. This drop was found to cover 5–6 V, which equals the reverse bias across a cell in reverse breakdown.
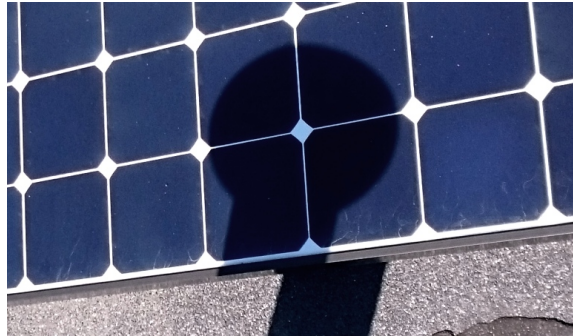

Figure 6.11: *Shading from the vent pipe during the PVPM measurement. Taken May 10th, 12:30.*
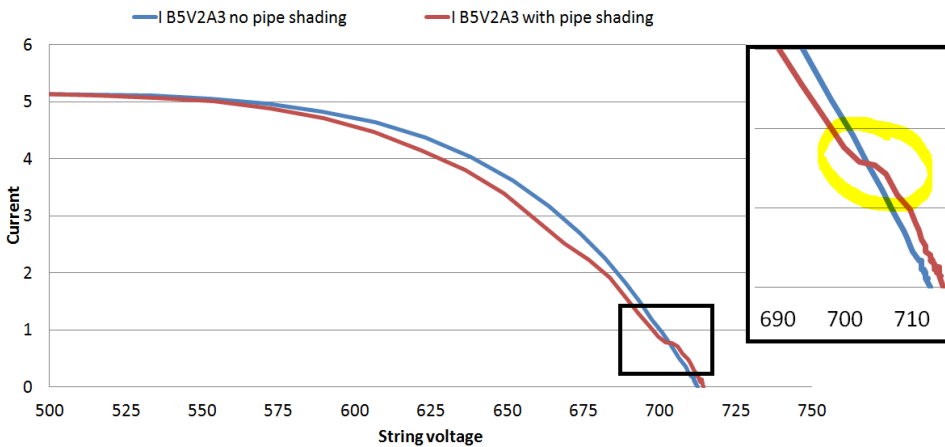

Figure 6.12: *Measured I-V curves of string B5_V2A3, shaded by the vent pipe (red) and with the pipe removed (blue). $E_{EFF} = 848$ W/m^2, $T = 44\,°C$. The reverse breakdown is highlighted.*

As the photo shows, one cell is shaded approximately 80–85 %, the rest by 50–60 %. This can be seen from the I-V curve, where the most shaded cell breaks down at around 0.8 A, which is 15 % of the SC current measured as 5.3 A. At about 2.4 A, there is an additional voltage drop, which is most likely due to the other shaded cells. This supports the earlier measurements and simulations in this thesis, relating the shaded area to the reduced SC

current. If the simulations are correct regarding the number of shaded cells needed for activating the bypass diode of a 24-cell substring, the bypass diode should be activated near half of the SC power, but the detail level of the I-V curve is too low to determine this.

The maximum power for the whole string B5_V2A3 was measured as 2795 W with the pipe shading and 2848 W without. This corresponds to a reduction of 53 W, which is a decrease by approximately 2 %. At the measured irradiance and temperature, the theoretical maximum power for one module was calculated to be 257 W. The power drop corresponds to 21 %, which may be reasonable as the shaded substring represents 1/4th of one module and the cells are not completely shaded. Assuming the two other strings at B5_V2 are unshaded, the 2 % power drop for string B5_V2A3 alone will appear as about 0.5 % for the whole inverter. The power drop due to this shading is not visible in the Sunny Portal data.
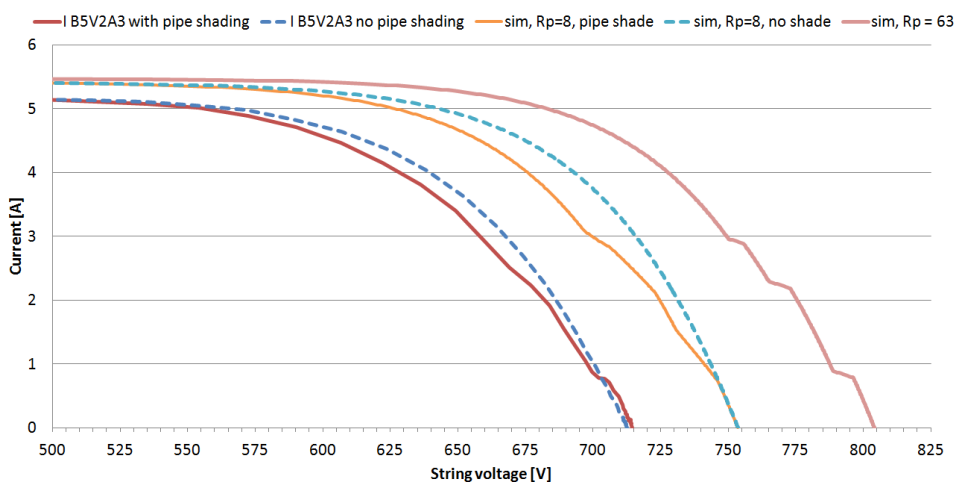

Figure 6.13: Measured and simulated I-V curves of string B5_V2A3 with and without vent pipe shading, with two values of R_P. Note that the simulated curves are deliberately shifted to the right for easier comparison.

Figure 6.13 shows a simulated recreation of the shading by the vent pipe for two values of R_P: One curve where $R_P = 63\ \Omega$, which was the values used in previous simulations, and one curve where $R_P = 8\ \Omega$, as was the average parallel resistance measured by the PVPM for the string. As can be seen in the figure, the curve with $R_P = 63\ \Omega$ appears to be a better fit at low currents, while the curve where $R_P = 8\ \Omega$ gives a better representation

for currents higher than where the first cell breakdown occurs. These measurements also support the theory that R_P changes value with reduced effective irradiance, and that a model of a PV module or system needs to implement the irradiance dependence for the model to give realistic results.

6.4.3   Shading on B5_V4: exhaust vent

The exhaust vents, roof window at Block 4 and roof hatch on Block 5 produce cast shadows affecting the short side of the modules, having the largest impact on a module as was demonstrated in the simulation chapter. The exhaust vents at both Block 4 and 5 may cause a large shading on the nearby modules at certain times of the day. The photo in Figure 6.14 shows that the exhaust vent casts a shadow on approximately 1/3 of the nearest module at B5_V4B, covering all substrings.

Figure 6.14: Cast shadow from the exhaust vent at Block 5, affecting string B5_V4B. Taken May 10th, 15:34 .

This is similar to the case simulated in the previous chapter (see Figure 5.18 on page 79) Figure 6.15 shows the measured I-V and power curve of string B_V4B at $E_\mathrm{EFF} = 735\,\mathrm{W/m^2}$, together with the simulation from Figure 5.18. The the reason for the measured curve being lower than the simulated is the lower irradiance, higher temperature, and potentially also soiling losses that are not accounted for in the simulations. Otherwise, the simulated curve seems to match the measured curve very well, capturing the same step down in current at approximately the same reduced SC current.

The voltage drop at the current step-down is measured as 59 V for the measured case and 62 V for the simulated case. Looking back to section 5.5.1 on page 69, the bypass diodes of the substrings activate after a voltage drop of 16.7 and 33 V for the 24-cell and 48-cell substring. This implies that all bypass diodes should be activated at around 66.4 V, which is close to the measured and simulated voltage drops. In theory, this voltage drop would be almost equal to the OC voltage of the module (64.9 V) plus the forward voltages of the three bypass diodes. If all bypass diodes are activated after a voltage drop of 66.4 V, subtracting the OC voltage gives exactly 0.5 V per diode.
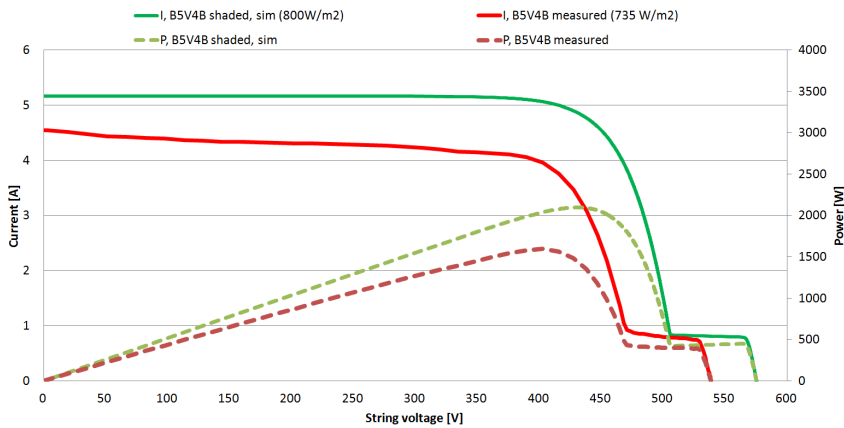

Figure 6.15: Measured and simulated I-V curves of string B_V4B, shaded by the exhaust vent.
$E_{\text{EFF}} = 735 \, \text{W/m}^2$, $T = 47.5\,^\circ\text{C}$.

Regarding power loss, the theoretical maximum power for one module at the given irradiance and temperature is calculates as 219 W per module. Multiplying this by 9, the theoretical maximum power for the string B5_V4 is 1971 W compared to the measured power of 1594 W. This corresponds to a loss of 19 %, which is higher than the 11.5 % loss estimated for the simulations in section 5.5.4 on page 78. Looking at the table in Appendix F.4, it is observed that there is an average error of estimated P_{MAX} at STC of about 6 %. Accounting for this, the new estimate for maximum power is 211 W per module, and the loss due to shading by the exhaust vent is calculated to be 16 %. Assuming that the only shaded module is the one shaded by the exhaust vent, the maximum power loss should be about 1/9th, corresponding to 11.1 %, which corresponds to the simulation estimates. The corrected measured loss of 16 % is still significantly above the simulated value, but

most likely there are some extra losses come from mismatches and soiling.

6.4.4 Shading on B5_V1 and V3: roof hatch

Figure 6.16 shows the cast shadow from when the hatch is opened to ventilate. The shade covers some of the cells on the short edge of the nearby modules the strings B5_V1B and string B5_V3B. At the time the I-V curve measurements were taken, the irradiance was approximately the same for the NW and SE modules: 669 and 665 W/m^2, respectively. As can be seen from the photo in Figure 6.16, the hatch's shadow affects four cells at string B5_V3B and 15 cells on B5_V1B. Both strings, two of the substrings are affected. Judging by the number of shaded cells, both bypass diodes may be activated at B5_V1B, while only the lower substring for B5_V3B may have a negative voltage. It should be noted that the cast shadow is not the same as for the other cases, as the hatch has a transparent top causing shading. It has not been studied how this affects the reduced irradiance in the shaded area, which could be an interesting topic for another study.

Figure 6.16: Cast shadow from the open roof hatch, affecting string B5_V1B and string B5_V3B. Taken May 10th, 10:24.

The I-V curves for shading by the open roof hatch are presented together in Figure 6.17. The blue dashed curve is a calculated I-V curve for 9 unshaded modules based on the I-V curve of the unshaded string B5_V1A1, measured at nearly the same irradiance. As noted above and as can be observed in the curves, string B5_V1B experiences a larger drop

in voltage due to shading of a larger number of cells. In these curves it is also unclear if and where the bypass diode is activated due to the poor detail level on the PVPM measurement.
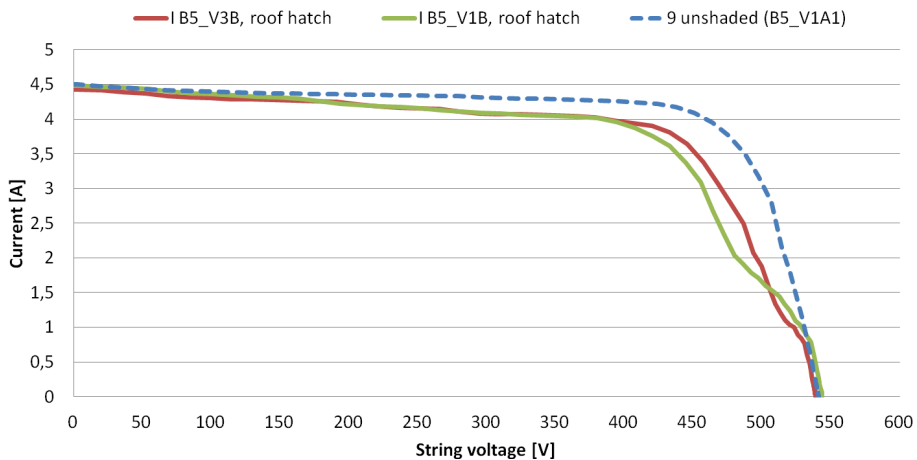

Figure 6.17: I-V curves for the string B5_V1B and string B5_V3B, with an estimated unshaded curve in blue. E_{EFF} = 665–669 W/m^2, T = 43.0 °C

Estimating the power loss referred to the estimated unshaded case, the drop in power is 80,5 W for B5_V3B and 151.5 W for B5_V1B, which correspond to a loss of 4.65 and 8.76 %, respectively. Using the equation for estimating maximum power as before, the new calculated power losses are 9.7 % for B5_V3B and 13.6 % for B5_V1B. Once again, the estimated power losses are significantly higher when comparing them to the theoretical maximum power calculated using P_{MAX} 327 W. This could either mean that the study by Energimyndigheten in Sweden were correct about the 6 % lower performance than given in the data sheet (as discussed in section 6.3.3 on page 93, [67]), that the formula is incorrect in terms of temperature coefficient, or simply consistent measurement errors by the PVPM.

6.4.5 Shading on B5_V1: safety wire (and roof hatch)

Figure 6.18 presents the power production of B5_V1 for the selected dates. March 16th is included to show that the impact is much greater when the Sun's altitude is low. The shadings affecting the modules of inverter B5_V1, are the roof hatch (B5_V1B) and the

South-eastern safety wire (B5_V1A1). As seen in the figure, there appears to be two main shading events through the day for B5_V1: the dip that occurs around midday, and the lowered power in the morning which disappears around 9:30–10:00. The latter is most likely the shading from the wire at B5_V1A1, since the shading from the wire was gone when the I-V curve measurements were started at 12:30 on May 10th. The dip around midday is therefore likely caused by the roof hatch shading on string B5_V1B.
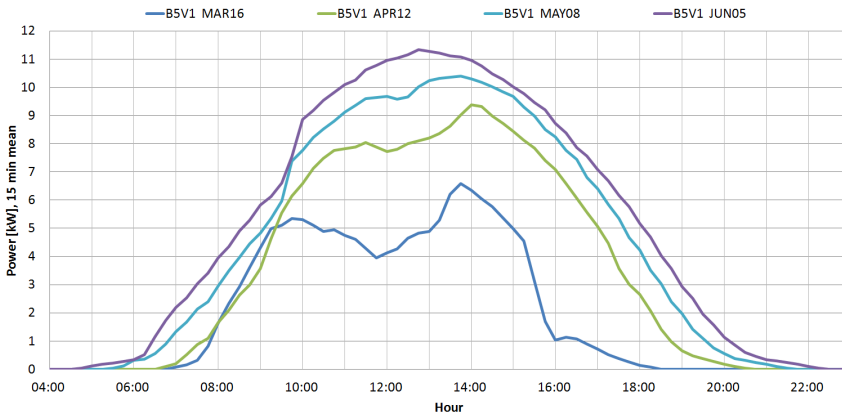

Figure 6.18: Sunny Portal power production from March 16th, April 12th, May 8th and June 5th.
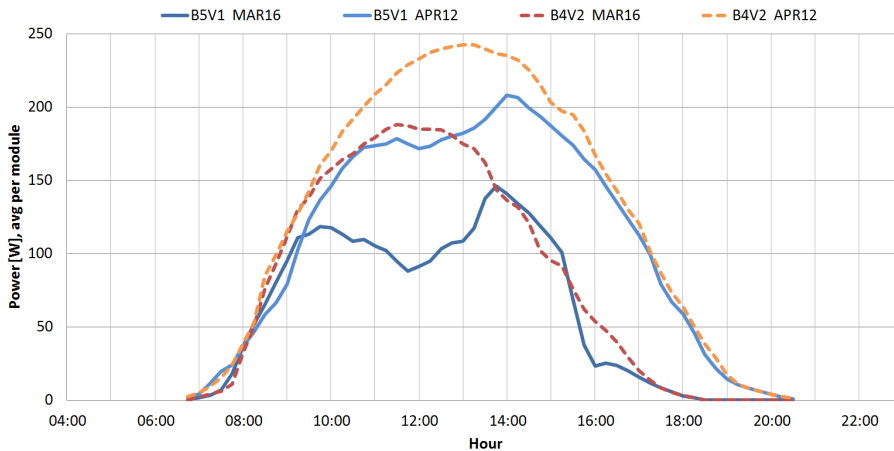

Figure 6.19: Average power per module for B5_V1 and B4_V2 from March 16th and April 12th.

The average power per module for B5_V1 is compared to B4_V2, which seems to be little to not affected by shading while B5_V1 is under shading. The power per module for

these two inverters are plotted in Figure 6.19 for March 16th and April 12th, where the shading has the largest impact. As the curves show, B5_V1 looses its peak production due to this partial shading. As the simulations and experiments showed, the wire by itself did not cause a dramatic loss in power. When the wire's mount was included, the power loss went from 3 % to 25.6 %, even if the shading only occurred on one substring. When the Sun's altitude is low, the shade from the mount will most likely be even larger, which may be the cause of the large power drop seen in Figure 6.18.

Table 6.5: *A rough estimate of energy loss due to partial shading by the wire and roof hatch on B5_V1, where B4_V2 used for comparison.*

Date	B5V1 lost energy compared to B4V2	Daily energy yield B5V1	Shading loss
16/3/16	13.12 kWh	38.59 kWh	34.0 %
12/4/16	12.16 kWh	69.34 kWh	17.5 %

The estimated lost energy due to shading on B5_V1 compared to B4_V2 is calculated between 8:30 and 13:30 for March 16th and between 8:00 and 16:00 for April 12th. The results are presented in Table 6.5 Note that the loss of energy after 13:30 and 16:00 are not included, as shading seems to be affecting B4_V2. The estimated losses are from the shading that is most likely caused by the wire and roof hatch combined. Lack of production data on a string level makes it impossible to separate the losses.

6.4.6 Shading on B4_V3: weather station

Figure 6.20 shows the shading from the weather station during the I-V curve measurements, affecting two modules in string B4_V3A1. As shown in the photo, this cast shadow is more transparent and blurry than the cast shadow from e.g. the exhaust vent. This is because the source of the shadow is located further away, as explained in the theoretical chapter. The I-V and power curve for the string affected by the shadow is shown in Figure 6.21 together with an unshaded string in the same orientation. This study has not conducted any experiments or simulations directed at the weather station, but the figures below indicate that there is a visible impact of the shading. Even though the shadow affects more than one module, the shadow is spread across several cells on the long side of the

module in this particular case. This will make the impact less severe, just like the case of shading by wire along a row of modules resulted in a small simulated loss of 3 %.

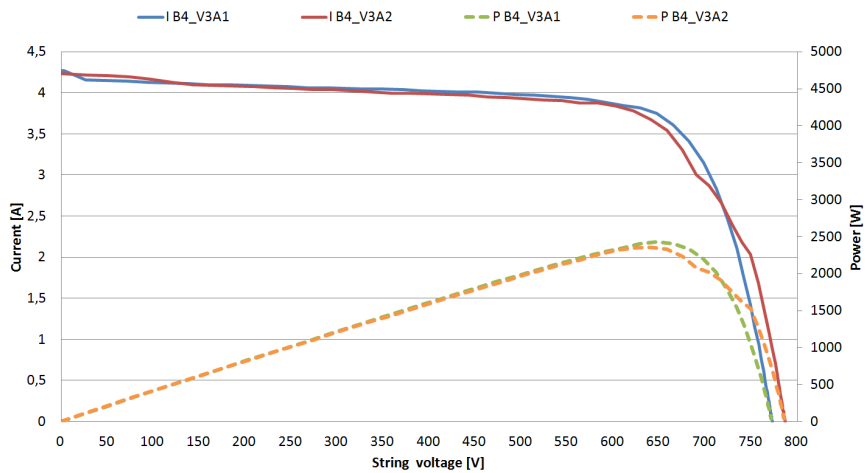*Figure 6.20: A photo showing the shading by the weather station. Taken May 10th, 16:07.*

Figure 6.21: I-V and power curves for B4_V3A1 and A2, where V3A1 is under shading by the weather station as in Figure 6.20. $E_{\mathrm{EFF}} = 596W/m^2$, $T = 38\,^{\circ}$C.

6.5   Summary of the On-Site Findings

This chapter has presented results from thermal imaging, the impact of cleaning a single or several strings of modules, and I-V measurements for various sources of cast shadows at PK. The images from the IR camera did not find any hot spots or other anomalies at Block 4 and 5, neither did the IR camera capture any dangerously high temperatures. The highest temperature recorded was 80 °C, which according to theory is far below the limit of harmful temperatures (150 °C).

The cleaning of one single module soiled by seagull droppings and road dust showed a improvement in terms of I-V characteristics, but not by more than 0.5 %. It did also show a rather large increase in the parallel resistance of 80 Ω (+12.4 %) and an increase in SC current of 0.053 A. The results of cleaning a all the modules connected to an inverter showed an increased daily energy yield of up to almost 11 % compared to the uncleaned modules of another inverter with the same orientation. The daily energy yield was observed to be decreasing the next days, and dropping below 1.7 % after the first rainfall, indicating that the rain is able to remove most of the soiling that held back the performance of the soiled strings. However, there was still a consistent higher energy yield of the cleaned inverter the next days, even if it was small.

When investigating the shading impacts of some selected sources for shading at Block 5 and 4, it was demonstrated that shading impacts could be identified by various methods: comparing production data, performing I-V characteristic measurements, or studying the instantaneous current and voltage values. It was found that the shading-tolerant SP-E20 modules have a great advantage in terms of minimizing power loss. For most of the cases of shading, only a small drop was observed in the I-V characteristics. In the case for shading by the exhaust vent, this clearly showed the largest drop in power. This was because of the way the shadow hit the affected module and causes lost power from all its substrings.

The PVPM measurements summarized in Table F.2 of Appendix F.4, show that there are generally significant errors between the theoretical peak power value calculated at STC and the rated value of 327 W, even for the unshaded strings. The exception is for the

measurements conducted at Block 4, when the sky became slightly cloudy and actually overestimated the peak power at STC. Shading impacts during cloudy days has not been investigated, as there has been no available irradiance data that separated the diffuse and direct irradiance. Also, for cloudy days, the differences in power production between the inverters is little to none, regardless of orientation, see the example in Figure 6.23. These differences in production are clearly seen in the figures of Appendix F.2.2, which were measured at cloud-free days.
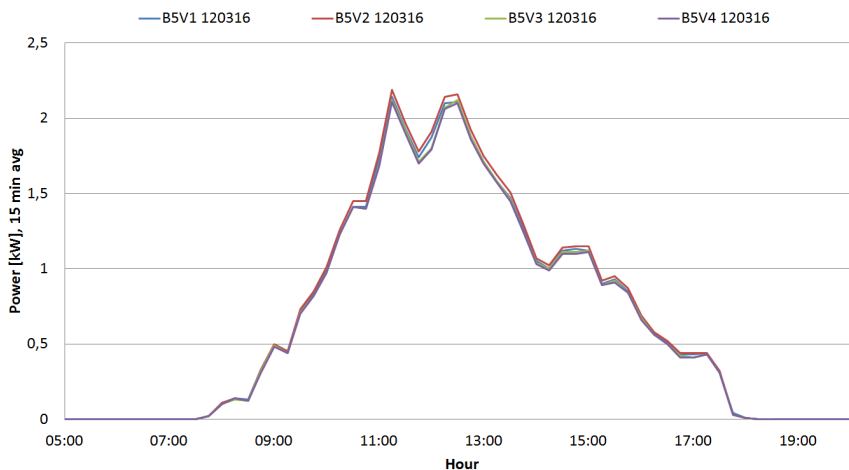
Figure 6.22: Power production for Block 5, March 12th, showing how the power production follows the same pattern for all inverters.

Judging by the obtained I-V curves during partial shading conditions, there was not observed any issues with local maxima, regarding erroneous operation of the MPPTs. Neither of the curves showed any protruding local maxima, perhaps except for the case of shading by the exhaust vent. However, the power curve at the step-down is rather flat and may not even be regarded as a maximum point by the MPPT.

For most of the shading conditions, the impacts have not been quantified with certainty. When relating the lost power to the theoretical maximum power value of 327, the losses are significantly larger than for the simulations. When relating the losses to the maximum power of similar strings with no shading, the losses were closer to what was found in the simulations due to the lower theoretical maximum power. However, there is a risk

in comparing with other strings, as the strings may be exposed to different amounts of soiling in terms of seagull droppings (dust accumulation is usually more uniformly spread, as mentioned earlier), which may affect the measurements. In general, the unshaded strings appeared to have similar characteristics, with little or no indication of large mismatches. And example is shown in Figure 6.23, which displays the power curves for the three strings at input A of inverter B5_V1.
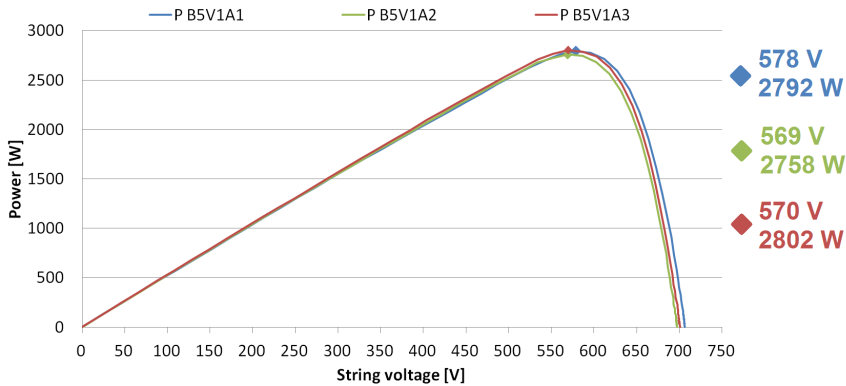

Figure 6.23: Power curves for the three strings at input A of inverter B5_V1, showing a small mismatch in MPP voltages.

Chapter 7 | Summary and Conclusion

This thesis has been dedicated to confirming or discarding the claim that soiling and partial shading conditions at Powerhouse Kjørbo's PV system has a significant negative impact on the PV system performance. The study has sought to find the potential causes of such partial shading conditions, and to evaluate their impact on PV system performance by gaining an in-depth understanding of PV cells and modules and how they operate under illuminated, shaded and soiled conditions though a theoretical, experimental and simulation study. The focus has been aimed towards Powerhouse Kjørbo and PV systems in Nordic climates, and the answer to the following research questions have been sought:

1. Is the concern expressed by the hypothesis reality or not?

2. How does the reverse bias I-V characteristic of PV cells affect the performance of PV modules and systems under partial shading conditions?

3. How do shading-tolerant PV modules perform compared to conventional modules, and what are their advantages in a PV system exposed to partial shading?

4. Will manual cleaning of soiled PV modules lead to a significant increase in performance, or is the environmental conditions sufficient for preventing large soiling losses?

During on-site inspections at the PK PV system, several sources of partial shading were found, including an exhaust vent, a roof hatch, a vent pipe, a steel safety wire and a weather station. It was also found a significant layer of dust deposit on the module surface, along with large amounts of bird droppings and an occasional mussel shell. All these are sources of reduction of PV system performance to some extent, and it has been proven through experimental and on-site measurements that the impact of the suspected partial shading sources are all measurable. It has also been demonstrated that performing I-V curve measurements on a string level can be very useful for identifying partial shading conditions and parallel mismatches.

The main limitation of the results in this thesis is the lack of sufficiently detailed data for quantifying the impacts of partial shading. There has therefore not been drawn any certain conclusions regarding quantification of the impact of the different sources for cast shading. It was shown that the largest power loss (estimated at 16–19 % loss on a string level) occurs when shading modules on their short edge. By a simulated study of the SunPower module, it was found that it may have two or four cells shaded – depending on where on the module the shading occurs – before the bypass diodes are activated. The SunPower E20 modules used at PK are of a shading-tolerant type, which are constructed to minimize power losses by exploiting the property of soft reverse breakdown at small negative voltages, instead of relying on bypass diodes like conventional modules. Under small shading conditions, this may salvage power which would have been lost to a conventional module, without harming the PV module. This property has been observed during on-site measurements at PK, the main observations summarized in section 6.5.

By cleaning all the modules connected to two of the inverters at the garage building, it was found that the daily energy yield increased by 6–11 % compared to uncleaned modules under the same operating conditions. It was also found that cleaning a single PV module increased its output by 1.3 W, corresponding to 0.5 % of its rated output power. Regarding research question number 4, it was observed that after the firs rainfall after cleaning the modules, the daily energy yield was still higher than for the modules that had not been cleaned, but the yield was limited to 1.7 %. Considering the statistical precipitation in Sandvika, it is most likely that the rainfall will clean the modules sufficiently. There was also found that the bird droppings were not removed easily.

It has been proven that PV modules may successfully be modelled by mathematical equations using MATLAB, as the well-used single-diode circuit model, giving realistic results. According to the findings in the experimental measurements, the assumption of assuming a constant parallel resistance is not valid when modelling partial shading. The parallel resistance has been shown by studies to change value with the effective irradiance, meaning the parallel resistance of a PV cell will increase when shaded. This was found in measurements for both the conventional PV module and the SoloSol E20 module. It was also demonstrated that shading conditions could be recreated,

correlations between shaded area, strength of shading and the equivalent short-circuit current of the shaded cell could be estimated, and these parameters could produce realistic values in a computer simulation.

7.1   Recommendations for Further Work

Since this study was not comprehensive and detailed enough to present qualified estimations on the impacts of partial shading, it is recommended that an updated and more detailed model of the PK PV system is created in PVSyst, including the sources of cast shadows that was identified in this thesis. It is also suggested to perform further shading experiments for better understanding and evaluating the different sources of partial shading at PK. Such a study also requires more time than just the months March to June. It is also proposed to find a way for logging the instantaneous currents and voltages on a string level. These data would be most useful for a continuation of studies similar to this thesis. It should also be done more studies of the SunPower E20 module on a module level, as the series-connection of a string may include interconnection and mismatch errors.

Regarding cleaning of the modules, it is suggested that periodical inspections are performed to evaluate whether the modules should be cleaned or not, as the dropping stains were proved to have a negative impact on the power output. It may also be wise to clean the PV modules if a sufficiently long time has passed since the last rainfall, as it has been shown to increase the daily energy yield. For a better investigation of the impact of bird droppings, the amount of droppings on each string should be mapped and then evaluated by the corresponding power production.

Findings in this thesis indicated that the SunPower E20 modules may have a lower maximum power output than specified in the data sheet, having a maximum power of 5–7 % lower than the specified power of 327 W. A study conducted by Energimyndigheten in Sweden that claims that the SunPower E20 module gives a power output that is 6 % below the rated output of 327 W, which are in accordance with the values estimated in this thesis. There is however some uncertainties regarding this, as these results could

just be measurement errors. If they are *not* simply measurement errors, however, this may have an impact on the scheduled energy production from the PV system, giving lower values than what was planned. Since PK is an energy-positive building, it requires a certain yearly energy production.

As the production data have shown, there is little to no production while the modules are covered in snow. It could be conducted a study of the gain by removing the snow during winter, but as other studies have shown this is often not economically feasible.

Regarding computer modelling and simulation of PV systems and modules under partial shading, it is suggested to make the resistances variable as a function of effective irradiance or reduced short-circuit current for each cell. This is suggested because the findings of these studies have proven that there are large errors compared to real-life measurements in the obtained I-V curves when simulating with a too low parallel resistance.

Bibliography

[1] IEA-PVPS, "Snapshot of global photovoltaic markets," *Report IEA PVPS T1-29:2016*, 2016.

[2] Multiconsult, "Vekst i solkraftmarkedet i 2015," n.d. http://www.multiconsult.no/vekst-i-solkraftmarkedet-i-2015/ [Accessed: June 10 2016].

[3] NVE, Enova, Innovasjon Norge, and Norges Forskningsråd, "Solenergi – 3. produksjon og marked," n.d. http://www.fornybar.no/solenergi/produksjon-og-marked/3-produksjon-og-marked [Accessed: May 15 2016].

[4] T. Lang, E. Gloerfeld, and B. Girod, "Don't just follow the sun–a global assessment of economic performance for residential building photovoltaics," *Renewable and Sustainable Energy Reviews*, vol. 42, pp. 932–951, 2015.

[5] C. Drefvelin, Teknisk Ukeblad, "Bygger Norges første plusshus – med 1550 m2 solceller," Oct 25 2013. http://www.tu.no/artikler/bygger-norges-forste-plusshus-med-1550-m2-solceller/235294 [Accessed: June 10 2016].

[6] J. Nilsen, Teknisk Ukeblad, "Tirsdag åpner det som blir Norges største solcelleanlegg," Oct 6 2014. http://www.tu.no/artikler/tirsdag-apner-det-som-blir-norges-storste-solcelleanlegg/232519 [Accessed: Jun 11 2016].

[7] Ø. Lie, Teknisk Ukeblad, "Her bygger de Norges desidert største solkraftverk," Des 16 2015. http://www.tu.no/artikler/her-bygger-de-norges-desidert-storste-solkraftverk/276246 [Accessed: Jun 11 2016].

[8] J. Nilsen, Teknisk Ukeblad, "Nå er Norges største solcelle-anlegg blitt nesten tre ganger så stort," May 6 2016. http://www.tu.no/artikler/na-er-norges-storste-solcelle-anlegg-blitt-nesten-tre-ganger-sa-stort/346914 [Accessed: Jun 11 2016].

[9] NorgesGruppen, "Bygger Norges største Solcelleanlegg," May 4 2016. `http://www.norgesgruppen.no/presse/nyhetsarkiv/aktuelt/bygger-norges-storste-solcelleanlegg/` [Accessed: Jun 11 2016].

[10] Powerhouse, "Powerhouse kjørbo – trinn 1," n.d. `http://www.powerhouse.no/prosjekter/kjorbo/` [Accessed: June 29 2016].

[11] Powerhouse, "Powerhouse kjørbo – trinn 2," Feb 01 2016. `http://www.powerhouse.no/prosjekter/kjorbo-trinn-2/` [Accessed: June 29 2016].

[12] SMA Solar Technology AG, "User manual: Plant Monitoring Sunny Portal. version 2.3," 2011.

[13] SunPower Corporation, "Data sheet: SunPower E20 Series solar panels," 2013.

[14] SunPower Corporation, "SunPower Safety and Installation Instructions."

[15] SunPower Corporation, "White paper: SunPower Module Degradation Rate," n.d.

[16] Z. Ahmed, H. A. Kazem, and K. Sopian, "Effect of dust on photovoltaic performance: review and research status," *Latest trends in renewable energy and enviromental informatics*, pp. 193–199, 2013.

[17] M. H. Naeem, *Soiling of Photovoltaic Modules: Modelling and Validation of Location-Specific Cleaning Frequency Optimization.* PhD thesis, ARIZONA STATE UNIVERSITY, 2014.

[18] L. Ødegården, "Test and demonstration of pv systems," 2015. [Specialization project]. Norwegian University of Science and Technology, Institute of Electric Power Engineering.

[19] NVE, Enova, Innovasjon Norge, and Norges Forskningsråd, "Solenergi – 1. ressursgrunnlag," n.d. `http://www.fornybar.no/solenergi/ressursgrunnlag` [Accessed: May 6 2016].

[20] NVE, Enova, Innovasjon Norge, and Norges Forskningsråd, "Types of solar radiation," Dec 28 2015. `http://www.aeronsystems.com/types-of-solar-radiation/` [Accessed: Apr 21 2016].

[21] G. M. Masters, *Renewable and efficient electric power systems.* John Wiley & Sons, 2004.

[22] NVE, Enova, Innovasjon Norge, and Norges Forskningsråd, "Solenergi – 2. teknologi,"

n.d. http://www.fornybar.no/solenergi/teknologi [Last accessed: March 01 2016].

[23] PVeducation.org, "Screen printed solar cells," n.d. http://www.pveducation.org/pvcdrom/manufacturing/screen-printed [Accessed: May 27 2016].

[24] O.-M. Midtgård, "The current-voltage characteristic of standard silicon pv cells and modules," n.d. [Lecture note TET4175]. Norwegian University of Science and Technology, Institute of Electric Power Engineering.

[25] PVeducation.org, "Ideality factor," n.d. http://www.pveducation.org/pvcdrom/solar-cell-operation/ideality-factor [Accessed: May 6 2016].

[26] PVeducation.org, "Bypass diodes," n.d. http://www.pveducation.org/pvcdrom/modules/bypass-diodes [Accessed: May 6 2016].

[27] E. Rodrigues, R. Melício, V. Mendes, and J. Catalão, "Simulation of a solar cell considering single-diode equivalent circuit model," in *International conference on renewable energies and power quality, Spain*, pp. 13–15, 2011.

[28] T. Esram, P. L. Chapman, *et al.*, "Comparison of photovoltaic array maximum power point tracking techniques," *IEEE Transactions on Energy Conversion EC*, vol. 22, no. 2, p. 439, 2007.

[29] C. S. Ruschel, F. P. Gasparin, E. R. Costa, and A. Krenzinger, "Assessment of pv modules shunt resistance dependence on solar irradiance," *Solar Energy*, vol. 133, pp. 35–43, 2016.

[30] G. P. Willeke and E. R. Weber, *Advances in Photovoltaics*, vol. 89. Newnes, 2013.

[31] PVeducation.org, "Shunt resistance," n.d. http://www.pveducation.org/pvcdrom/solar-cell-operation/shunt-resistance [Accessed: May 27 2016].

[32] L. Cerna, V. Benda, and Z. Machacek, "A note on irradiance dependence of photovoltaic cell and module parameters," in *Microelectronics (MIEL), 2012 28th International Conference on*, pp. 273–276, IEEE, 2012.

[33] M. N. Islam, M. Z. Rahman, and S. M. Mominuzzaman, "The effect of irradiation on different parameters of monocrystalline photovoltaic solar cell," in *Developments in Renewable Energy Technology (ICDRET), 2014 3rd International Conference on*

the, pp. 1–6, IEEE, 2014.

[34] H. Bellia, R. Youcef, and M. Fatima, "A detailed modeling of photovoltaic module using matlab," *NRIAG Journal of Astronomy and Geophysics*, vol. 3, no. 1, pp. 53–61, 2014.

[35] D. L. King, J. Kratochvil, W. E. Boyson, *et al.*, "Temperature coefficients for pv modules and arrays: measurement methods, difficulties, and results," in *Photovoltaic Specialists Conference, 1997., Conference Record of the Twenty-Sixth IEEE*, pp. 1183–1186, IEEE, 1997.

[36] F. Fertig, S. Rein, M. Schubert, and W. Warta, "Impact of junction breakdown in multi-crystalline silicon solar cells on hot spot formation and module performance," *cell*, vol. 40, no. 60, p. 80, 2011.

[37] PVeducation.org, "Mismatch for cells connected in series," n.d. http://www.pveducation.org/pvcdrom/modules/mismatch-for-cells-connected-in-series [Accessed: May 15 2016].

[38] O. Breitenstein, J. Bauer, K. Bothe, W. Kwapil, D. Lausch, U. Rau, J. Schmidt, M. Schneemann, M. C. Schubert, J.-M. Wagner, *et al.*, "Understanding junction breakdown in multicrystalline solar cells," *Journal of applied physics*, vol. 109, no. 7, p. 071101, 2011.

[39] H. Yang, H. Wang, and M. Wang, "Investigation of the relationship between reverse current of crystalline silicon solar cells and conduction of bypass diode," *INTERNATIONAL JOURNAL OF PHOTOENERGY*, 2012.

[40] Wikipedia, "Breakdown voltage," n.d. https://en.wikipedia.org/wiki/Breakdown_voltage [Accessed: June 27 2016].

[41] STMicroelectronics, "Application note: How to choose a bypass diode for a silicon panel junction box," 2011.

[42] A. Woyte, J. Nijs, and R. Belmans, "Partial shadowing of photovoltaic arrays with different system configurations: literature review and field test results," *Solar energy*, vol. 74, no. 3, pp. 217–233, 2003.

[43] K. A. Kim and P. T. Krein, "Reexamination of photovoltaic hot spotting to show inadequacy of the bypass diode," *IEEE Journal of Photovoltaics*, vol. 5, no. 5,

pp. 1435–1441, 2015.

[44] S. Davis, "Schottky diodes: the old ones are good, the new ones are better," *Power*, 2011.

[45] F. Salem and M. A. Awadallah, "Detection and assessment of partial shading in photovoltaic arrays," *Journal of Electrical Systems and Information Technology*, 2016.

[46] D. Sera and Y. Baghzouz, "On the impact of partial shading on pv output power," in *WSEAS/IASME International Conference on Renewable Energy Sources (RES'08)*, 2008.

[47] H. Chu, L. J. Koduvelikulathu, V. D. Mihailetchi, G. Galbiati, A. Halm, and R. Kopecek, "Soft breakdown behavior of interdigitated-back-contact silicon solar cells," *Energy Procedia*, vol. 77, pp. 29–35, 2015.

[48] D. D. Smith, P. J. Cousins, A. Masad, S. Westerberg, M. Defensor, R. Ilaw, T. Dennis, R. Daquin, N. Bergstrom, A. Leygo, *et al.*, "Sunpower's maxeon gen iii solar cell: High efficiency and energy yield," in *2013 IEEE 39th Photovoltaic Specialists Conference (PVSC)*, pp. 0908–0913, IEEE, 2013.

[49] H. Patel and V. Agarwal, "Matlab-based modeling to study the effects of partial shading on pv array characteristics," *IEEE transactions on energy conversion*, vol. 23, no. 1, pp. 302–310, 2008.

[50] Y.-H. Ji, D.-Y. Jung, J.-G. Kim, J.-H. Kim, T.-W. Lee, and C.-Y. Won, "A real maximum power point tracking method for mismatching compensation in pv array under partially shaded conditions," *IEEE Transactions on power electronics*, vol. 26, no. 4, pp. 1001–1009, 2011.

[51] SMA Solar Technology AG, "Shade Management - Efficient operation of partially shaded PV systems with OptiTrac Global Peak, Version 1.2," n.d. Technical information paper, available from http://files.sma.de/dl/7418/GlobalPeak-TI-en-12.pdf.

[52] K. Ishaque and Z. Salam, "A review of maximum power point tracking techniques of pv system for uniform insolation and partial shading condition," *Renewable and Sustainable Energy Reviews*, vol. 19, pp. 475–488, 2013.

[53] IBC Solar AG, "Data sheet: IBC SoloSol 100 CS."

[54] PVE Photovoltaik Engineering, "Data sheet: PVPM 1000CX."

[55] S. Silvestre, A. Boronat, and A. Chouder, "Study of bypass diodes configuration on pv modules," *Applied Energy*, vol. 86, no. 9, pp. 1632–1640, 2009.

[56] E. V. Paraskevadaki and S. A. Papathanassiou, "Evaluation of mpp voltage and power of mc-si pv modules in partial shading conditions," *IEEE Transactions on Energy Conversion*, vol. 26, no. 3, pp. 923–932, 2011.

[57] B. A. Alsayid, S. Y. Alsadi, S. J. Ja'far, and M. H. Dradi, "Partial shading of pv system simulation with experimental results," 2013.

[58] Linear Technology Corporation, "Design simulation and device models," n.d. http://www.linear.com/designtools/software/#LTSpice [Accessed: June 18 2016].

[59] LITE-ON Semiconductors, "Data sheet: Schottky barrier rectifiers 10SQ050," 2013.

[60] N.N, "Spice models chapter 3 - diodes and rectifiers," n.d. http://www.allaboutcircuits.com/textbook/semiconductors/chpt-3/spice-models/ [Accessed: May 01 2016].

[61] M. Boztepe, F. Guinjoan, G. Velasco-Quesada, S. Silvestre, A. Chouder, and E. Karatepe, "Global mppt scheme for photovoltaic string inverters based on restricted voltage window search algorithm," *iEEE Transactions on industrial Electronics*, vol. 61, no. 7, pp. 3302–3312, 2014.

[62] A. Mäki and S. Valkealahti, "Power losses in long string and parallel-connected short strings of series-connected silicon-based photovoltaic modules due to partial shading conditions," *IEEE Transactions on Energy Conversion*, vol. 27, no. 1, pp. 173–183, 2012.

[63] FLIR, "How Does an IR Camera Work?," n.d. http://www.flir.com/corporate/display/?id=41523 [Accessed: Jun 15 2016].

[64] FLIR, "Thermal imaging cameras: a fast and reliable tool for testing solar panels," n.d. http://www.flir.co.uk/instruments/building/display/?id=41872 [Accessed: Jun 15 2016].

[65] Torsten Hoffmann, 2015–2016. Available at: http://www.suncalc.org/#/59.

8864,10.5272,20/2016.05.10/12:26/7.

[66] S. Wendlandt, A. Drobisch, T. Buseth, S. Krauter, and P. Grunow, "Hot spot risk analysis on silicon cell modules," in *25th European Photovoltaic Solar Energy Conference, Valencia, Spain*, 2010.

[67] T. U. J. Nilsen, "Stor test: Disse solcellene er best for norske forhold," Jun 9 2015. http://www.tu.no/artikler/ stor-test-disse-solcellene-er-best-for-norske-forhold/223888 [Accessed: Jun 30 2016].

[68] Atonometrics, Inc, "White paper: The Effects of Soiling on PV Performance - a brief litterature survey," 2012.

[69] H. B. Pedersen, "Experimental study of soiling on photovoltaic modules in a nordic climate," 2015.

[70] SMA Solar Technology AG, "Data sheet: STP 10000TL / 12000TL / 15000TL / 17000TL."

Appendix A | Inverters and Strings

A.1 Inverter Specifications

The tables below present the specifications for each of the inverters used at Powerhouse Kjørbo. They are named V1–V4 at Block 4 and 5, and V1–V8 at the garage building. More details can be found in the STP data sheet, [70].

Table A.1: Specifications of the three inverter models installed at PK. [70]

Inverter model	STP 12000TL-10	STP 15000TL-10	STP 17000TL-10
Max DC power (PF = 1)	12.5 kW	15.6 kW	17.6 kW
Max DC voltage	1000 V	1000 V	1000 V
MPP voltage range	150–800 V	150–800 V	150–800 V
Max input current input B / input B	22 A / 11 A	33 A / 11 A	33 A / 11 A
No. of MPP trackers	2	2	2
Max no. of strings (input A / input B)	4 / 1	5 / 1	5 / 1
Max AC power output (230 V, 50 Hz)	12 kVA	15 kVA	17 kVA
Max. efficiency/ European efficiency	98 % / 97.5 %	98 % / 97.5 %	98 % / 97.5 %

Table A.2: Properties of the PV system of Block 4, "B4".

BUILDING 4 PV SYSTEM	
Number of modules per string (A / B)	13 / 14
Number of strings per input utilized (A / B)	3 / 1
Inverter model	STP 15000TL-10
Number of inverters	4
Rated PV power per inverter	17.331 kWp
Tilt angle	10°
Azimuth V1–V	-35° (SE)
Azimuth V3–V4	+145° (NW)
Rooftop area covered	345.56 m^2

Table A.3: Properties of the PV system of Block 5, "B5".

BUILDING 5 PV SYSTEM	
Number of modules per string (A / B)	12 / 9
Number of strings per input utilized (A / B)	3 / 1
Inverter model	STP 12000TL-10
Number of inverters	4
Rated power per inverter	14.715 kWp
Tilt angle	10°
Azimuth V1–V	-35° (SE)
Azimuth V3–V4	+145° (NW)
Rooftop area covered	293.40 m^2

Table A.4: Properties of the PV system of the garage building, "P".

GARAGE BUILDING PV SYSTEM	
Number of modules per string (A / B)	12 / 10 (11 for V4 and V8)
Number of strings per input utilized (A / B)	5 / 1
Inverter model	STP 17000TL-10
Number of inverters	8
Rated PV power per inverter	22.890 kWp (23.217 kWp for V4 and V8)
Tilt angle	10°
Azimuth angle V1–V4	+70° (SW)
Azimuth angle V5–V8	-110° (NE)
Rooftop area covered	293.40 m^2 916.06 m^2

A.2 String Configuration

In Figure A.1 to A.3, each string has its own color. Each module is labeled with the name of the string it belongs to.
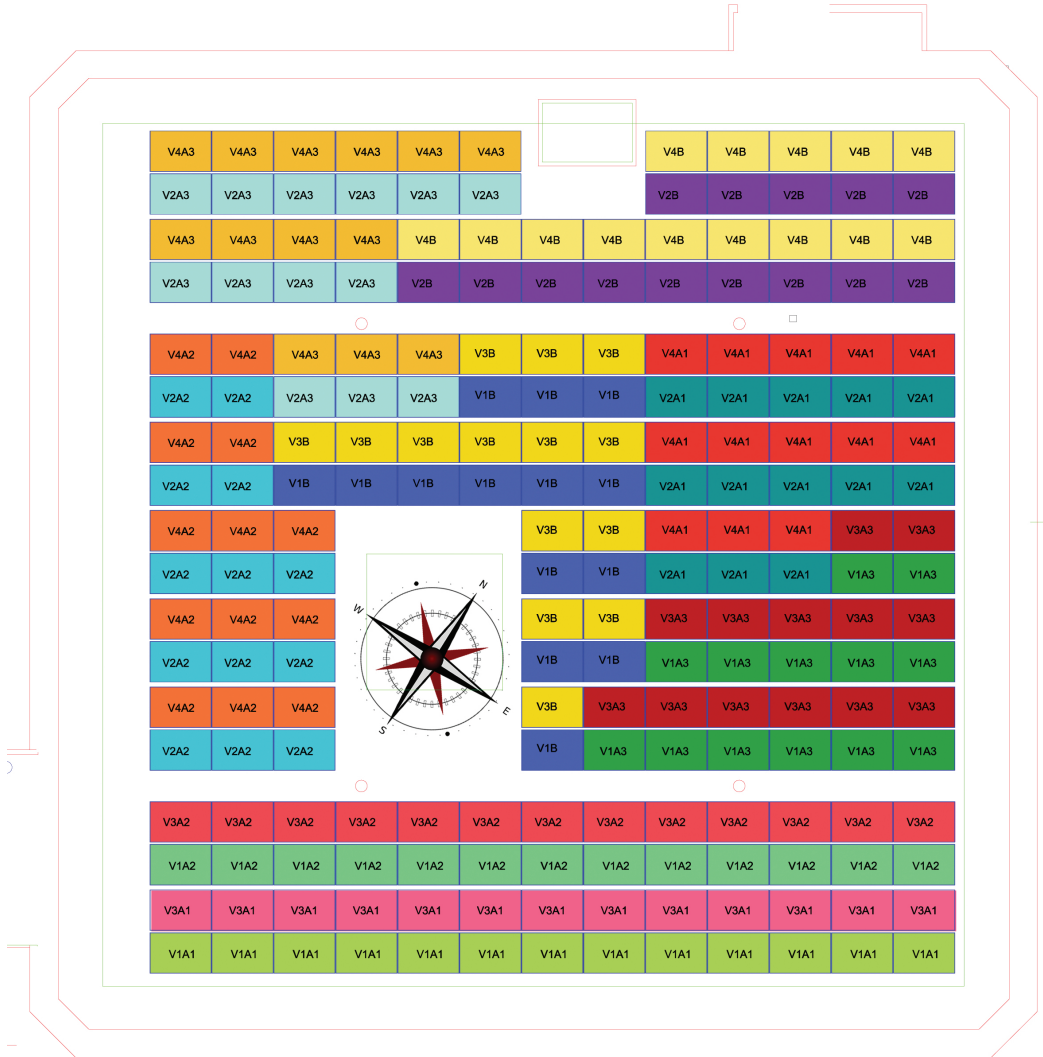
Figure A.1: Illustration showing the string configuration at Block 4. (Source: Asplan Viak, Skanska)
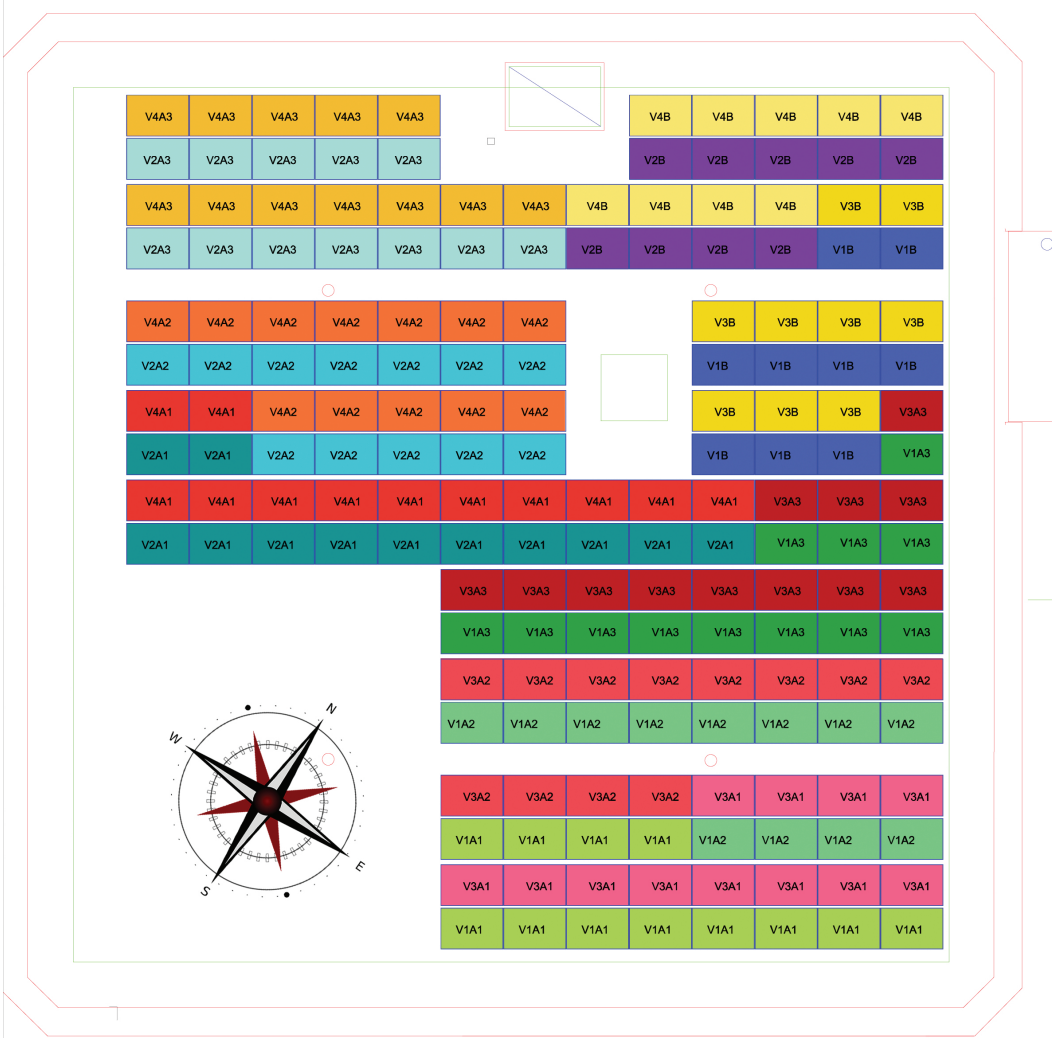
Figure A.2: Illustration showing the string configuration at Block 5. (Source: Asplan Viak, Skanska)
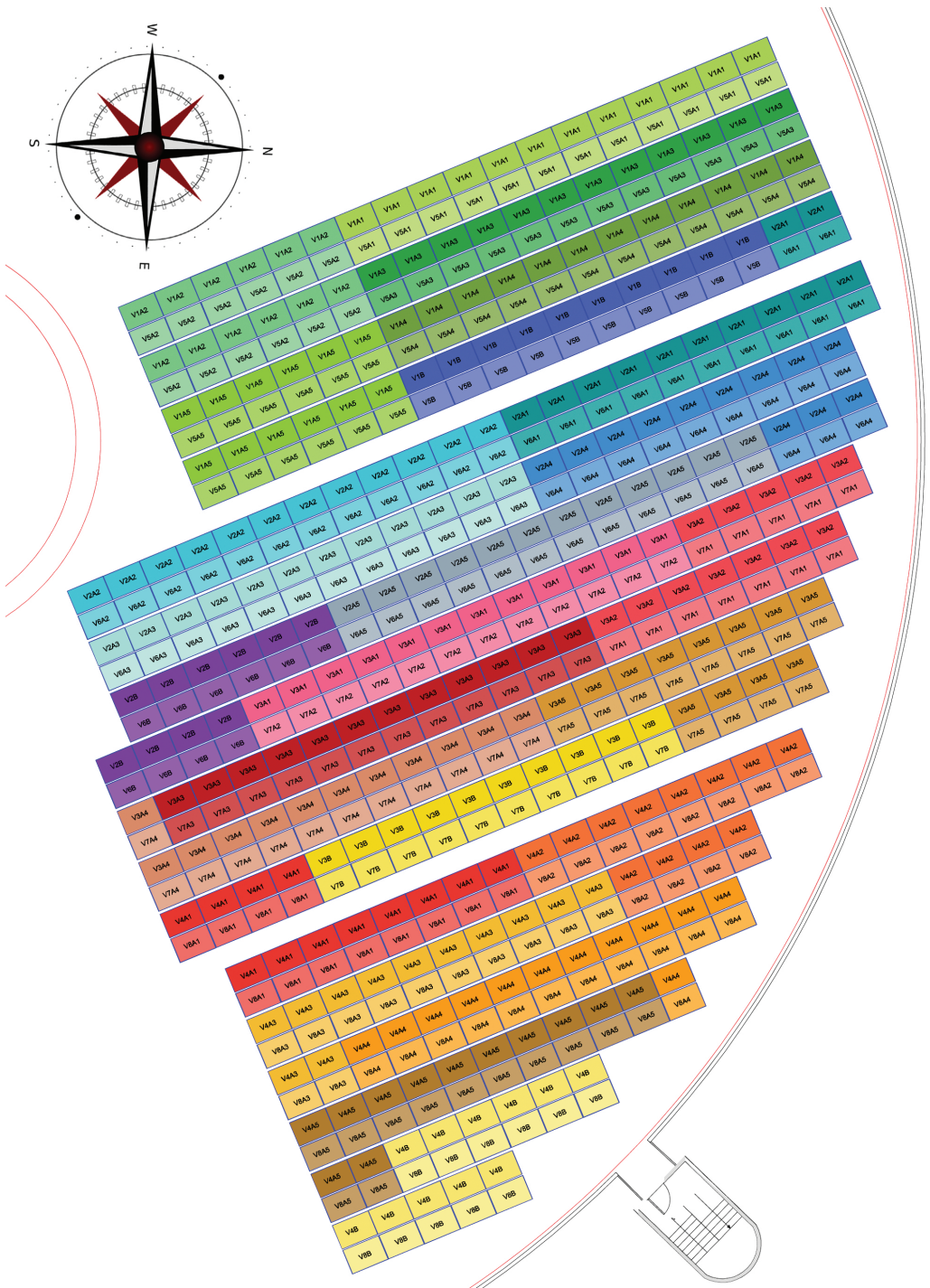
Figure A.3: Illustration showing the string configuration at the garage building. (Source: Asplan Viak, Skanska)

Appendix B | Precipitation

The table below shows the measured precipitation on a daily basis from February 1st to June 1st. This weather station is the closest one to Sandvika, located in Asker, 6.5 km away. The dates marked in yellow are the dates spent on site, and the dates marked in green are the dates studied when cleaning the modules on the garage.

Table B.1: Precipitation in Asker. Source: Norwegian Meteorological Institute via the web service eKlima.

Date	Precipitation [mm]	Snow depth [cm]		Date	Precipitation [mm]	Snow depth [cm]
01.02.2016	0	7		07.03.2016	6,1	36
02.02.2016	2,7	9		08.03.2016	0,3	32
03.02.2016	0,6	10		09.03.2016	0	33
04.02.2016	0	9		10.03.2016	0	31
05.02.2016	0	10		11.03.2016	0	27
06.02.2016	6,5	14		12.03.2016	**0**	26
07.02.2016	4,8	5		13.03.2016	**0**	26
08.02.2016	4,1	0		14.03.2016	**0,5**	24
09.02.2016	**16,7**	0		15.03.2016	0	18
10.02.2016	0,9	2		16.03.2016	0	12
11.02.2016	0,3	2		17.03.2016	0	11
12.02.2016	0	4		18.03.2016	0	7
13.02.2016	0,3	4		19.03.2016	0	7
14.02.2016	0,2	6		20.03.2016	0	4
15.02.2016	0	6		21.03.2016	0	0
16.02.2016	0	6		22.03.2016	0	0
17.02.2016	0	3		23.03.2016	0	0
18.02.2016	0	4		24.03.2016	0	0
19.02.2016	0	4		25.03.2016	0	0
20.02.2016	2,2	2		26.03.2016	**0,2**	0
21.02.2016	**9,4**	12		27.03.2016	**1,3**	0
22.02.2016	0	11		28.03.2016	**4,2**	0
23.02.2016	0	12		29.03.2016	**13**	0
24.02.2016	0	10		30.03.2016	**1,7**	0
25.02.2016	0	12		31.03.2016	0	0
26.02.2016	0	9		01.04.2016	0,1	0
27.02.2016	0	9		02.04.2016	1,2	0
28.02.2016	0	8		03.04.2016	1,5	0
29.02.2016	0	10		04.04.2016	2,9	0
01.03.2016	0	8		05.04.2016	8,9	0
02.03.2016	6,2	15		06.04.2016	0,6	0
03.03.2016	**22,2**	34		07.04.2016	0,8	0
04.03.2016	7,2	27		08.04.2016	5,2	0
05.03.2016	9,6	33		09.04.2016	2,1	0
06.03.2016	3,3	29		10.04.2016	0,4	0

Precipitation in Asker continued.

Date	Precipitation [mm]	Snow depth [cm]		Date	Precipitation [mm]	Snow depth [cm]
11.04.2016	0	0		07.05.2016	0	0
12.04.2016	1,3	0		08.05.2016	0	0
13.04.2016	0	0		09.05.2016	0	0
14.04.2016	0	0		10.05.2016	0	0
15.04.2016	0	0		11.05.2016	0	0
16.04.2016	0,9	0		12.05.2016	0	0
17.04.2016	14,7	0		13.05.2016	0	0
18.04.2016	1,3	0		14.05.2016	0	0
19.04.2016	1,4	0		15.05.2016	0,1	0
20.04.2016	0	0		16.05.2016	0	0
21.04.2016	0	0		17.05.2016	0	0
22.04.2016	0	0		18.05.2016	0	0
23.04.2016	0	0		19.05.2016	0,1	0
24.04.2016	0,4	0		20.05.2016	0,4	0
25.04.2016	0,1	0		21.05.2016	2,5	0
26.04.2016	0	0		22.05.2016	3	0
27.04.2016	0	0		23.05.2016	15,7	0
28.04.2016	0	0		24.05.2016	18,9	0
29.04.2016	9,8	0		25.05.2016	1,2	0
30.04.2016	12,5	0		26.05.2016	0	0
01.05.2016	**23,7**	0		27.05.2016	0	0
02.05.2016	0	0		28.05.2016	0	0
03.05.2016	2,7	0		29.05.2016	7,9	0
04.05.2016	3,1	0		30.05.2016	9,9	0
05.05.2016	0	0		31.05.2016	3,4	0
06.05.2016	0	0		01.06.2016	0	0

Appendix C | Simulation Models

This appendix presents a the visual interface of the models used for simulation of the IBC SoloSol 100 CS and the SunPower E20-327 PV modules. See also the digital attachment including the two LTSpice models and the MATLAB script.

C.1 LTSpice Models
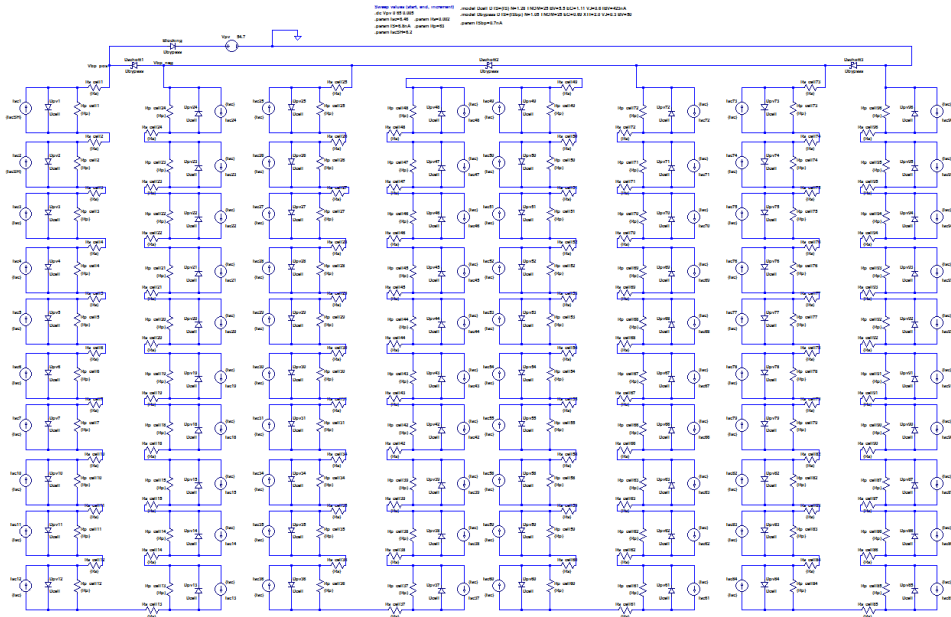
Figure C.1: The LTSpice model for the SunPower E320-327 module. The blocking diode connected.

Figure C.2: The LTSpice model for the IBC SoloSol 100 CS module. The blocking diode is not connected.

C.2   MATLAB Script Interface

Figure C.3 shows the user interfaces form the MATLAB script. The default values are set to those of the IBC SoloSol 100CS module.
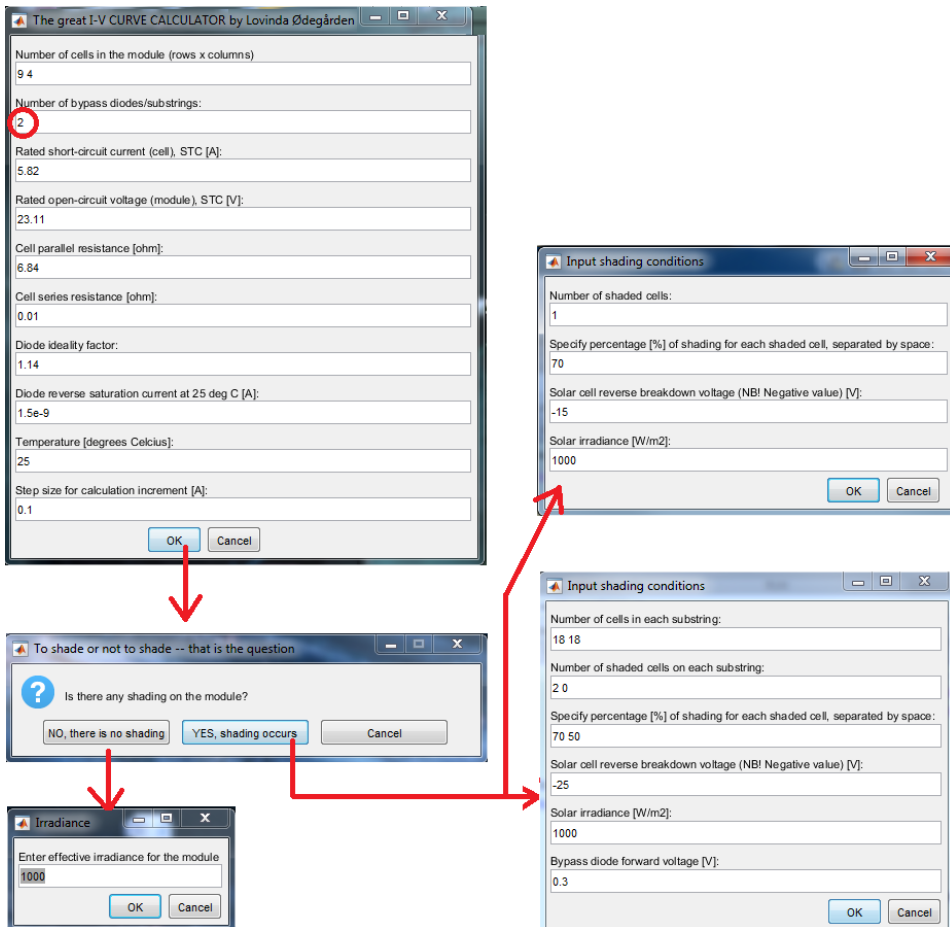
Figure C.3: Input dialogue from the MATLAB script, showing which inputs the user can specify.

C.3 LTSpice VS. MATLAB Simulations
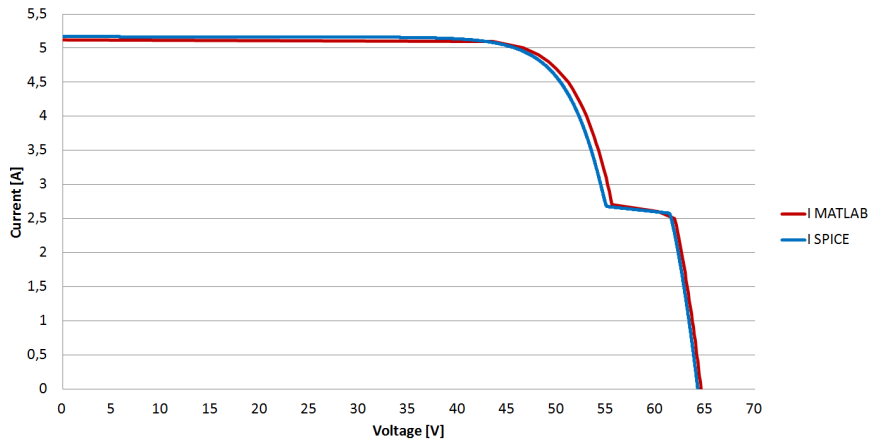
Figure C.4: I-V characteristics for the SP-E20 module, shaded 1 cell, simulated in MATLAB and LTSpice. Simulated without blocking diode in LTSpice.
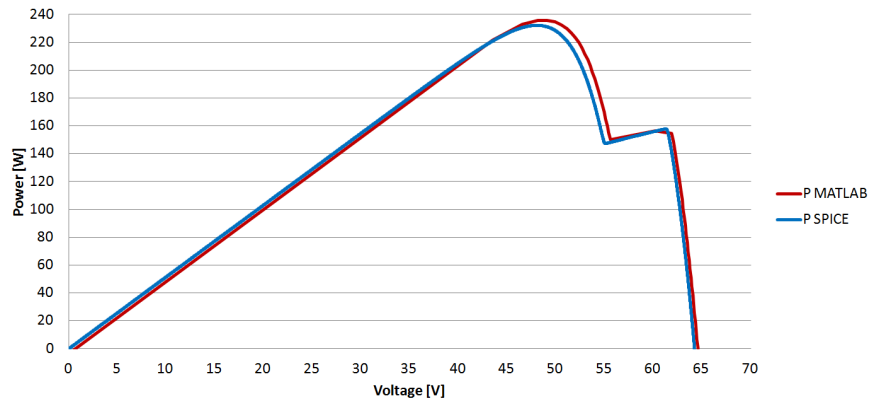
Figure C.5: P characteristics for the SP-E20 module, shaded 1 cell, simulated in MATLAB and LTSpice. Simulated without blocking diode in LTSpice.
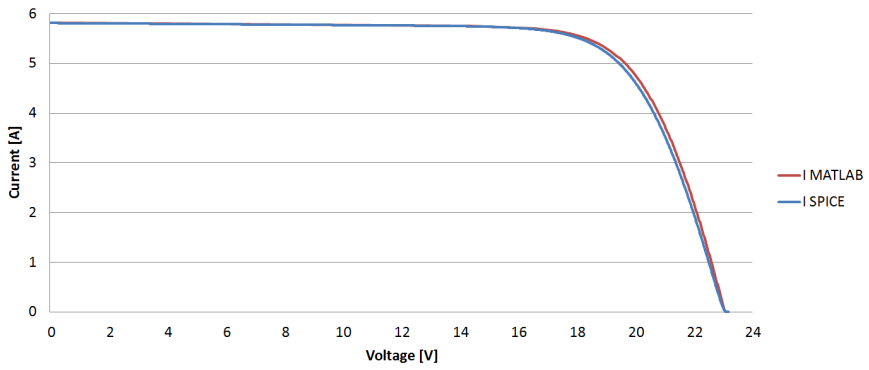
Figure C.6: I-V characteristics for the SoloSol module, unshaded case, simulated in MATLAB and LTSpice. Simulated with reduced ideality factor by 0.02 in MATLAB.
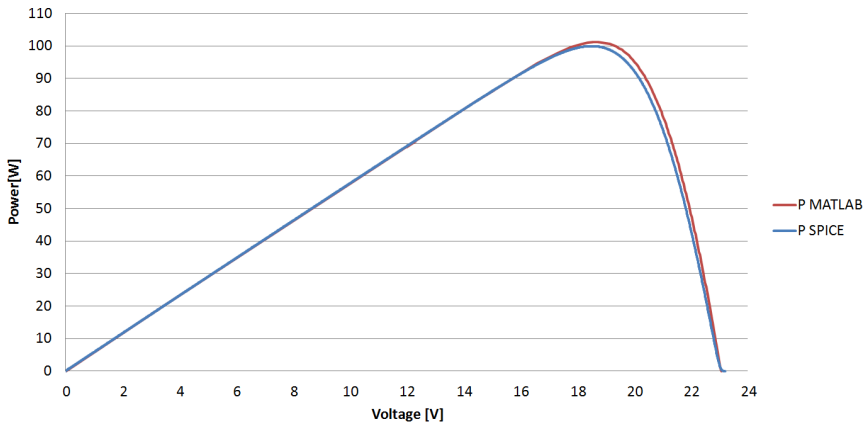
Figure C.7: I-V characteristics for the SoloSol module, unshaded case, simulated in MATLAB and LTSpice. Simulated with reduced ideality factor by 0.02 in MATLAB.

Figure C.8: Power characteristics for the SoloSol module, shaded case, simulated in MATLAB and LTSpice. Same ideality factor and blocking diode present.
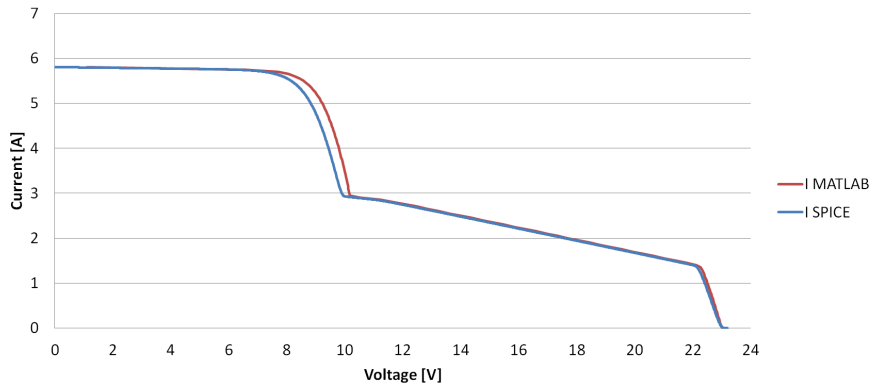
Figure C.9: Power characteristics for the SoloSol module, shaded case, simulated in MATLAB and LTSpice. Same ideality factor and blocking diode present.
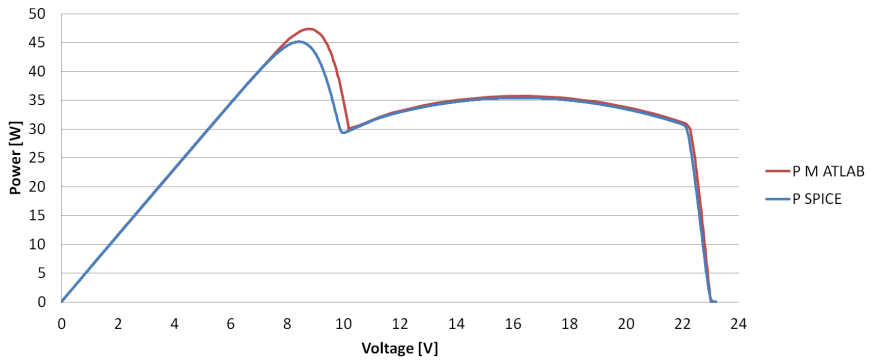
Appendix D │ PK Shading Diagrams

Figure D.1: Shading diagram for shading by blue mussel shell.
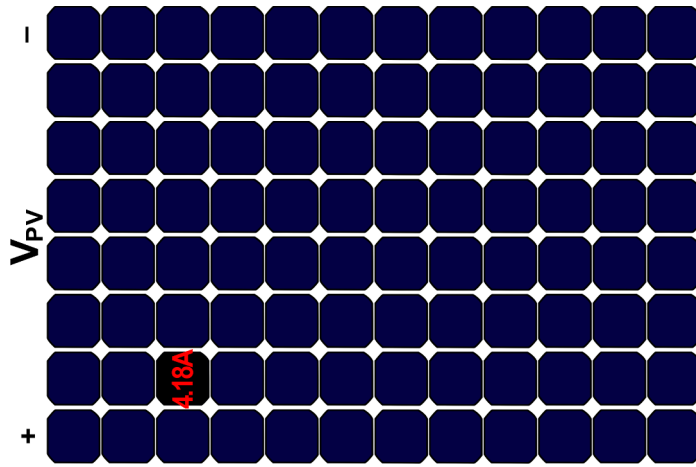
Figure D.2: Shading diagram for shading by steel wire (1/2).
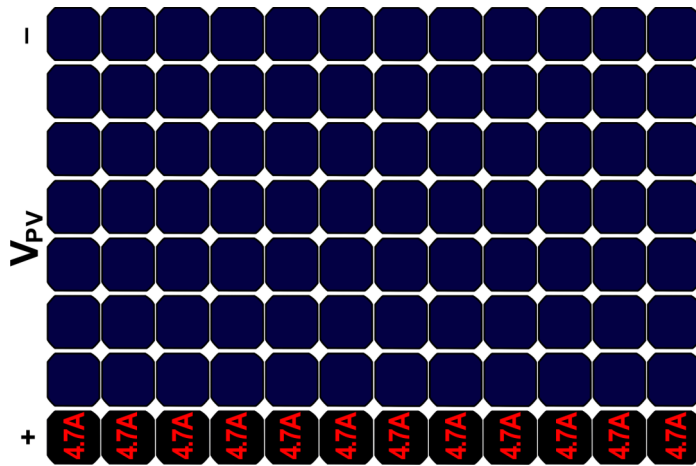
Figure D.3: Shading diagram for shading by steel wire (2/2).
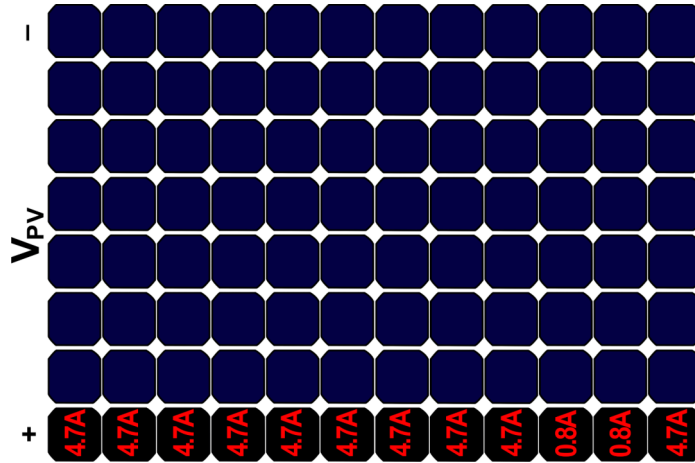
Figure D.4: Shading diagram for shading by vent pipe (1/2).

Figure D.5: Shading diagram for shading by vent pipe (2/2).

Figure D.6: Shading diagram for shading by roof vent or roof hatch.
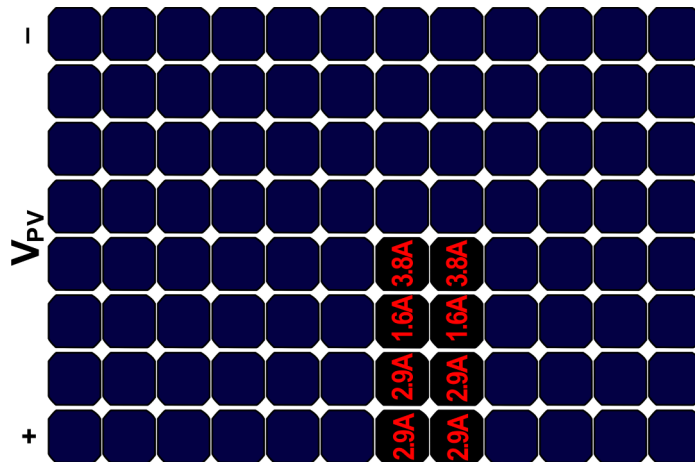
Figure D.7: Shading diagram for shading by roof vent.
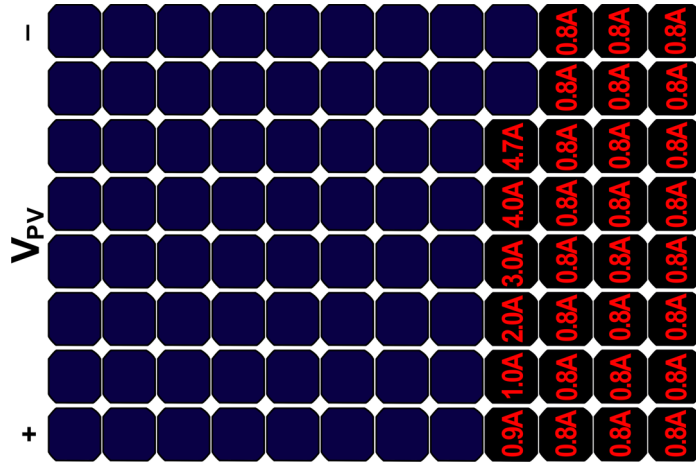
Appendix E | Cleaning of Strings
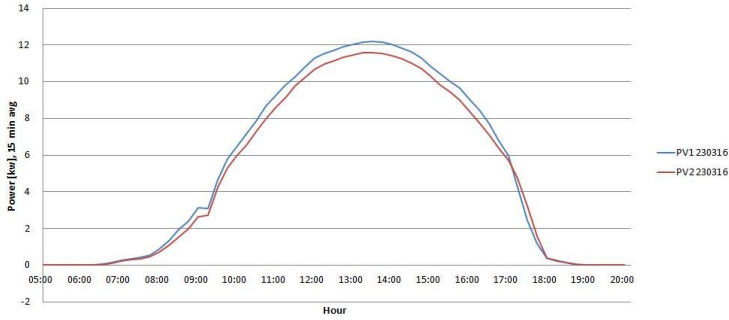
Figure E.1: Power of V1 and V2 for March 23rd.
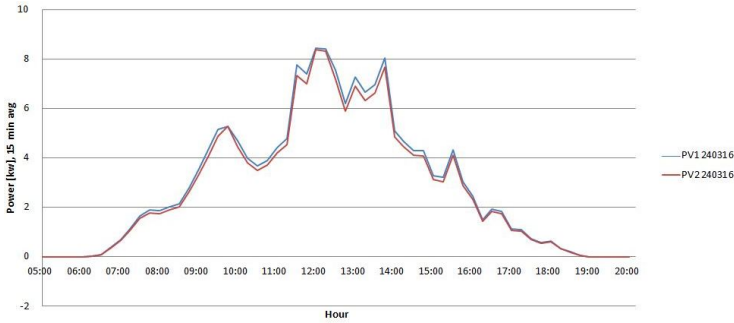
Figure E.2: Power of V1 and V2 for March 24th.
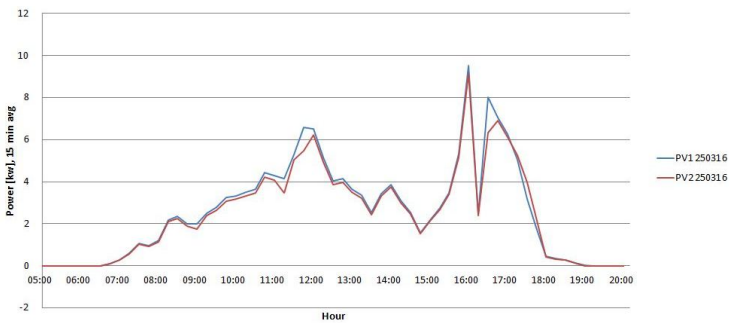
Figure E.3: Power of V1 and V2 for March 25th.
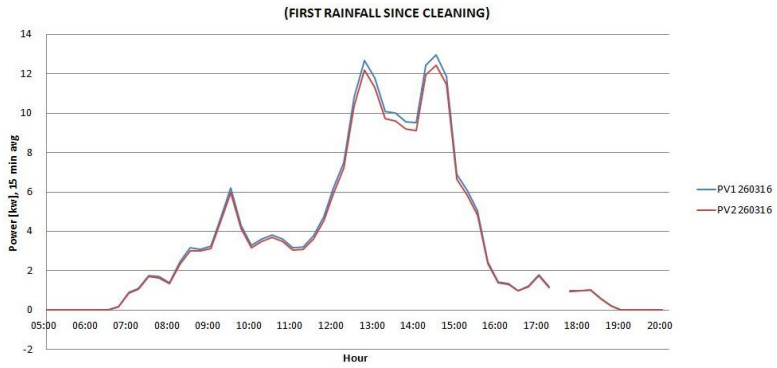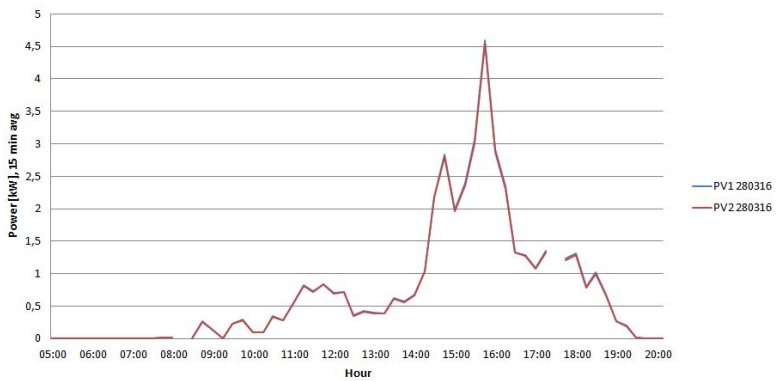
Figure E.4: Power of V1 and V2 for March 26th.
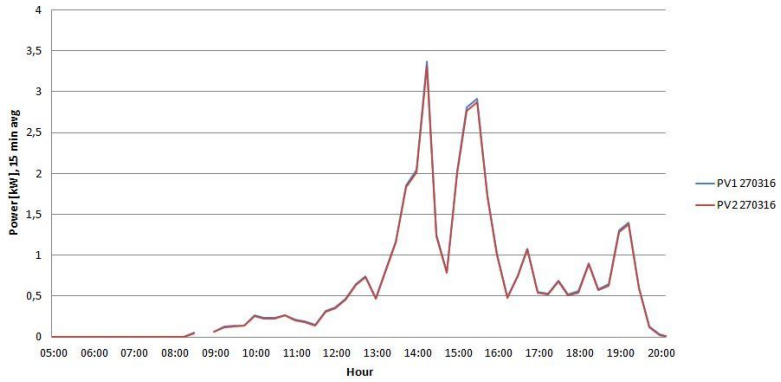
Figure E.5: Power of V1 and V2 for March 27th.

Figure E.6: Power of V1 and V2 for March 28th.

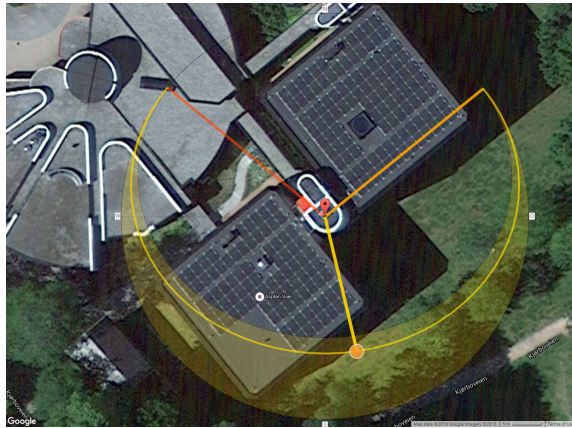# Appendix F | Supplement to Shading Measurements

F.1 SunCalc Images

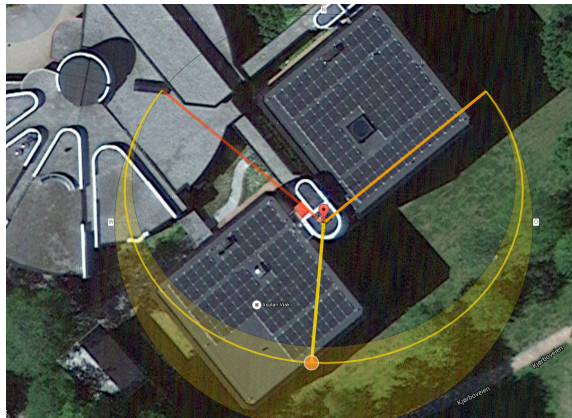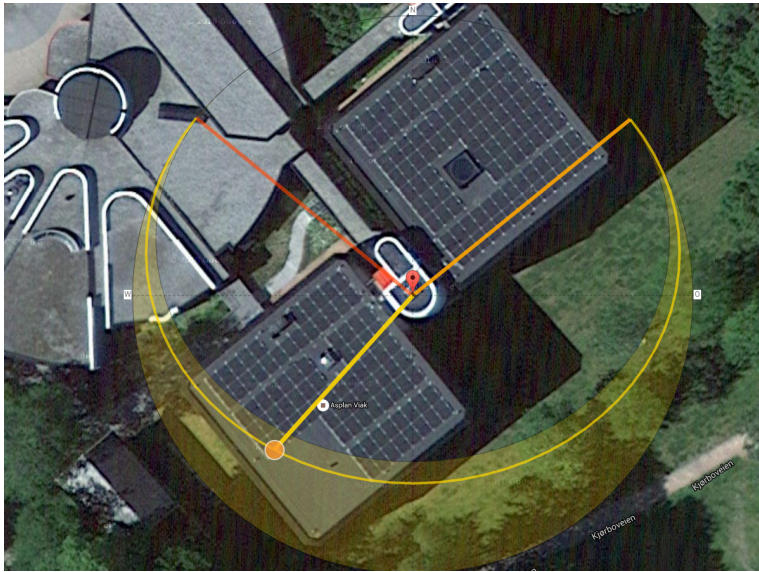*Figure F.1: SunCalc May 10th 12:30.*

Figure F.2: SunCalc May 10th 13:30.

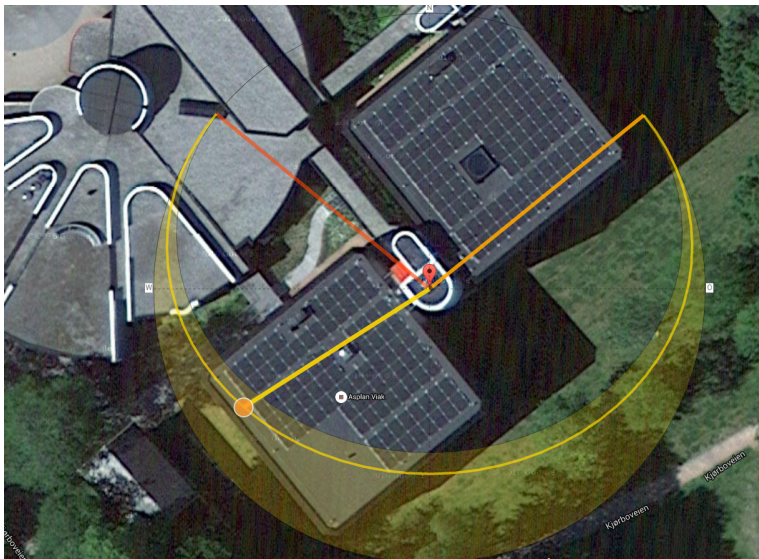*Figure F.3: SunCalc May 10th 15:20.*

Figure F.4: SunCalc May 10th 16:15.

F.2   Four Sunny Days

F.2.1   Global irradiance

The effective (global)irradiance from the Northeast (blue) and Southwest-oriented (red)
irradiance sensors for April 12th, May 8th and Jun 5th. The irradiance data for March
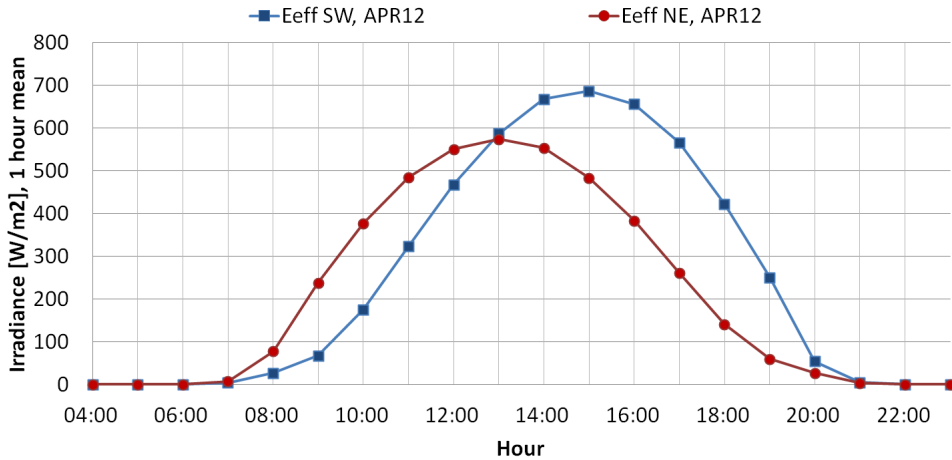16th is not available.

Figure F.5: 1 hour mean effective irradiance on April 12th.

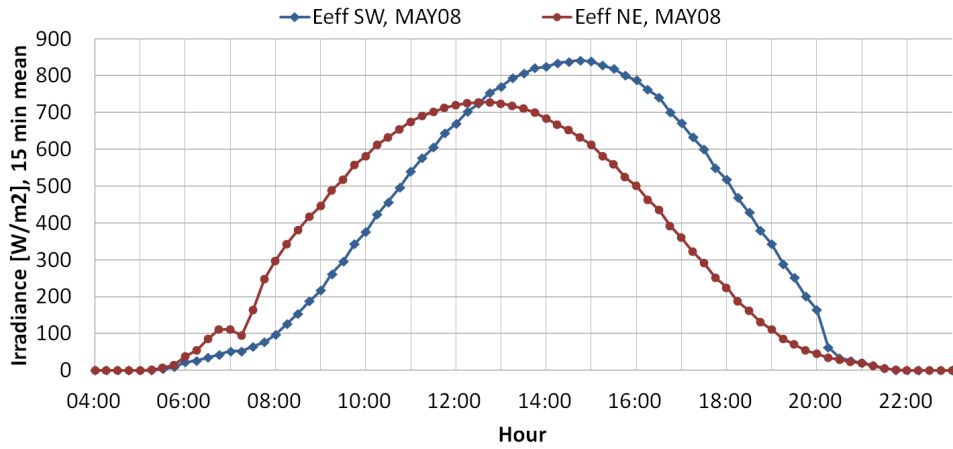*Figure F.6: 15 minute mean effective irradiance on May 8th..*
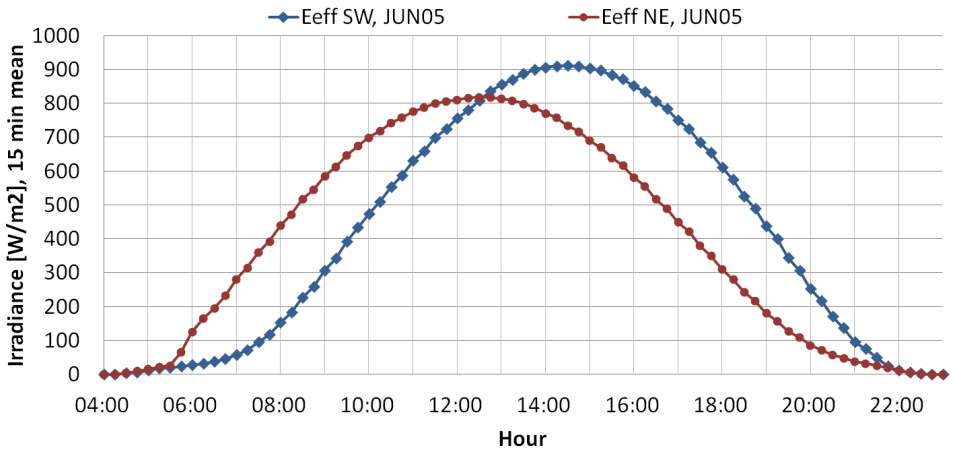
Figure F.7: 15 minute mean effective irradiance on June 5th.

F.2.2   Power for Block 4 and 5 for the three sunny days

Figure F.8: 15 minute mean power production on selected sunny days for B4_V1 and V2 (SE).

Figure F.9: 15 minute mean power production on selected sunny days for B5_V1 and V2 (SE).

Figure F.10: 15 minute mean power production on selected sunny days for B4_V3 and V4 (NW).

Figure F.11: 15 minute mean power production on selected sunny days for B5_V3 and V4 (NW).

F.3　Instantaneous Values from the WebBox, May 10th
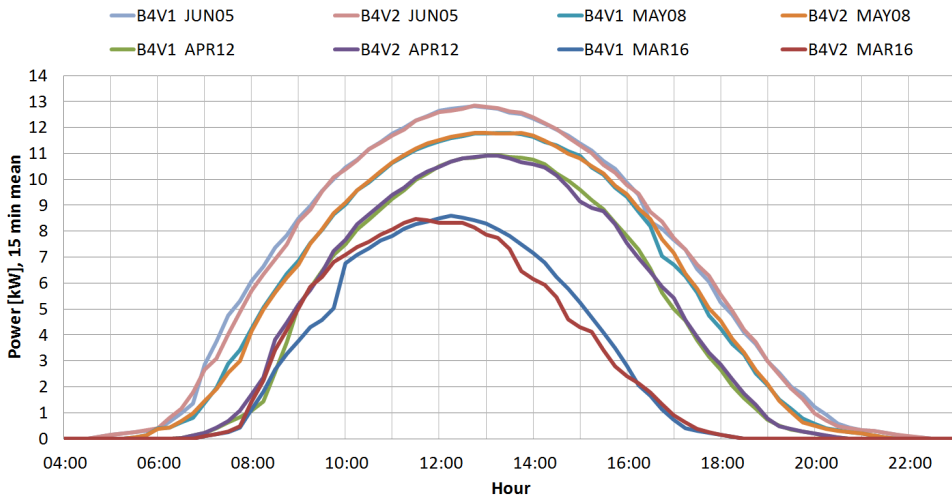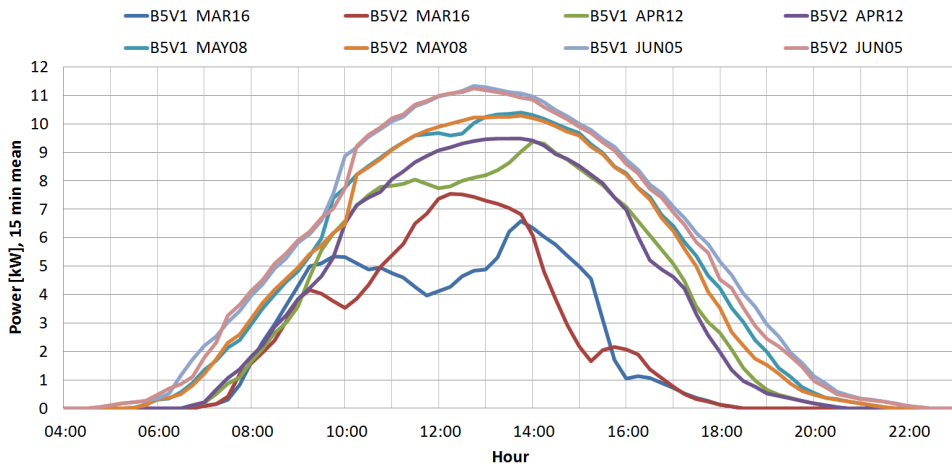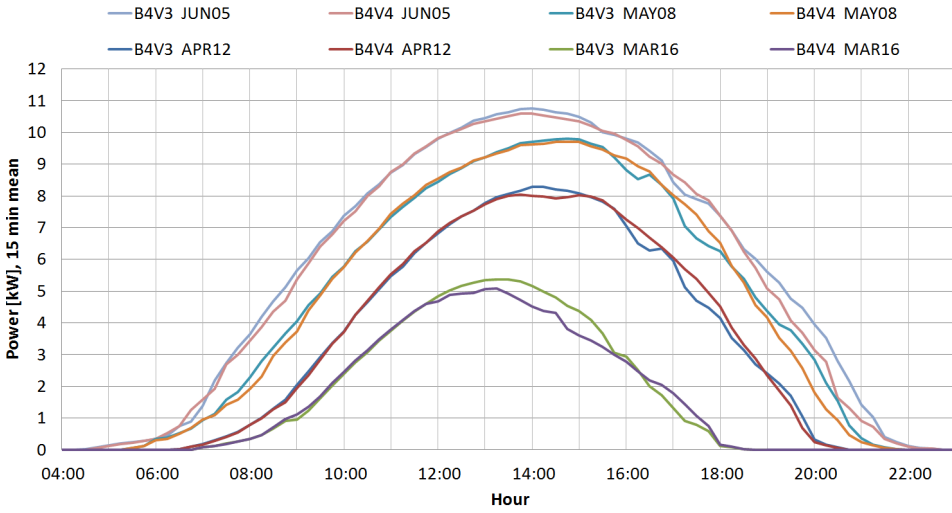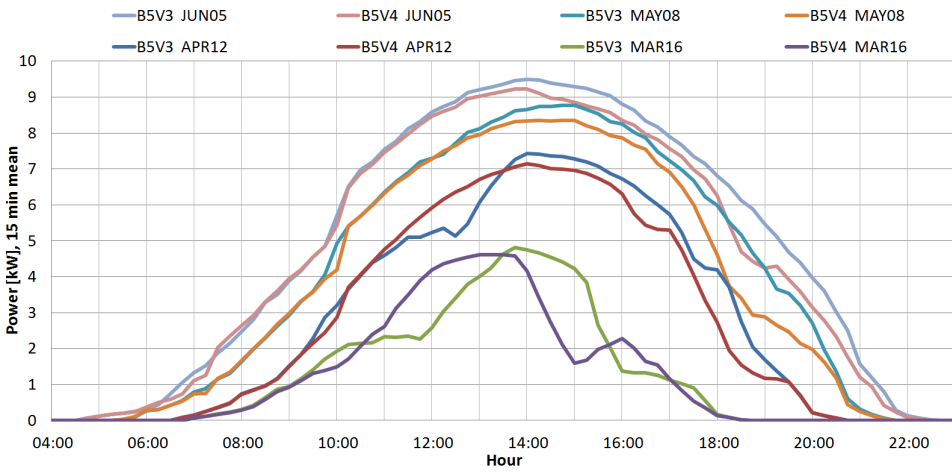
WebBox in Table F.1, the strings most affected by partial shading at these instances are: B4_V1A1, shaded by the South-eastern safety wire; B5_V1A1, also shaded by the safety wire; and B5_V2A3, shaded by the vent pipe of Block 5. These are marked in red, showing a reduced current of approximately 0.2–0.3 A for each shaded string.

Kl. 10:00								
INV\Param	I_A1 [A]	I_A2 [A]	I_A3 [A]	I_A [A] tot	I_B [A]	U_A [V]	U_B [V]	P_A [kW]	P_B [kW]
B5V1	3,56	3,8	3,82	**11,39**	3,78	614,6	458,3	**6,94**	**1,727**
B5V2	3,98	3,92	3,64	**11,74**	3,95	587,4	458	**6,95**	**1,73**
B5V3	2,43	2,56	2,54	**7,39**	2,44	628,8	466,7	**4,72**	**1,142**
B5V4	2,37	2,38	2,55	**7,446**	2,55	623,3	427	**4,63**	**1,201**
B4V1	3,7	3,93	3,97	**11,6**	3,97	669,1	711,98	**7,716**	**2,834**
B4V2	3,88	3,99	3,99	**11,905**	3,98	662,8	670,2	**7,9**	**2,66**
B4V3	2,55	2,48	2,56	**7,7**	2,56	675,7	724,9	**5,2**	**1,86**
B4V4	2,58	2,67	2,53	**7,68**	2,7	669,6	727,5	**5,16**	**1,97**
Kl. 11:00								
INV\Param	I_A1 [A]	I_A2 [A]	I_A3 [A]	I_A [A] tot	I_B [A]	U_A [V]	U_B [V]	P_A [kW]	P_B [kW]
B5V1	4,177	4,446	4,463	**13,208**	4,419	627,2	461,87	**8,294**	**2,041**
B5V2	4,542	4,478	4,336	**13,318**	4,585	615,88	455,72	**8,202**	**2,089**
B5V3	2,985	3,065	3,065	**9,287**	3,012	635,29	472,87	**5,899**	**1,424**
B5V4	2,955	2,971	3,098	**9,192**	3,12	623,32	472,22	**5,729**	**1,473**
B4V1	4,239	4,477	4,51	**13,303**	4,469	657,62	711,98	**8,748**	**3,181**
B4V2	4,431	4,51	4,509	**13,356**	4,47	663,12	674,77	**8,862**	**3,016**
B4V3	2,955	3,049	3,066	**9,256**	3,087	669,27	718,45	**6,194**	**2,217**
B4V4	3,033	3,112	3,128	**9,096**	3,161	681,56	732,68	**6,199**	**2,316**

Table F.1: Instantaneous values from the Sunny WebBox at 10:00 and 11:00, May 10th.

F.4 Summarized Results from I-V Measurements

String	Comment	Pmax per mod,	Pmax, calc	Difference [%]	Ppk [W]	Ppk per mod, avg	Error Ppk, ref 327 W [%]	Rp per cell [Ohm]
B5V2A3	pipe	232,935821	258,2373713	9,79778061	3610,837209	300,9031007	7,980703139	7,868964681
B5V2A3	no pipe	237,3036228	256,784005	7,586291161	3725,034103	310,4195086	5,070486659	7,586625215
B5V2A2	no shade	231,3050115	254,3942325	9,076157408	3659,680487	304,973374	6,735971267	7,947992217
B5V2A1	no shade	234,8409521	253,3509045	7,306053425	3767,369043	313,9474203	3,991614592	6,771258383
B5V2B	no shade	235,4008349	252,3284645	6,708569159	2830,566443	314,5073825	3,820372314	7,239232304
B5V1A1	no shade	232,638552	259,289051	10,27829711	3633,321693	302,7768077	7,407704054	7,117212366
B5V1A3	no shade	233,5660824	258,0007756	9,470782829	3678,076959	306,5064133	6,267151907	6,482264051
B5V1B	before hatch	229,6479907	257,3684329	10,77072344	2755,856159	306,2062399	6,358948048	4,679563796
B5V1A2	no shade	229,806949	255,9623331	10,2184504	3641,072992	303,4227493	7,210168411	6,931315125
B5V1B	hatch	175,5995517	202,7051979	13,37195421	2786,498224	309,6109138	5,317763368	5,262242449
B5V1A1	no shade	192,1799067	205,6984365	6,57201389	3945,499982	328,7916652	-0,547909839	8,45742849
B5V3B	hatch	183,5478487	202,810684	9,497939101	2917,377431	324,1530479	0,87062755	6,153893191
B5V3B	hatch	182,9091759	210,4798564	13,09896394	2810,656523	312,2951692	4,496890147	5,486263298
B5V4B	vent	177,5332919	219,7020028	19,1935942	2407,581312	267,5090347	18,19295575	8,271155838
B4V3A2	(CLOUDY)	181,4768658	186,585228	2,737817069	4577,674104	352,1287773	-7,684641366	7,259676997
B4V3A1	(CLOUDY)	186,8024112	185,1220866	-0,9076846	4978,039233	382,9260949	-17,10278131	6,144676003
B4V3A1	(CLOUDY)	186,6192194	184,5625469	-1,114349841	4995,544476	384,272652	-17,51457248	6,086816341

Table F.2: Summarized Results from I-V Measurements from May 10th.